Universidad Michoacana de San Nicolás de Hidalgo

Instituto de Investigaciones Químico Biológicas

Doctorado en Ciencias Químicas

Configuración absoluta de derivados de timol de la tribu Eupatorieae

Tesis

Que para obtener el grado de

Doctor en Ciencias Químicas

Presenta:

M.C. Héctor Manuel Arreaga González

Directores:

D.Q. Mario Armando Gómez Hurtado

D.C. Rosa Elva Norma del Río Torres

Morelia, Michoacán marzo de 2019

Cuando era niño mi madre me dijo: si eliges ser soldado, serás general; si eliges ser sacerdote, serás Papa. Fui pintor, y llegué a ser Picasso.

Pablo Picasso

A mis padres

Con infinito agradecimiento dedico esta tesis a mis padres, no existen las palabras suficientes para agradecer por todo lo que me han dado.

Mamá: por ser mi ejemplo de fortaleza.

Papá: por ser mi ejemplo de sacrificio.

AGRADECIMIENTOS

A la Universidad Michoacana de San Nicolás de Hidalgo, por permitirme culminar otro proyecto en sus instalaciones. Mi corazón ya es Nicolaita.

Al Instituto de Investigaciones Químico Biológicas porque a lo largo de los años, los compañeros se han vuelto familia.

A la Doctora Rosa Elva del Río Torres, Por tener la dicha de conocer a una excelente persona como lo es usted, por enseñarme el valor de la honestidad y por darme la oportunidad de demostrar que hago las cosas con pasión.

Al Doctor Mario Armando Gómez Hurtado por si infinita paciencia, por compartir conmigo sus conocimientos y permitirme formarme como Doctor y persona en su laboratorio.

A los Doctores: Hugo Alejandro García Gutiérrez, Juan Diego Hernández Hernández y Carlos Martín Cerda García-Rojas, por sus valiosas aportaciones y consejos que han permitido llevar a buen término este proyecto.

Al Doctor Pedro Joseph Nathan por las facilidades otorgadas en el uso de su laboratorio y equipos.

Al Doctor Jesús Martín Torres Valencia por permitirme realizar una estancia de Investigación en su laboratorio, pero principalmente por permitirme conocerle como persona.

Al Doctor José de Jesús Manríquez Torres por el apoyo obtenido en el procesamiento de datos computacionales.

A los técnicos del IIQB y del CINVESTAV, Coni, José Manuel, Verito, Angie, Azucena Alvina, Celina, Yola, por el procesamiento de las muestras y sus buenos consejos.

A CONACyT por la beca 295638.

A mis hermanas Verónica y Guadalupe por ser mis compañeras de vida, porque sé que siempre cuento con ustedes, por alegrar y hacer crecer la vida y la felicidad de esta familia con Xime y Esteban.

A Moni por compartir tu tiempo, tu espacio y tu vida conmigo, por no dejarme caer en los momentos de desesperación y ansiedad, por los buenos momentos que hemos pasado.

A la Doctora Gabriela Rodríguez García por todos los consejos y buenas vibras.

Al Doctor Julio Cesar Pardo Novoa, solo tengo una palabra para agradecerte: Hermano.

A la Maestra Ana Karen Villagómez Guzmán por tantos años de amistad y buenos momentos en el laboratorio.

A todos los buenos amigos que he conocido en el IIQB, han sido tantos que intentare nombrarlos a todos: Bedolla, Galileo, Fredy, Juan Carlos, Mayra Yunuen, Vargas, Techi, Salvador Gallardo, Alejandro, Ismael, Cristian, Juan Antonio, Tere, David, Karen, Estefanía, Antonio, Paulina, Yesenia, Sinuhe, Doris, Karina, Donaldo, Lirenny, Mayra torres, Itzel, Rebeca, Salvador López y a todos los tesistas y chicharitos. Ustedes saben que a todos los quiero.

A los amigos de la UAEH: Raúl, Elena, Erika, Adriana, Alexia, Oswaldo, Miguel, Curie y René por tantos buenos momentos compartidos durante mi estancia en su universidad.

A Yesenia Romero, Erika Ramírez, Guadalupe Garnica y Juan Diego Rivas por permitirme guiarlos en este camino, ustedes han hecho mi estancia en el laboratorio una de las mejores experiencias de mi vida académica, siempre estaré orgulloso de sus logros.

Llegar a la meta no es vencer
Lo importante es el camino y en el:
Caer, levantarse, insistir y aprender.

Esta investigación se realizó en el laboratorio de Química de Productos Naturales del Instituto de Investigaciones Químico Biológicas de la Universidad Michoacana de San Nicolás de Hidalgo bajo la dirección del D.Q. Mario Armando Gómez Hurtado y de la D.C. Rosa Elva Norma del Río Torres, con la beca de doctorado 295638 otorgada por el Consejo Nacional de Ciencia y Tecnología (CONACyT).

Los resultados obtenidos en la presente tesis doctoral permitieron la generación de las siguientes publicaciones, participaciones en congresos, tesis dirigidas y capítulos en libros:

ARTÍCULOS

1. Pardo-Novoa J. C., **Arreaga-González** H. M., Gómez-Hurtado M. A., Rodríguez-García G., Cerda-García-Rojas C. M., Joseph-Nathan P., del Río R. E. *Absolute Configuration of Menthene Derivatives by Vibrational Circular Dichroism*. *Journal of Natural Products*, (2016) **79**: 2570-2579.

2. **Arreaga-González** H. M., Pardo-Novoa J. C., del Río R. E., Rodríguez-García G., Torres-Valencia J. M., Manríquez-Torres J. J., Cerda-García Rojas C. M., Joseph-Nathan P., Gómez-Hurtado M. A., *Methodology for the Absolute Configuration Determination of Epoxythymols Using Constituents of Ageratina glabrata*. *Journal of Natural Products*. (2018) 81: 63-71.

3. Pardo-Novoa J. C., **Arreaga-González** H. M., Galván-Gómez S., Rodríguez-García G., Cerda-García-Rojas C., Joseph-Nathan P., Gómez-Hurtado M. *Biomimetic Transformation of p-Menthene Glucosides into p-Cymenes and Carvotanacetone*. *Journal of Natural Products* (en prensa).

4. **Arreaga-González** H. M. y colaboradores, *Absolute Configuration Determination by VCD and Seasonal Variations of Enantiomeric ratio of 10-cinnamoyloxy-7-oxo-8,9-epoxythymol isobutyrate by ^{1}H MNR and (S)-BINOL* (en proceso).

TRABAJOS EN CONGRESOS

1. “Asignación posicional y espectroscópica de derivados de timol de *Ageratina glabarta*”, **Arreaga**-**González** H. M., Rosa E. del Río, Gabriela Rodríguez-García, Carlos M. Cerda-García-Rojas, Pedro Joseph-Nathan, Mario A. Gómez-Hurtado. 12ª Reunión Internacional de Investigación en Productos Naturales. Celebrada en Xalapa, Veracruz, del 18 al 20 de Mayo de 2016.

2. “Epoxitimoles minoritarios de *Ageratina glabrata*”, **Arreaga**-**González** H. M., Rodríguez-García G., López-Castro Y., Torres-Valencia J. M., del Río R. E., Gómez-Hurtado M. A. Tercera Semana del Posgrado en Ciencias Químicas. Celebrado en el IIQB de la UMSNH, Morelia, Michoacán, el 29 de junio de 2016.

3. “Configuración absoluta de derivados de timol por Dicroísmo Circular Vibracional”, **Arreaga**-**González** H. M., Rodríguez-García G., Torres-Valencia J. M., Manríquez-Torres J. J., del Río R. E., Cerda-García-Rojas C. M., Joseph-Nathan P., Gómez-Hurtado M. A. 1er Foro del Posgrado en Ciencias Químicas. Celebrado en el IIQB de la UMSNH, Morelia, Michoacán, del 31 de julio al 4 de agosto de 2017.

4. “Elucidación estructural de un derivado de timol de *Ageratina glabrata*”, **Arreaga**-**González** H. M., 12º Congreso Estatal de Ciencia, Tecnología e Innovación y 6º. Encuentro de Jóvenes Investigadores del Estado de Michoacán. Celebrado en Morelia, Michoacán, México el 6 de octubre de 2017.

5. “Caracterización espectroscópica y configuración absoluta de derivados de timol de *Piptothrix areolare*”, **Arreaga**-**González** H. M., del Río R. E., Gómez-Hurtado M. A., Rodríguez-García G., García-Gutiérrez H. A., Cerda-García-Rojas C. M., Joseph-Nathan P. 2do Foro del Posgrado en Ciencias Químicas. Celebrado en el IIQB de la UMSNH, Morelia, Michoacán, del 2 al 6 de julio de 2018.

6. “Absolute configuration determination of epoxythymol derivatives from *Ageratina glabrata*”, **Arreaga**-**González** H. M., Rodríguez-García G., Torres-Valencia J. M., Manríquez-Torres J. J., del Río R. E., Cerda-García-Rojas C. M., Joseph-Nathan P., Gómez-Hurtado M. A. 54th Annual Meetingof the Phytochemical Society of North America (PSNA). Celebrada en la Facultad de Ciencias Químicas de la Universidad Autónoma de San Luis Potosí, San Luis Potosí, del 4 al 8 de agosto de 2018.

7. “Estudios sobre la susceptibilidad a la racemización de un derivado de timol”, **Arreaga**-**González** H. M., Rivas-Gervacio J. D., Ramírez-Guzmán E. J., Rodríguez-García G., del Río R. E., Gómez-Hurtado M. A. 13º Congreso Estatal de Ciencia, Tecnología e Innovación y 7º Encuentro de Jóvenes Investigadores del Estado de Michoacán. Celebrado en Morelia, Michoacán, el 19 de octubre de 2018.

TESIS DIRIGIDAS

1. “Aislamiento y actividad antioxidante de timoles funcionalizados” Tesis para obtener el título de Química Farmacobióloga de Yesenia Romero Colín. Fecha de examen 6 de marzo de 2016, con mención honorifica. Tema co-dirigido con el D.Q. Mario Armando Gómez Hurtado.

CAPÍTULO DE LIBRO

1. del Río R. E., Rodríguez-García G., Gómez-Hurtado M. A., Talavera-Alemán A., **Arreaga**-**González H**. **M**. Comprendiendo científicamente los efectos de la hierba del golpe *Ageratina glabrata*. Instituto de Ciencia, Tecnología e Innovación. Año 2018 no. 4. Cuadernos de Divulgación Científica y Tecnológica del Instituto de Ciencia, Tecnología e Innovación. ISBN 04-2018-011610464800-102.

ÍNDICE

1 SÍMBOLOS Y ABREVIATURAS

Δ	Desplazamiento químico
®	Marca registrada
ºC	Grados Celsius
AcOEt	Acetato de etilo
Ang	Grupo angelato
ATM	Atmósfera
B3LYP	Becke, three-parameter, Lee-Yang-Parr
BINOL	1,1´-bi-2-naftol
CA	Configuración absoluta
Cm	Centímetro
CONAGUA	Comisión nacional del agua
D	Señal doble
Dd	Señal doble de dobles
DCV	Dicroísmo circular vibracional
DFT	Density functional theory
DGDZVP	DGauss Double-Zeta Valence Polarization
e.e.	Exceso enantiomérico
G	gramo
H	hora
Hz	Hertz
i-Bu	Grupo isobutirato
IR	Infrarrojo
J	Constante de acoplamiento
K	Grados Kelvin
Kcal	Kilocalorias
Km	kilómetro
M	Señal múltiple
OMe	Grupo metoxilo
MeBu	Grupo metilbutirato
mL	Mililitro
Mm	Milímetro
Mg	Miligramos
MHz	Mega Hertz

MMFF	Molecular mechanics force field
Ppm	Partes por millón
RMN de ^{13}C	Resonancia Magnética Nuclear de carbono-13
RMN de ^{1}H	Resonancia Magnética Nuclear de Hidrógeno
S	Señal simple
S_E	Similitud espectral
Sept	Señal séptuple
T	Señal triple
Tt	Señal triple de triples
Tig	Grupo tiglato
TMS	Tetrametilsilano
UV	Ultravioleta
1D	Unidimensional
2D	Bidimensional

2 RESUMEN

En el presente trabajo se reporta el estudio químico de los derivados de timol de las especies vegetales: *Ageratina glabrata*; (+)-(8*S*)-isobutirato de 10-benzoiloxi-6-hidroxi-8,9-epoxitimol (**1**), (+)-(8*S*)-isobutirato de 10-isobutiriloxi-8,9-epoxitimol (**2**), (+)-(8*S*)-isobutirato de 10-acetoxi-6-metoxi-8,9-epoxitimol (**3**), (+)-(8*S*)-isobutirato de 10-benzoiloxi-6-metoxi-8,9-epoxitimol (**4**), isobutirato de 10-benzoiloxi-8,9-epoxitimol (**5**), isobutirato de 10-benzoiloxy-9-isobutiriloxi-6,8-dihidroxitimol (**6**) y *Piptothrix areolare*; (8*S*)-isobutirato de 10-cinamoiloxi-7-oxo-8,9-epoxitimol (**7**). Se estableció una metodología para la determinación del exceso enantiomérico de epoxitimoles por Resonancia Magnética Nuclear de ^{1}H empleando el reactivo de desplazamiento quiral 1,1'-bi-2-naftol (BINOL) y configuración absoluta (CA) por Dicroísmo Circular Vibracional (DCV) del derivado **1**, la eficacia de esta metodología fue probada al determinar la CA de los derivados **2**-**4**. El valor de la rotación específica de **5** mostró que este derivado existe como mezcla racémica. La susceptibilidad química a la racemización de estos derivados se evaluó en condiciones de reacción ácidas con el derivado mayoritario **1**. Adicionalmente, se realizó la asignación posicional de los ésteres del subproducto de racemización **6**. Con base en las propiedades ópticas observadas en los epoxitilmoes de *A*. *glabrata*, se analizaron los valores de rotación específica y el grado de escalemización natural del derivado **7** de *P. areolare* a partir de un estudio estacional anual. En cada lote se determinó el exceso enantiomérico por RMN de ^{1}H y BINOL. Los resultados demostraron que el grado de escalemización de este derivado está estrechamente relacionado con los cambios climáticos de la región, lo que sugiere que este tipo de derivados podrían cumplir una función regulatoria y defensiva para la especie vegetal. Finalmente, fue posible determinar la configuración absoluta de (−)-(8*S*)-**7** por DCV. Tomando como base aquel lote que mostró una mayor pureza enantiomérica.

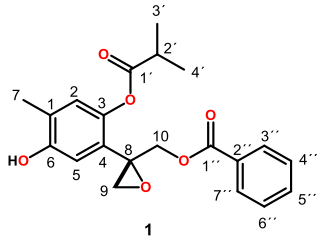

1

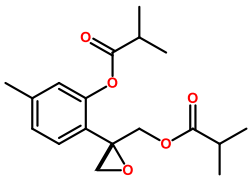

2

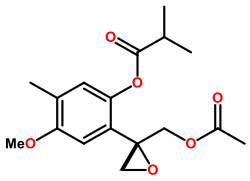

3

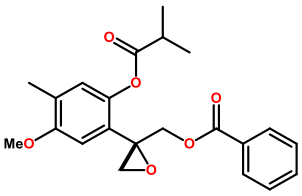

4

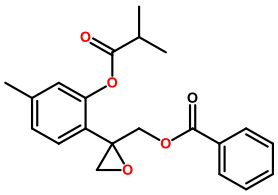

5

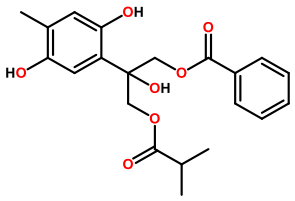

6

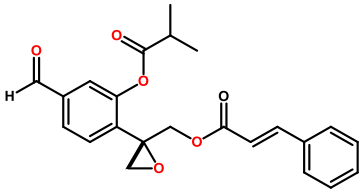

7

Palabras clave: Configuración absoluta, estudio estacional, epoxitimoles, *Ageratina glabrata*, *Piptothrix areolare*.

3 ABSTRACT

In the present research, we report the chemical study of epoxythymol derivatives of *Ageratina glabrata*: (+)-(8*S*)-10-benzoyloxy-6-hydroxy-8,9-epoxythymol isobutyrate (**1**), (+)-(8*S*)-10-isobutyryloxy-8,9-epoxythymol isobutyrate (**2**), (+)-(8*S*)-10-acetoxy-6-methoxy-8,9-epoxythymol isobutyrate (**3**), (+)-(8*S*)-10-benzoyloxy-6-methoxy-8,9-epoxythymol isobutyrate (**4**), 10-benzoyloxy-8,9-epoxythymol isobutyrate (**5**), 10-benzoyloxy-9-isobutyryloxy-6,8-dihydroxythymol isobutyrate (**6**) and *Piptothrix areolare*; (8*S*)-10-cinnamoyloxy-7-oxo-8,9-epoxythymol isobutyrate (**7**) plant species, on the one hand, the methodology for the determination of enantiomeric excess by ^{1}H NMR and chiral displacement reagent 1,1'-bi-2-naphthol (BINOL) and absolute configuration by Vibrational Circular Dichroism of **1** was established. The effectiveness of this methodology was tested by determining the absolute configuration of **2**-**4** derivatives, while the specific rotation value of **5** showed that this exist as a racemic mixture, the racemitation susceptibility of these derivatives was evaluated under acid reaction with **1**, adittionally, the positional assigment of the ester groups of **6** was determinated. Based on the optical properties observed in the epoxythymols of *A. glabrata*, the specific rotation values and the degree of natural scalemization of the **7** were analyzed in a anual seasonal study. In each lot was determinated the enantimeric excess by ^{1}H NMR and chiral displacement reagent 1,1'-bi-2-naphthol (BINOL). The results showed that the scalemization degree of **1** has a close relationship with climate change of the region and suggest that these derivatives could meet a regulatory and defensive function for this plant. Finally, the absolute configuration of (-)-(8*S*)-**7** was determined by VCD using the sample with the higher enantiomeric purity.

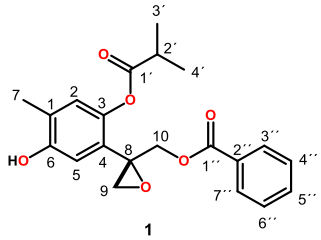

1

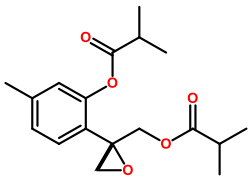

2

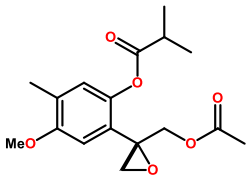

3

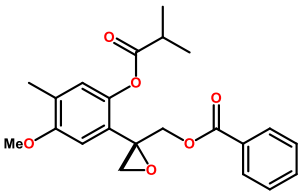

4

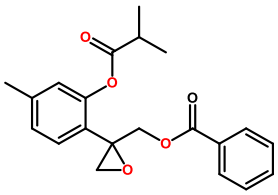

5

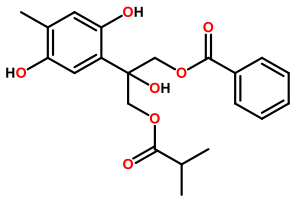

6

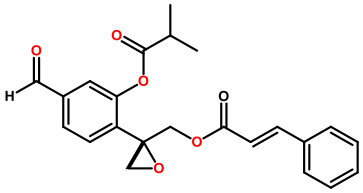

7

Key words: Absolute configuration, epoxythymols seasonal study, *Ageratina glabrata*, *Piptothrix areolare*.

4 INTRODUCCIÓN

Los derivados de epoxitimoles constituyen un extenso grupo de monoterpenos aromáticos con funcionalizaciones principalmente en las posiciones C-3, C-6, C-7 y/o C-10 que incluyen grupos éster, y algunos, un anillo de oxirano en C-8/C-9. Un grupo de 63 derivados de epoxitimol con estas características estructurales han sido reportados de 67 especies vegetales distribuidos en 32 géneros de la familia Asteraceae (Talavera-Alemán *et al*, 2016). La rotación específica de este tipo de estructuras ha sido reportada solo en algunos casos. Se pueden encontrar epoxitimoles levorotatorios en *Callilepis laureola* (Bohlmann e*t al*, 1977), *Eupatorium fortunei* (Tori *et al*, 2001) y *Gaillarda aristata* (Bohlmann *et al*, 1969), epoxitimoles dextrorotatorios han sido reportados de *A. glabrata* (Bohlmann *et al*, 1977), *A. cylindrica* (Bustos-Brito, *et al*, 2014), *Arnica acaulis* (Herz *et al*, 1989), *Brasilia sickii* (Bohlmann *et al*, 1983) e *Inula crithmoides* (Marco *et al*, 1993). Los epoxitimoles aislados de *Eupatorium stoechadosmum* (Trang *et al*, 1993) y *P. areolare* (Hernández *et al*, 1986) fueron descritos como mezclas racémicas. La presencia de epoxitimoles racémicos de *P. areolare* fue corroborada mediante reactivos de desplazamiento quiral (Hernández *et al*, 1986). Algunas explicaciones acerca de la racemización de 8,9-epoxitimoles hacen referencia al proceso de aislamiento (Tori *et al*, 2001) o a su generación como artefactos en extractos que permanecieron almacenadas por prolongados periodos (Delle Monache *et al*, 1984). Sin embargo, algunos derivados de timol enantiomericamente puros y racémicos han sido reportados de la misma planta (Tori *et al*, 2001, Wang *et al*, 2014), a pesar de esto, hasta la fecha no se han llevado a cabo estudios acerca de la susceptibilidad de racemización de epoxitimoles. En el presente trabajo se describe la determinación de la configuración absoluta (CA) de los derivados de timol **1**-**4** de *A. glabrata*, estableciendo una metodología basada en el análisis de la pureza enantiomérica y cálculos de DCV, se determinó el grado de escalemización de **1** en condiciones de reacción ácidas y se realizó la asignación posicional de los ésteres de **6**. Esta metodología fue validada al determinar la CA de **7**, compuesto mayoritario aislado de las raíces de *P. areolare* y se evaluó el grado de escalemización natural del mismo al realizar un estudio estacional anual, basado en las mediciones de rotación específica y RMN de ^{1}H con BINOL.

5 ANTECEDENTES

Una de las familias de plantas ampliamente distribuidas en el mundo son las asteráceas, la cual cuenta con alrededor de 950 a 1450 géneros y entre 20 000 y 30 000 especies. En México podemos encontrar 182 géneros, entre los que cuentan con mayor número de especies se encuentran *Ageratina*, *Stevia*, *Verbesina* y *Acourtia*, se localizan ampliamente distribuidas en el centro del País, principalmente en los estados de Querétaro, Michoacán y Guanajuato (Villaseñor 2012). Dentro de esta familia se encuentran las especies: *A*. *glabrata* y *P*. *areolare*, los cuales están ampliamente distribuidas en el continente Americano desde el norte al sur y el caribe (King, 1978).

A. *glabrata* es un arbusto de hasta 2.5 m de altura de tallos leñosos; hojas opuestas, haz y envés glabro y glanduloso-punteado, numerosos capítulos de 7 a 15 mm de largo dispuestos en corimbos compuestos terminales, sus flores de 15 a 18; corola de 7 mm de largo, blanca, a veces con tinte rosado en los lóbulos, cerdas blancas (figura 1) (Calderón de Rzedowski, 2005). En la medicina tradicional es conocida como “Chamizo blanco”, “Hierba del golpe”, y/o “Hierba de la mula” (Sánchez-González, 2008), se utiliza como analgésico para el tratamiento de golpes y fracturas (Bello *et al*, 2007).

P. *areolare* es un arbusto de 1 a 4 m de altura, presenta hojas pecioladas de 6 a 14 cm de largo por 2.5 a 6.5 cm de ancho, trinervias desde la base, los márgenes serrulados, el ápice angostamente acuminado; peciolo de 1 a 1.5 cm. Capitulescencia: una panícula tirsoide alargada con ramas corimbosas en las axilas de las hojas distales, terminalmente piramidal en el ápice; pedúnculos de 2 a 7 mm. Cabezuelas de 6 a 8 mm. Flores: de 12 a 18 con corola de 5 a 5.5 mm, corola de blanco a rosado (figura 1) (King, 1970).

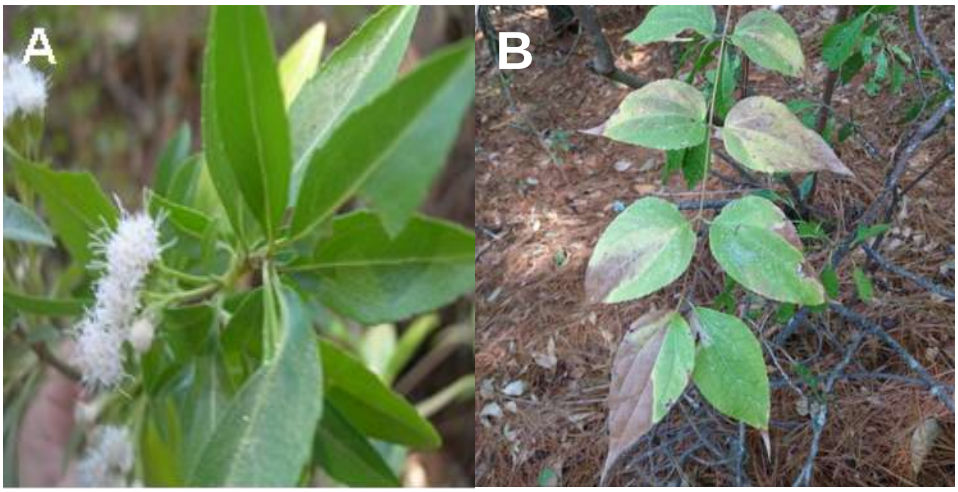

Figura 1. A) *A*. *glabrata*, B) *P*. *areolare*.

5.1 Actividad biológica

El timol es un compuesto aromático presente en los aceites esenciales de *Thymus vulgaris* formado por dos unidades de isopreno en la ruta biosintética del mevalonato, y posee el esqueleto típico de un monoterpeno cíclico (Dewick, 2009). En el año 2016 Talavera-Alemán *et al*, realizaron una revisión bibliográfica de derivados de timol que poseen un centro estereogénico o proestereogénico, reportando la existencia de 163, distribuidos en 38 géneros y 88 especies, de estos, 68 presentan funciones hidroxilo, éter o éster en la posición C-8, 62 están funcionalizados con un anillo de epóxido y presentan un centro estereogénico en C-8, mientras que 23 poseen un doble enlace y 5 presentan otras funcionalidades, incluyendo acetónidos (Figura 2).

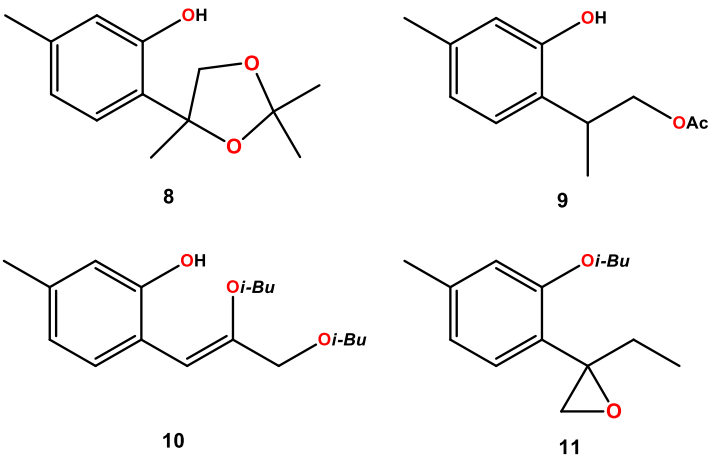

Figura 2. Diferentes tipos de sustituciones en derivados de timol.

En cuanto a la actividad bilógica de este tipo de estructuras, hasta el año 2016 solo se ha reportado la actividad de cerca del 10% de los derivados y estos han presentado una amplia gama de actividades como: alelopática (Zhou *et al*, 2003) anti-inflamatoria (Wang *et al*, 2014, Kos *et al*, 2005,) antiprotozoal (Bustos-Brito *et al*, 2014), antimicrobiana (Zhao *et al*, 2010, Liang *et al*, 2007), citotóxica (Jiang *et al*., 2006), antiproliferativa (Chen *et al*, 2014). En un estudio previo nuestro grupo de trabajo reportó el efecto analgésico de los extractos de cloruro de metileno de hojas de *A*. *glabrata* en animales de experimentación en modelos térmicos de dolor agudo de plato caliente y retirada de la cola demostrando su efecto analgésico 5 h posteriores a su aplicación (García *et al*, 2011).

5.2 Racemización

De los tallos de *Ageratina glechonophylla* aislaron los derivados de timol **12** y **13** (Delle-Monache *et al*, 1984) considerándose que el derivado **13** podría ser un artefacto de **12**, producto de la apertura del epóxido presente en su estructura (Figura 3).

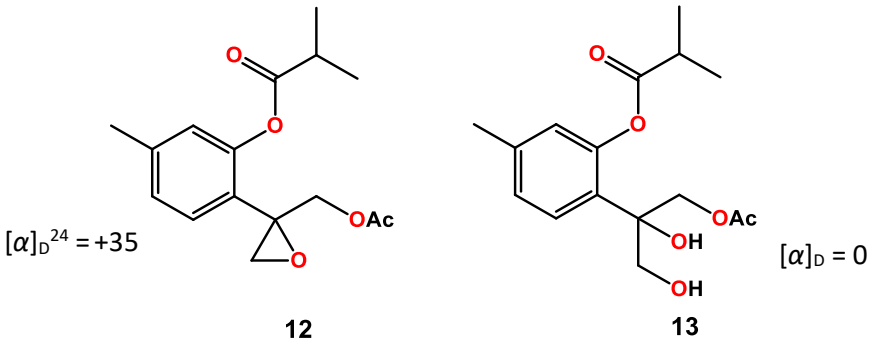

Figura 3. Derivados de timol de *A*. *glechonophylla*.

De las partes aéreas de *Eupatorium fortunei* (Figura 4), aislaron los compuestos **14**-**20**, con valores de rotación específica de cero para **14**-**19**. El autor demostró que estos compuestos existen como mezclas racémicas, y pueden ser artefactos formados durante la etapa de aislamiento (Tori, *et al* 2001).

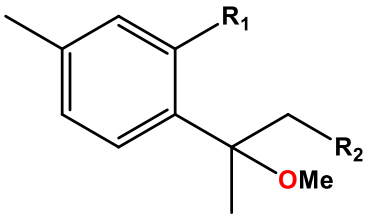

	R_1	R_2	[α]
14	OH	OH	$[\alpha]^{20}$±0
15	O*i*-Bu	OH	$[\alpha]^{24}$±0
16	OTig	OH	$[\alpha]^{20}$±0
17	OH	OAng	$[\alpha]^{20}$±0
18	OH	O*i*-Bu	$[\alpha]^{20}$±0
19	OH	OMeBu	$[\alpha]^{20}$±0
20	H	OH	$[\alpha]^{23}$+18.2

Figura 4. Derivados de timol de *Eupatorium fortunei*.

5.3 Pureza enantiomérica

Con base en la nula actividad óptica del areolal (**7**), fue descrito que para determinar su pureza enantiomérica, se empleó $Eu(THC)_3$ como agente de solvatación quiral, una alternativa eficaz, accesible y de fácil manejo (Hernández *et al*, 1986). En dicho ensayo, el racemato fue revelado al observar el desdoblamiento de la señal del CH_2-10, atribuida a los hidrógenos de metileno adyacente al centro estereogénico (Figura 5).

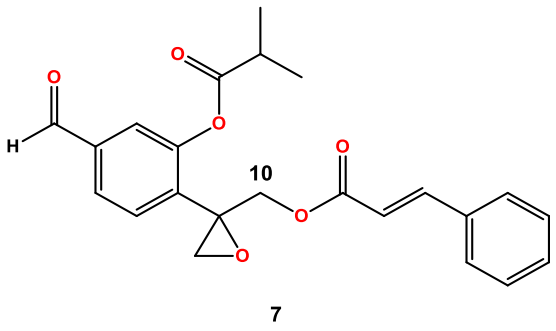

7

Figura 5. Areolal aislado de *P. areolare*.

Como alternativa al empleo de reactivos metálicos, en 2010 fue cuantificada la pureza enantiomérica del (*S*)-omeprazol (**21**) y su análogo: lansoprazol (**22**) (Figura 6), usando (*S*)-BINOL como reactivo de desplazamiento quiral mediante RMN de ^1H y ^{19}F. Esta técnica representa un método analítico rápido y confiable ya requiere una mínima cantidad de muestra y la preparación es sencilla, no destructiva y de fácil purificación por métodos convencionales (Redondo *et al*, 2010).

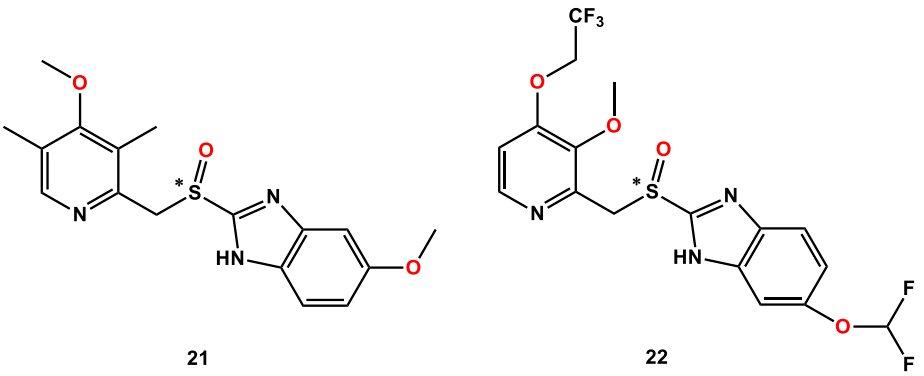

Figura 6. (*S*)-omeprazol (**21**), lansoprazol (**22**).

Derivados del BINOL se han empleado satisfactoriamente para la determinación de la pureza enantiomérica, así como la CA en productos naturales. Du *et al*, emplearon (*S*)-3,3'-dibromo-1,1'-bi-2-naftol para determinar la pureza óptica y quiralidad de la bavachinina (**23**) (Du *et al*, 2015) (Figura 7).

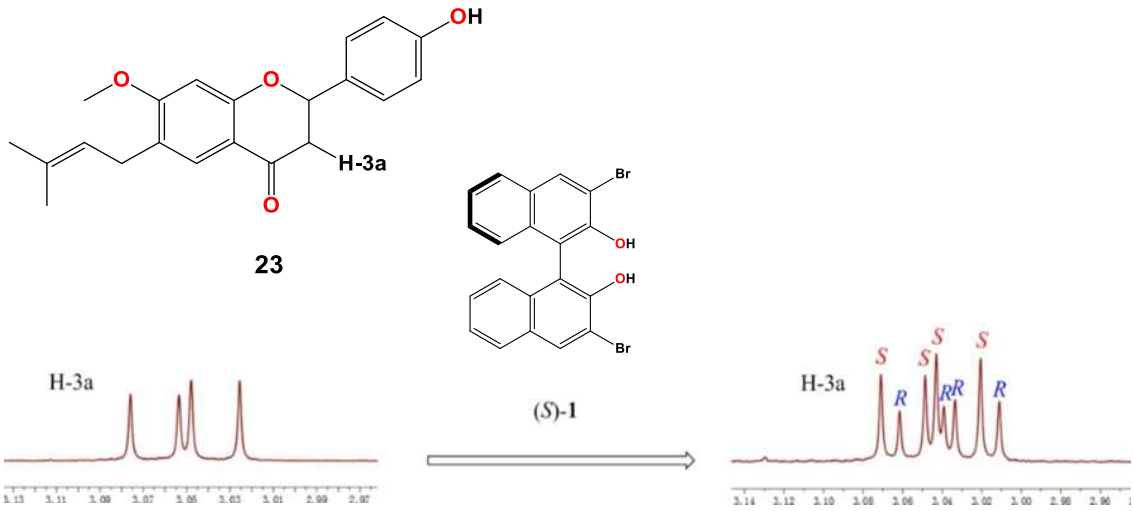

Figura 7. Relación enantiomérica entre bavachinina (*R*) y (*S*).

En 2016 Yi *et al*, también utilizaron de manera exitosa al (*R*)- BINOL y (*S*)-BINOL para la pureza óptica de las isoflavanonas **24** y **25** (Figura 8), y establecieron su CA con base en sus desplazamientos químicos (Yi *et al*, 2016).

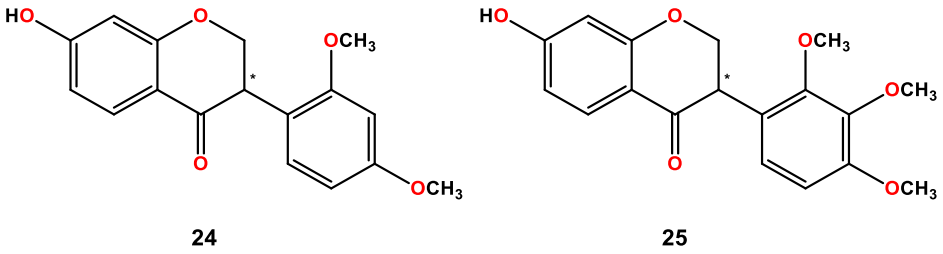

Figura 8. Isoflavanonas **30** y **31**.

5.4 Transesterificaciones

En 1969, Bohlmann *et al*, reportaron los primeros 10 derivados de timol a partir de *Gaillardia aristata* y *Hellenium mexicanum*, los cuales fueron caracterizados con base en sus desplazamientos de RMN de ^{1}H. El autor sugirió que el compuesto **27** se derivó del tratamiento ácido de **26** (Figura 9).

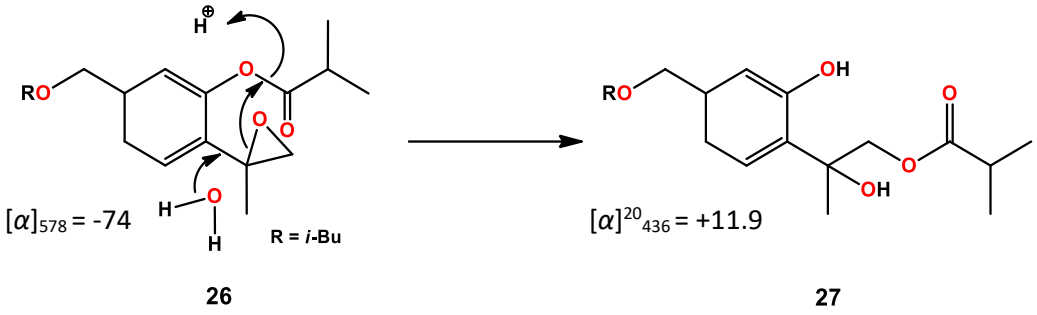

Figura 9. Derivados de timol aislados *Gaillardia aristata* y *Hellenium mexicanum.*

En 1992 Maldonado *et al*, aislaron de *Calea nelsonii* al derivado de timol **28**, sugirieron la posible transterificación a **27**, atribuido al uso de metanol durante el proceso de purificación (Maldonado *et al*, 1992) (Figura 10).

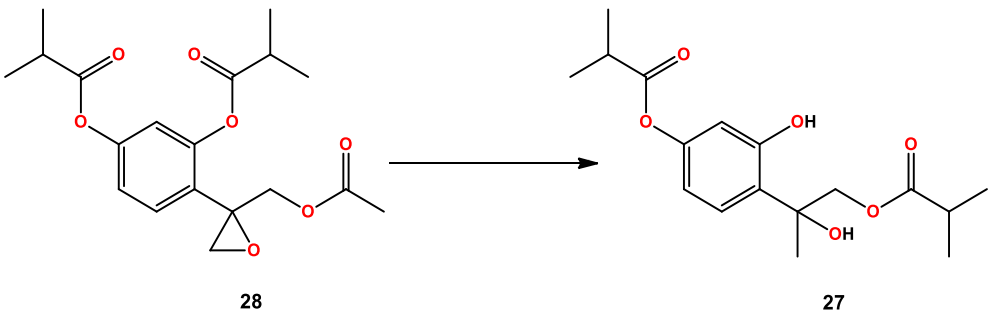

Figura 10. Derivados de timol de *Calea nelsonii.*

5.5 Configuración absoluta

La CA de una molécula se puede determinar a partir de distintas estrategias experimentales, una de ellas es por correlación química mediante una serie de reacciones, que pueden proceder con retención o inversión de la configuración y donde no se modifican los enlaces que están directamente unidos al centro estereogénico, como se demostró con el (−)-ácido láctico en base a la configuración del (+)-gliceraldehído (Juaristi, 2010) (Esquema 1).

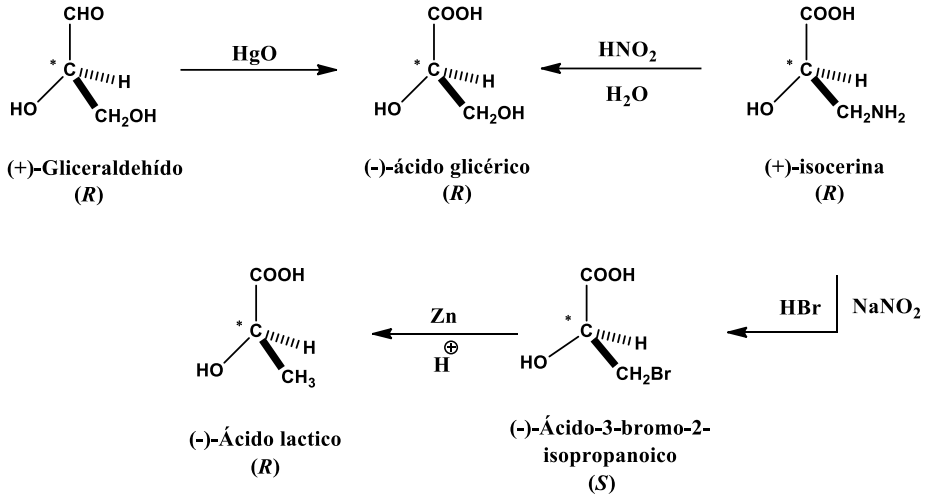

Esquema 1. Determinación de la CA por correlación química.

En el caso de moléculas de origen natural, dado que en la naturaleza los organismos no suelen producir metabolitos secundarios en forma racémica y las reacciones de biosíntesis siguen la misma ruta para una familia de compuestos, se puede determinar la CA de todos ellos con base en su biogénesis (Dewick, 2009). En 2011 Gómez-Hurtado *et al*, proponen la correlación biogenética de los *ent*-clerodanos y labdanos de *Chromolaena pulchella* con base en los resultados de la determinación de la CA de estos derivados (Gómez-Hurtado *et al*, 2011) (Esquema 2).

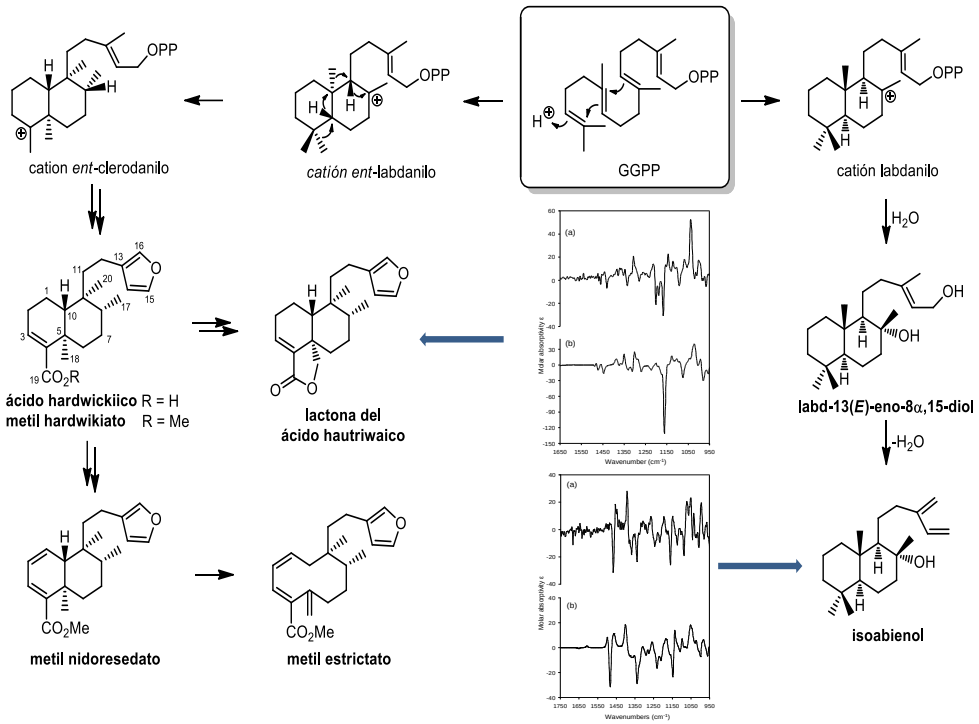

Esquema 2. Correlación biogenética de los *ent*-clerodanos y labdanos.

Otra alternativa para la determinación de la CA es la difracción de rayos X, que es capaz de distinguir entre estructuras cristalinas enantiomórficas, así como los enantiómeros de una molécula quiral tomando en cuenta información esencial como la geometría molecular, la distancia de enlace, los ángulos y el empaquetamiento de las moléculas dentro de la estructura. Se puede determinar la CA de un compuesto mediante la determinación de los parámetros de Flack y Hooft, el primero establece la relación que hay entre los cristales perfectamente orientados de forma opuesta dentro de un monocristral, por lo que se pueden definir las dos posibles configuraciones de un centro estereogénico (Flack, 2008); el segundo, es un parámetro estadístico computacional que se lleva a cabo al término del refinamiento y proporciona una ruta de sustento al parámetro de Flack (Thompson, 2009).

En el año 2014 Bustos-Brito *et al*, aislaron de *Ageratina cylindrica* al compuesto **29** (figura 11) reportaron el primer estudio para la determinación de la CA del centro estereogénico (C-8) de un derivado de timol mediante las técnicas de rayos X bajo los parámetros de Flack y Hooft y DCV (Bustos-Brito, *et al*, 2014).

Configuración absoluta
Flack *x* = -0.1 (2)
Hooft *y* = 0.02 (5)
Configuración opuesta
Flack *x* = 1.1 (2)
Hooft *y* = 0.98 (5)
R = 3.9%

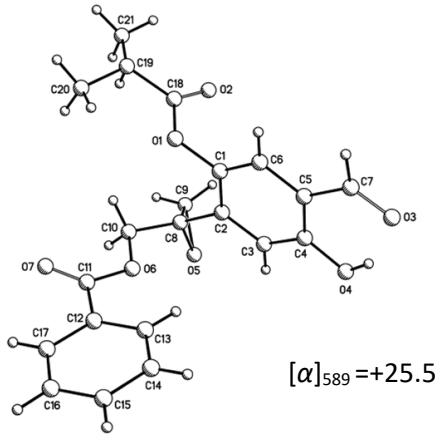

$[\alpha]_{589}$ =+25.5

29

Figura 11. Determinación de la CA del compuesto **29**.

Posteriormente, en 2016 Bustos-Brito *et al*, reportaron la CA por difracción de rayos X con base en el parámetro de Flack del (8*S*)-isobutirato de 10-benzoiloxi-6-hidroxi-8,9-epoxitimol (**1**) de *A. glabrata* (Bustos-Brito *et al* 2016) (figura 12).

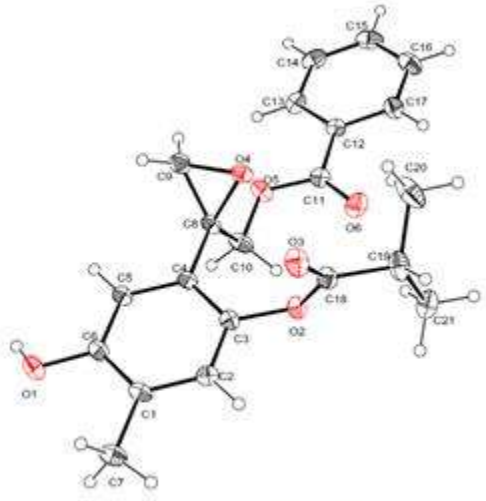

Figura 12. Difracción de rayos X de **1**.

Como propiedad espectroscópica, todas las moléculas orgánicas absorben irradiación de IR, por lo que las moléculas quirales pueden generar espectros IR de haz dicroico, es decir, IR_{DCV}, el cual es esteroespecífico, por tanto, los pares de enantiómeros generarán el mismo espectro de IR pero sus espectros de DCV serán imágenes especulares. La magnitud en las bandas en un espectro de DCV es aproximadamente 10,000 veces más pequeña que la de IR, lo que representa una desventaja del método, no obstante, cada banda de

absorción en el espectro de IR tiene una correspondiente banda en DCV. Es posible hacer una comparación entre un espectro DCV calculado y el experimental para determinar inequívocamente la CA.

En nuestro grupo de trabajo se determinó la CA de tres diterpenos de tipo cassano **30**-**32** de *Caesalpinia platyloba* por el método de DCV (Gómez-Hurtado, *et al*, 2013), contribuyendo con esto a la aplicación exitosa de esta técnica en moléculas terpénicas naturales (Figura 13).

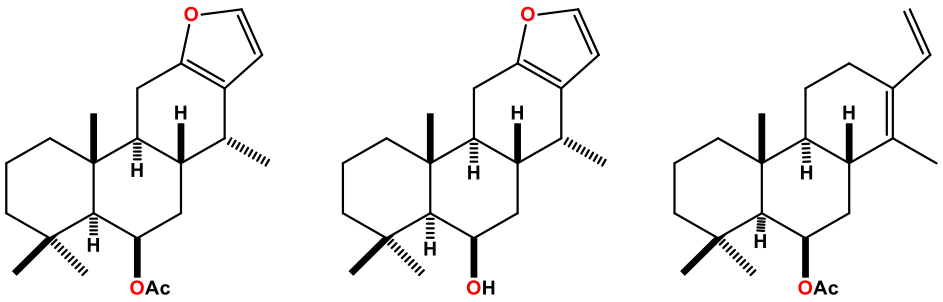

Figura 13. Diterpenos de *Caesalpinia platyloba*.

Adicionalmente, la CA por DCV de derivados del *p*-menteno **33** y **34** aislados de las partes aéreas de *A. glabrata*, permitió determinar la CA por correlación química de otras moléculas análogas en esta especie (Pardo-Novoa *et al* 2016) (Figura 14).

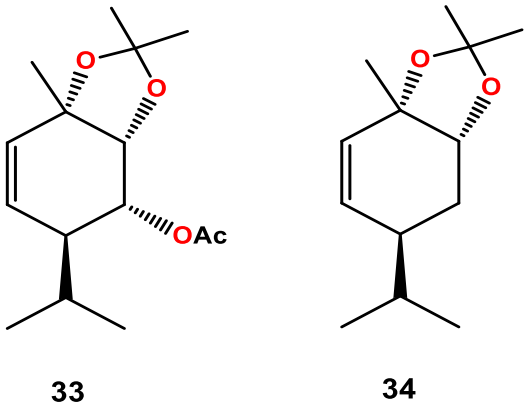

Figura 14. Mentenos aislados de *A. glabrata*.

De igual manera, se ha demostrado que dicha técnica es capaz de diferenciar diasteroisómeros, como en 2014, cuando García *et al* determinaron la CA de dos terpenos de tipo labdano mediante esta técnica y confirmaron la coexistencia de 13-*epi*-labdanos en *Ageratina jocotepecana* (Figura 15).

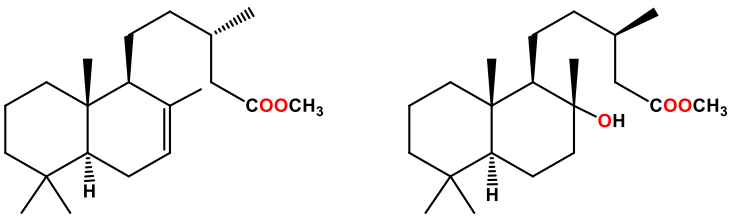

35 36

Figura 15. Estructuras del éster de ácido catívico (**35**) y éster del ácido 13-*epi*-labdanólico (**36**).

A pesar de que existen técnicas adecuadas, hasta el 2019 solo se ha determinado la CA de uno de los 163 derivados de timol reportados y no se han llevado a cabo ningún estudio experimental para determinar, por un lado la susceptibilidad química a la racemización del anillo de oxirano presente en 62 de ellos y por otro, si el medio ambiente puede propiciar la racemización natural. Con base en lo anterior, en este trabajo se plantea determinar la configuración absoluta de los derivados de timol presentes en las partes aéreas de *A. glabrata* y de las raíces de *P. areolare*, así como, determinar su capacidad de racemización en condiciones de reacción acidas como se ha sugerido anteriormente y corroborar en un estudio estacional anual si la relación enantiomérica de un epoxitimol reportado anteriormente como mezcla escalémica varía de acuerdo a las condiciones ambientales y el ciclo anual de la especie vegetal.

6 JUSTIFICACIÓN

Hasta el 2019 se han reportado 161 derivados de timol. Existen reportes donde se sugiere que pueden sufrir transesterificaciones y aperturas del anillo de epóxido por las condiciones de aislamiento, racemizaciones sugeridas en base a los valores de rotación específica. Solo hay un reporte de la CA de un derivado de timol y solo se ha reportado la actividad biológica del 10% de estos derivados, por lo que es pertinente llevar a cabo una investigación dirigida a determinar la configuración absoluta de los epoxitimoles aislados de dos especies vegetales de la tribu Eupatorieae y su capacidad de racemización por en condiciones de laboratorio y de forma natural en un estudio estacional.

7 OBJETIVOS

Objetivo general

Establecer una metodología para determinar la configuración absoluta de derivados de timol presentes en especies vegetales de la tribu Eupatorieae que pueda ser empleada de manera eficiente en estructuras análogas, y contribuir a la quimiotaxonomía de esta tribu vegetal.

Objetivos particulares

1. Aislar los derivados de timol mayoritarios de *A. glabrata*.
2. Determinar la pureza enantiomérica de **1**-**5**.
3. Propiciar la escalemización de epoxitimoles enantioméricamente puros mediante reacciones químicas.
4. Determinar la CA de los epoxitimoles aislados.
5. Aislar areolal (**7**) de *P. areolare*, y establecer su pureza enantiomérica.
6. Realizar un estudio estacional con colectas periódicas para el aislamiento de **7**, y determinar la pureza enantiomérica a lo largo del estudio.
7. Determinar la CA por DCV de **7**.

8 DISCUSIÓN DE RESULTADOS

8.1 Aislamiento de epoxitimoles de *Ageratina glabrata*

A. glabrata se colectó en febrero de 2015 en la desviación a Cuanajo a 1 km de la carretera Pátzcuaro-Santa Clara del Cobre, se secó a la sombra, posteriormente se separó en sus diferentes partes (raíces, tallos, hojas y flores), se maceró por separado con disolventes de polaridad ascendente por triplicado para obtener los correspondientes extractos.

Del extracto hexánico de hojas, en la polaridad (9:1) hexanos-AcOEt se obtuvo una miel amarilla, en su espectro de RMN de ^{1}H (figura 16), se observan entre 4.0 y 1.0 ppm las señales correspondientes a un grupo isobutirato, metilo aromático y metoxilo, alrededor de 4.5 y 3.0 ppm, las señales de sistemas AB de CH_2-9 y CH_2-10, en la región de los aromáticos, se aprecian las señales del anillo de benzoato entre 8.1 y 7.4 ppm y las señales para los hidrógenos en posición *para* del anillo de timol alrededor de 7.0 ppm. Con base en los datos anteriores, este espectro corresponde al isobutirato de 10-benzoiloxi-6-metoxi-8,9-epoxitimol **4** que fue aislado anteriormente de *A. glabrata* por Bohlmann en 1977 y de *Ageratina semialata* (Bohlmann *et al* 1977).

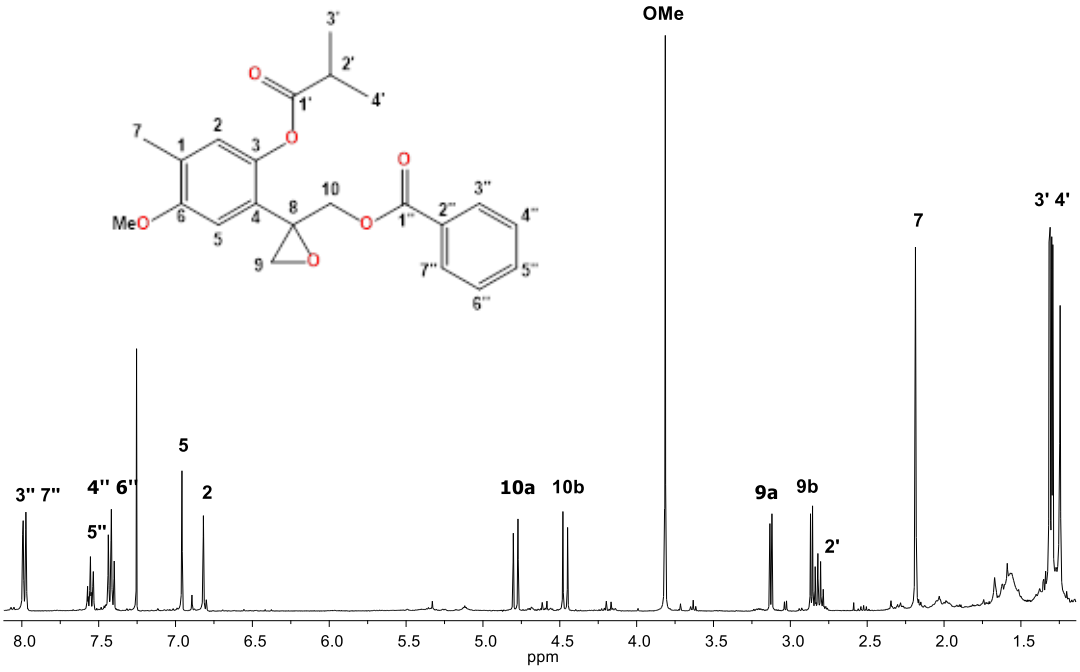

Figura 16. Espectro de RMN de ^{1}H a 400 MHz en $CDCl_3$ del isobutirato de 10-bezoiloxi-6-metoxi-8,9-epoxitimol (**4**).

En la misma polaridad se aisló un compuesto (figura 17), que presenta el patrón de señales para el grupo isobutirato y el anillo de epóxido, así como para el grupo benzoato. Adicionalmente, se aprecia que el anillo de timol presenta un patrón típico de trisustitución con constantes de acoplamiento *orto* y *meta* de 7.6 y 0.6 Hz, con base en estos datos se establece la obtención del isobutirato de 10-benzoiloxi-8,9-epoxitimol **5**, reportado anteriormente en *Ageratina glabrata* (Bohlmann *et al* 1977) y *en A. anisochroma* (Tamayo-Castillo, 1988).

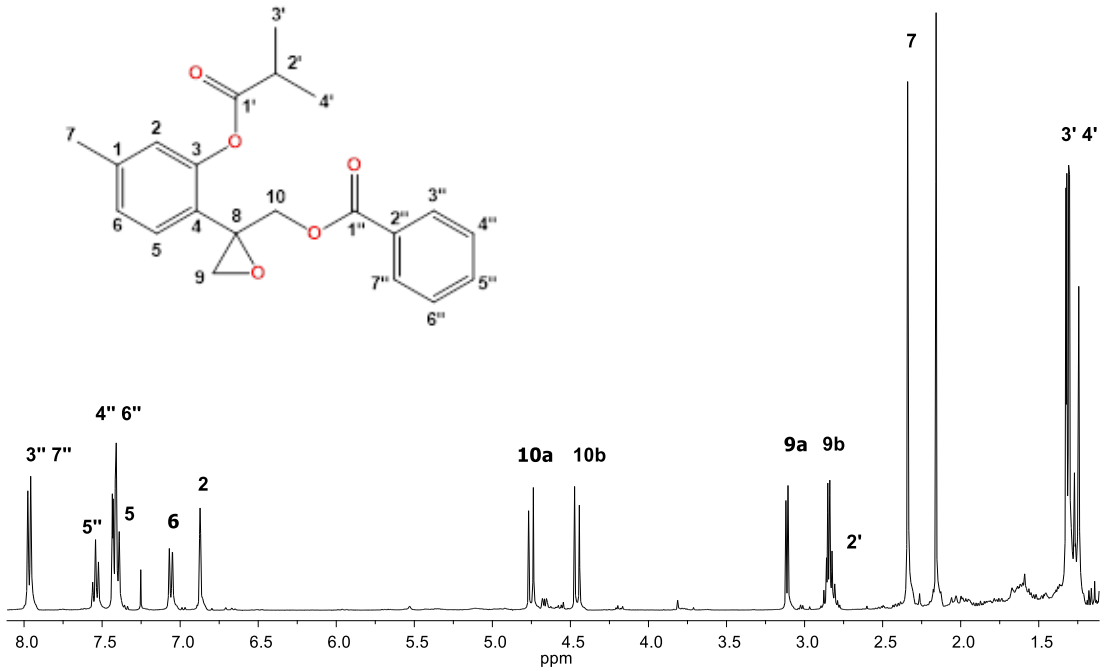

Figura 17. Espectro de RMN de ^{1}H a 400 MHz en $CDCl_3$ del isobutirato de 10-benzoiloxi-8,9-epoxitimol (**5**).

8.2 Evaluación de la pureza óptica

La pureza óptica de los epoxitimoles aislados **1**-**5**, se evaluó mediante la medición de la rotación específica. Los derivados **1**-**4** presentaron valores de $[\alpha]_{589}$ entre +10 y +28, mientras que para **5** se observó un valor de $[\alpha]_{589}$ +0.8 (*c* 0.8, $CHCl_3$), la cual difiere en signo y magnitud con la reportada por Bustos-Brito *et al*, en 2016 ($[\alpha]_{589}$ -3.9 en $CHCl_3$) en su estudio de *Ageratina glabrata*.

Esta variación sugiere que hay diferencias en la pureza óptica, donde probablemente prevalecen los enantiómeros opuestos, esto concuerda con los reportes donde algunos epoxitimoles existen como mezclas racémicas, o cuyo

valor de rotación específica es muy cercano a cero (Talavera *et al*, 2016). Por esta razón, se llevó a cabo la determinación de la pureza enantiomérica de todos los epoxitimoles aislados en este trabajo mediante el uso de (*S*)-BINOL como agente de solvatación quiral en mediciones de RMN de ^{1}H. Anteriormente, este método fue empleado exitosamente en la discriminación enantiomérica de algunos isoflavonoides (Yi *et al*, 2016), alcaloides (Antkowiak *et al*, 2002) y péptidos (Hu *et al*, 2016), así como en principios activos farmacológicos (Redondo *et al*, 2010, Redondo *et al*, 2013).). En los cinco compuestos estudiados fueron observados cambios en los desplazamientos químicos después del uso del reactivo de desplazamiento quiral (BINOL), los más significativos son los de los átomos localizados cerca del centro estereogénico concordando con la tendencia observada para otros compuestos (Gómez-Hurtado *et al*, 2013, García-Sánchez *et al*, 2014, Pardo-Novoa *et al*, 2016).

El análisis de BINOL-RMN de ^{1}H de **1**, **3** y **4** reveló que estos se encuentran enantiomericamente puros, ya que se observó un solo patrón de señales ligeramente desplazadas a campo alto con respecto al espectro original de RMN de ^{1}H. En el caso del epoxitimol **5** el espectro de RMN de ^{1}H-BINOL mostró dos conjuntos de señales para H-10b en 4.17 y 4.16 ppm ($\Delta\delta$ 0.013) con una marcada diferencia en la intensidad de las señales. El desdoblamiento de H-9a con $\Delta\delta$ 0.007 y H-9b con $\Delta\delta$ 0.004 también fue observado, las señales restantes mostraron los desplazamientos típicos observados en los espectros originales de RMN de ^{1}H. Con base en este experimento, fue posible establecer que este compuesto existe como una mezcla escalémica 3:1, por lo tanto un *e.e.* de 50% (Figura 18).

Por otro lado, el análisis de ^{1}H-BINOL de **5** reveló dos conjuntos de señales para H-10a y H-10b con similares intensidades, en este caso se observó que H-10b mostró el mayor desplazamiento químico ($\Delta\delta$ 0.021) en comparación con el observado para H-10a ($\Delta\delta$ 0.006), también H-9a mostró $\Delta\delta$ 0.009 y H-9b $\Delta\delta$ 0.003, mientras que para el resto de las señales no se observó un desplazamiento significativo. Con base en la intensidad de las señales desdobladas, es posible establecer una mezcla escalémica 56:44 (Figura 19), que tiene una relación directa con el valor de rotación específica observada $[\alpha]_{589}$ +0.8.

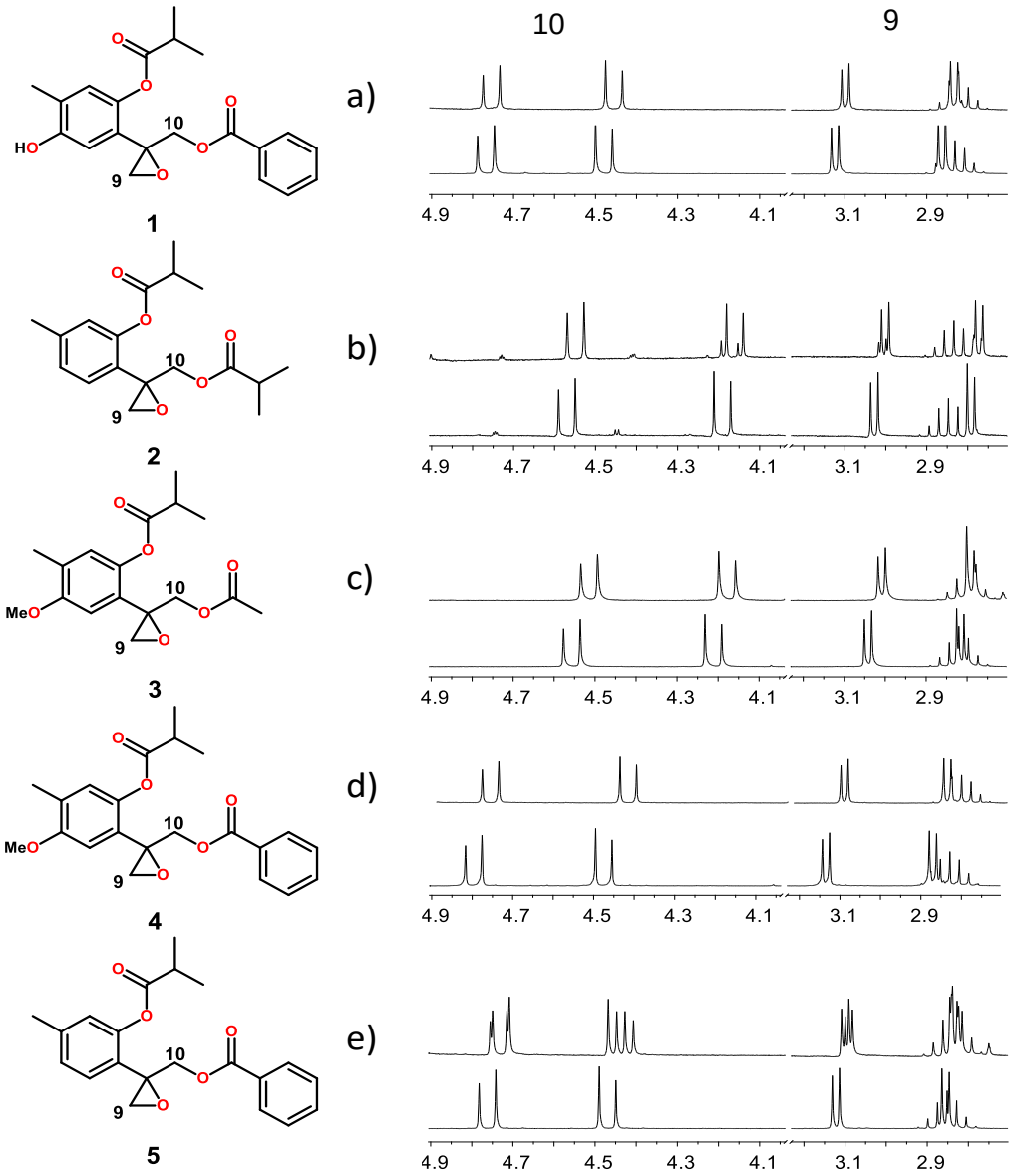

Figura 18. Comparación entre los espectros de RMN de ^{1}H de los epoxitimoles **1**-**5** (trazos inferiores) y aquellos donde se adicionó BINOL (trazos superiores) mostrando las proporciones escalémicas de (a) **1** 100:0; (b) **2** 75:25; (d) **3** 100:0; y (e) **4** 100:0; (c) **5** 56:44.

8.3 Determinación de la configuración absoluta por DCV

Se decidió llevar a cabo la determinación de la CA de derivados de timol por DCV siguiendo la metodología descrita por Bustos-Brito en 2014. Se modeló el enantiómero (*S*)-**1** (figura 19) en el programa Spartan´04. Posteriormente, se realizó una búsqueda conformacional empleando el protocolo Monte Carlo

obteniendo 139 confórmeros en un rango de energía relativa entre 0-9.62314891 kcal/mol.

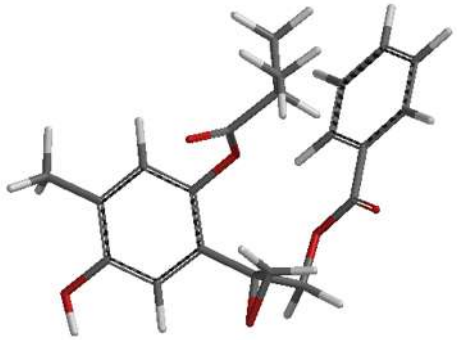

Figura 19. Confórmero de mínima energía y mayor contribución poblacional mediante el método MMFF de (*S*)-**1**.

Posteriormente, se optimizaron las energías de los 139 confórmeros con un nivel de teoría DFT B3LYP/6-31G**, aquellos confórmeros en el rango de 0-3 kcal/mol (109 confórmeros) fueron sometidos a una optimización de la geometría mediante DFT al nivel PBEPBE/DGDZVP y se seleccionaron los confórmeros en el rango de 0-2 kcal/mol y se emplearon para calcular los espectros de DCV e IR_{DCV} al mismo nivel de teoría. La comparación estadística de los espectros calculados y experimentales empleando el algoritmo Compare*VOA* indicó una pobre similitud espectral. Para solucionar este inconveniente, se realizó una búsqueda sistemática de posibles confórmeros faltantes. Esto se llevó a cabo a partir de un análisis de los ángulos diedros de enlaces con libre giro, lo que condujo a la incorporación de 13 confórmeros faltantes. Con esta incorporación, el análisis estadístico de los espectros experimentales contra los espectros calculados por compare*VOA*, mostró una buena similitud espectral para el enantiómero correcto (Figura 20) y un nivel de confianza del 100%, (tabla 2), sus datos termoquímicos pueden apreciarse en el anexo 1. Su CA se estableció como (+)-(8*S*)-Isobutirato de 10-benzoiloxi-6-hidroxi-8,9-epoxitimol (**1**).

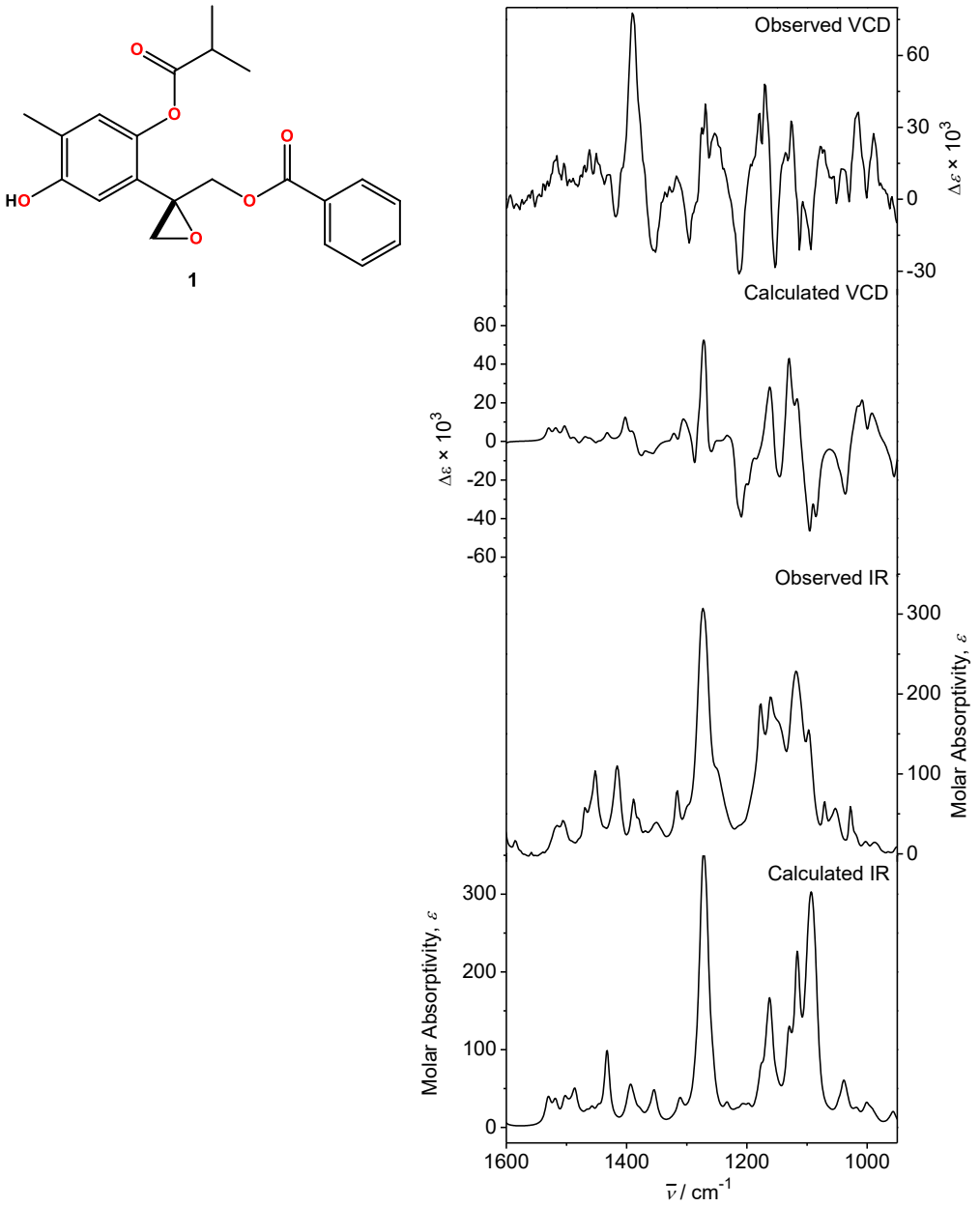

Figura 20. Comparación de los espectros experimentales y calculados de IR y DCV en PBEPBE/DGDZVP de (+)-(8*S*)-Isobutirato de10-benzoiloxi-6-hidroxi-8,9-epoxitimol (**1**).

La ausencia de algunos confórmeros en el epoxitimol **1** generó incertidumbre en cuanto a la eficiencia del método de Monte Carlo ya que se observaron diferentes resultados al utilizar modelos de partida diferentes, este factor fue asociado con las barreras energéticas presentes en la estructura molecular, las cuales fueron observables con un análisis rotacional realizado a los derivados **3** y **4** empleando el programa PCModel 7.0. Dichas barreras

rotacionales (>10 kcal/mol) se ubicaron en los ángulos diedros C-3−O-3−C-1´−C-2´ y C-4−C-8−C-10−0-10 (Figura 21). Con base en este análisis se determinó el uso de cuatro modelos de partida para el análisis de **3** y **4** como estrategia para disminuir la probabilidad de omisión de confórmeros imprescindibles para el estudio.

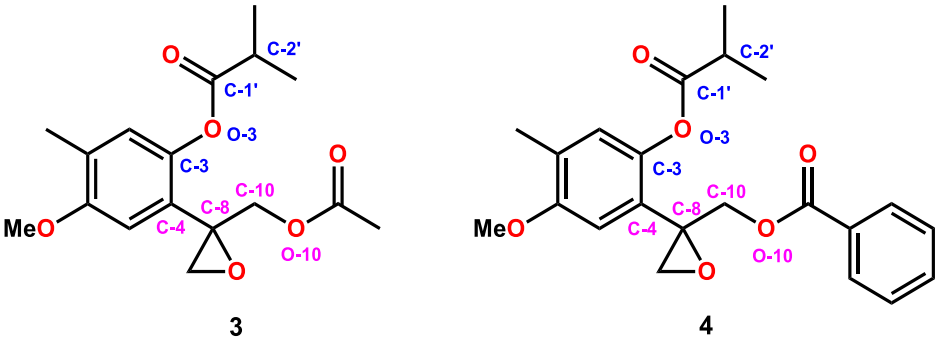

Figura 21. Análisis de ángulos diedros de **3** y **4**.

Para el epoxitimol **3** se obtuvieron 20 confórmeros con el protocolo de Monte Carlo; Posteriormente, sus energías se optimizaron en DFT B3LYP/6-31G**, los confórmeros en el rango de las 0-3 kcal/mol fueron depurados con base en sus energías libres y ángulos diedros para posteriormente optimizar su geometría con DFT PBEPBE/DGDZVP. Finalmente, aquellos confórmeros en el rango de las 0-2 kcal/mol fueron empleados para generar los espectros calculados de IR y DCV mediante DFT PBEPBE/DGDZVP (Tabla 1). La comparación estadística de los espectros calculados y experimentales de DCV e IR_{DCV} (Figura 22) mostraron valores de nivel de confianza en Compare*VOA* del 100% para el enantiómero correcto y su CA se estableció como (+)-(8*S*)-Isobutirato de 10-acetoxi-6-metoxi-8,9-epoxitimol (**3**).

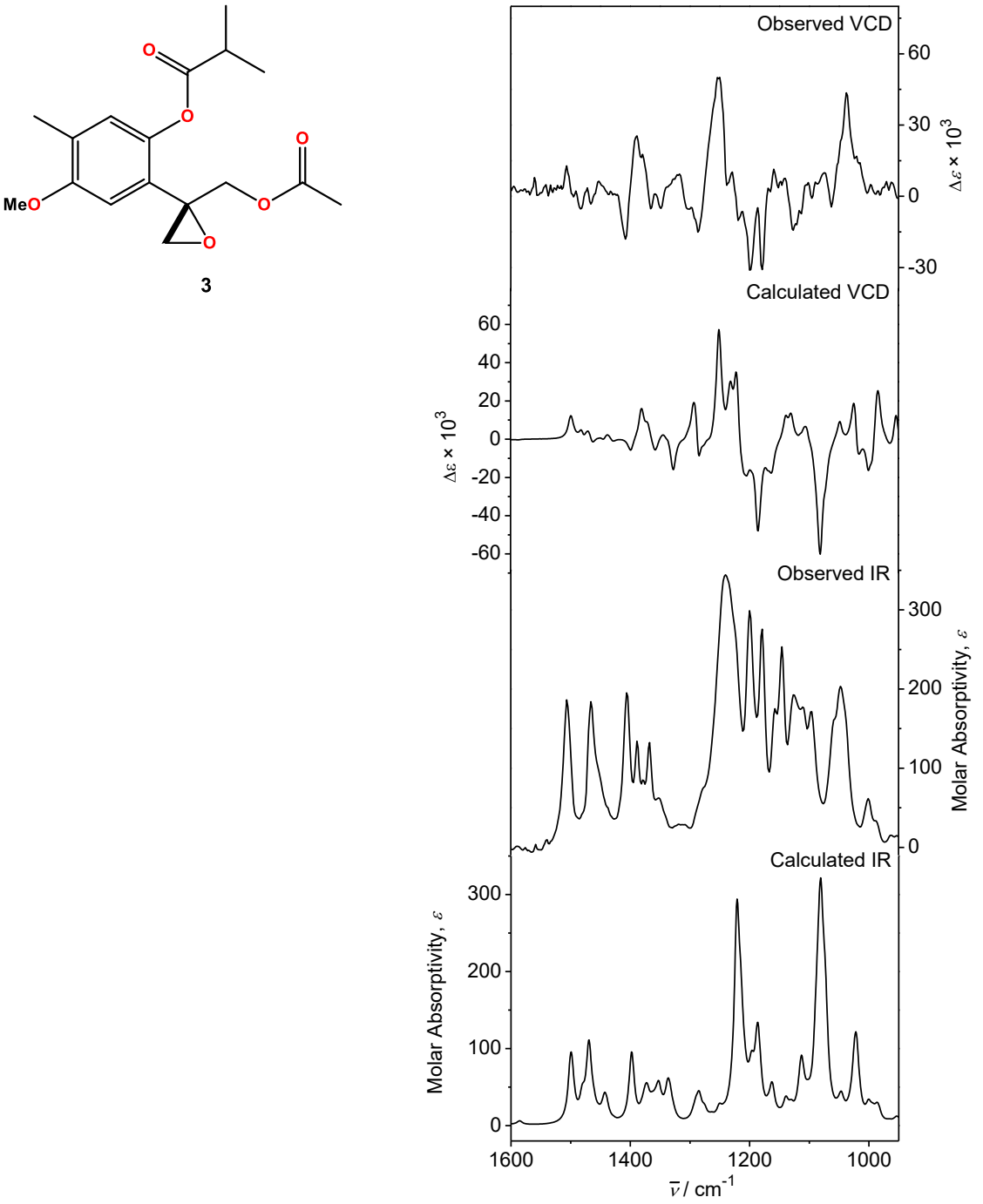

Figura 22. Comparación de los espectros experimentales y calculados de IR y DCV en PBEPBE/DGDZVP de (+)-(8*S*)-Isobutirato de10-acetoxi-6-metoxi-8,9-epoxitimol (**3**).

El análisis de la CA del compuesto **4** se llevó a cabo bajo la misma metodología empleada para **3** (Tabla 1). Los espectros calculados de DCV e IR_{DCV} comparados con los experimentales en el algoritmo estadístico

Compare*VOA* arrojaron un nivel de confianza del 100% (Tabla 2) para el (+)-(8*S*)-Isobutirato de 10-benzoiloxi-6-metoxi-8,9-epoxitimol (**4**) (Figura 23).

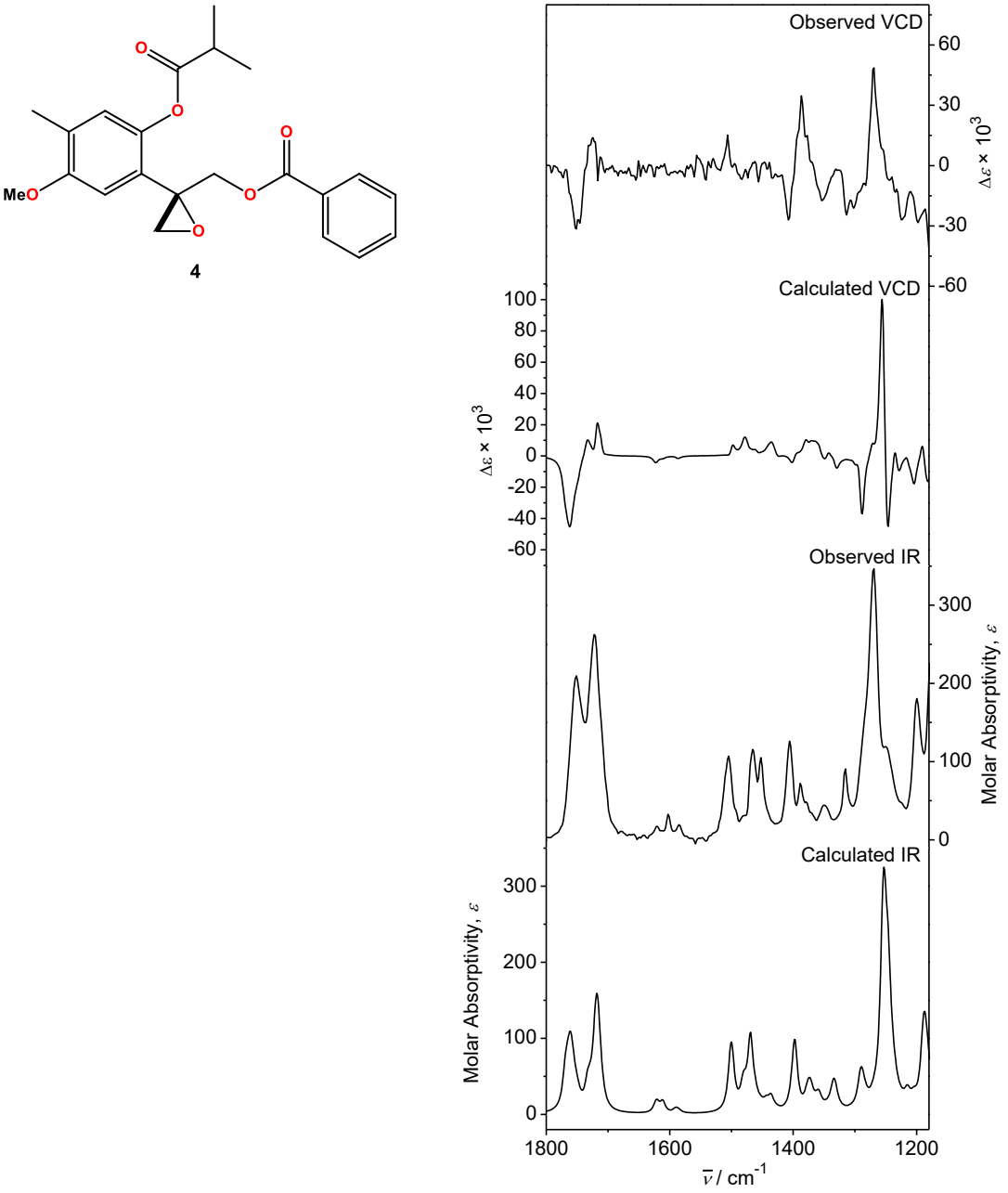

Figura 23. Comparación de los espectros experimentales y calculados de IR y DCV en PBEPBE/DGDZVP para (+)-(8*S*)-Isobutirato de 10-benzoiloxi-6-metoxi-8,9-epoxitimol (**4**).

La efectividad de la técnica sugerida para la determinación de la CA fue validada, por lo que se empleó para determinar la CA del enantiómero **2** mayoritario de la mezcla escalémica con un *e.e.* del 50%. En la tabla 1 se resume

la metodología empleada. La comparación estadística de los espectros ponderados DCV e IR_{DCV} contra los correspondientes experimentales en Compare*VOA* dio un nivel de confianza del 100% al considerar el rango de frecuencias de 1000 a 1400 cm^{-1}, que corresponde a la región de las bandas con mayor intensidad (Figura 24). La CA se determinó como (+)-(8*S*)-Isobutirato de 10-Isobutiriloxi-8,9-epoxitimol (**2**). Con base en estos resultados, puede establecerse que la técnica propuesta para determinar la CA de epoxitimoles puede emplearse para mezclas racémicas con exceso enantiomérico del 50% o mayores.

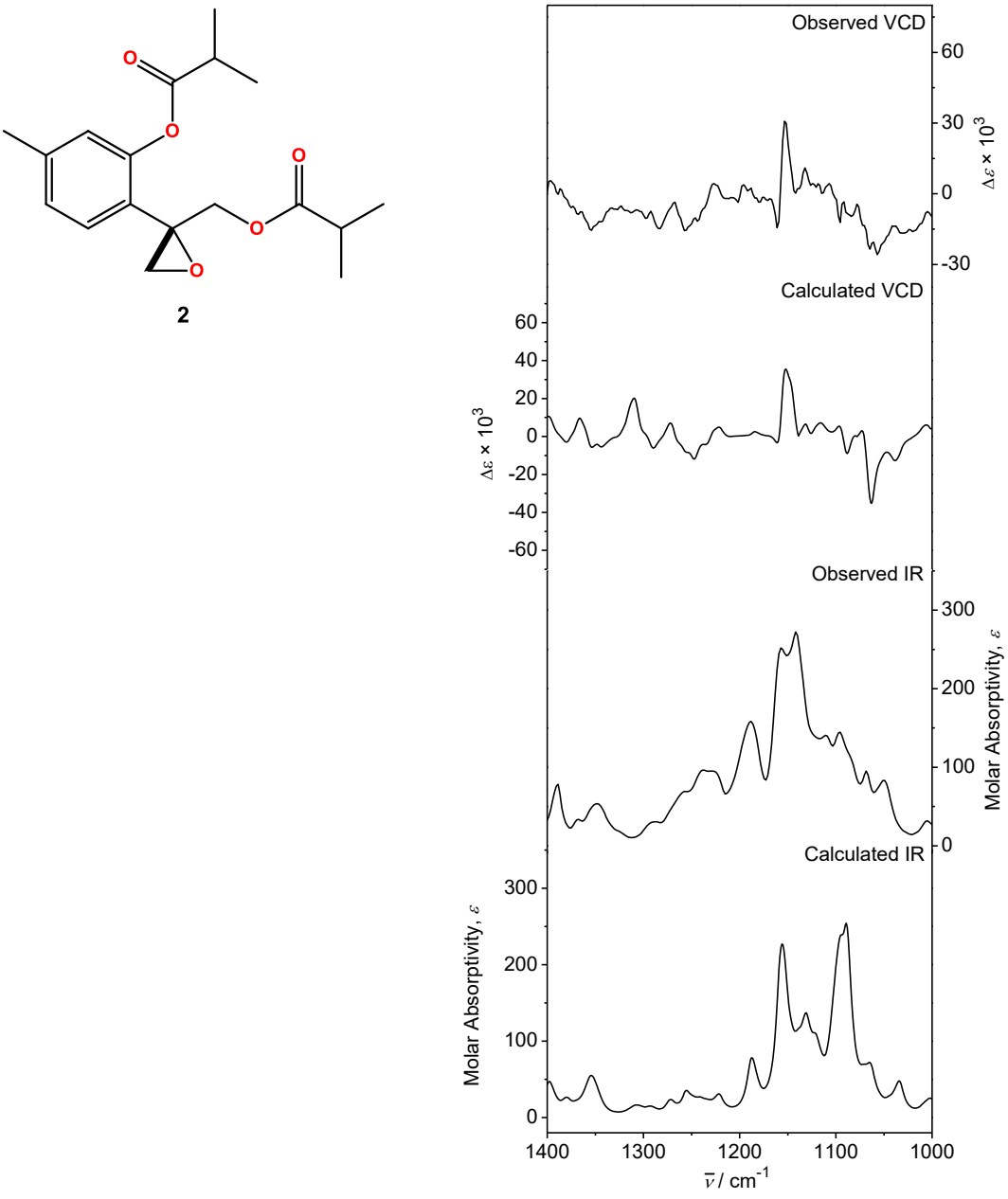

Figura 24. Comparación de los espectros experimentales y calculados de IR y DCV en PBEPBE/DGDZVP para (+)-(8*S*)-Isobutirato de 10-Isobutiriloxi-8,9-epoxitimol (**2**).

Es importante mencionar que el epoxitimol **2** se encuentra reportado en cerca de la mitad de las especies vegetales que contienen epoxitimoles (Talavera, 2016), por lo que, con la determinación de la CA de este epoxitimol, la CA de todos los derivados de timol presentes en tales especies vegetales podría ser inferida.

En los anexos **1**-**4**, se resumen los datos correspondientes a los análisis termoquímicos de los epoxitimoles **1**-**4**.

Tabla 1. Número de confórmeros encontrados en los diferentes niveles de cálculo empleados en la metodología.

	MMFF				DFT B3LYP/6-31G**	DFT PBEPBE/DGDZVP
	I	II	III	IV	(0-3kcal/mol)	(0-2kcal/mol)
1	139[a]				109	31
2	100	100	100	100	105	48
3	68	86	79	81	64	20
4	90	83	78	61	62	49

[a]Confórmeros obtenidos a partir de un solo cálculo de MMFF.

Tabla 2. Nivel de confianza para los espectros de IR y DCV de **1**-**5** calculados con el nivel de teoría PBEPBE/DGDZVP.

Compuesto	*anH*[a]	S_{IR}[b]	S_E[c]	S_{-E}[d]	ESI[e]	*C*[f]
1	1.020	90.9	70.9	17.3	53.5	100
2	1.014	89.6	73.2	23.7	49.5	100
3	1.009	80.7	71.5	11.8	59.7	100
4	1.000	84.7	71.2	19.2	51.9	100

[a]Factor de anharmonicidad. [b]IR similitud espectral. [c]VCD similitud espectral para el enantiómero correcto. [d]VCD similitud espectral para el enantiómero incorrecto. [e]Índice de similitud enantiomérica calculada como $S_E - S_{-E}$. [f]Nivel de confianza en porcentaje para las asignaciones configuracionales.

8.4 Reacciones de racemización/escalemización

Una vez que la presencia de mezclas escalémicas en **2** y **3** fue demostrada fue conveniente evaluar la capacidad de racemización de los epoxitimoles. Para este ensayo se eligió al epoxitimol **1**, ya que este es aislado en buenos rendimientos y posee pureza enantiomérica (Figura 25a). Tres alícuotas de **1** fueron calentadas bajo reflujo de benceno en presencia de gel de sílice como catalizador heterogéneo, usando una trampa de Dean Stark durante 2, 4 y 6 h. Los productos del crudo de reacción fueron purificados por

cromatografía en columna y analizados por ^{1}H-BINOL-RMN revelando una escalemización gradual relacionada directamente con el tiempo de reacción. Después de 2 h de reacción (figura 25b) se observó la presencia de una mezcla escalémica 90:10 (*e.e.* 80%), después de 4 h (figura 25c) de tratamiento esta proporción se modificó a un 87:13 (*e.e.* 74%); y después de 6 h de reacción (figura 25d), la proporción escalémica se incrementó a un 75:25 (*e.e.* 50%). Este experimento sugirió la susceptibilidad química de estos compuestos a la racemización (Figura 25).

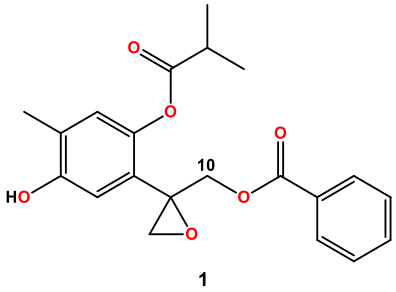

1

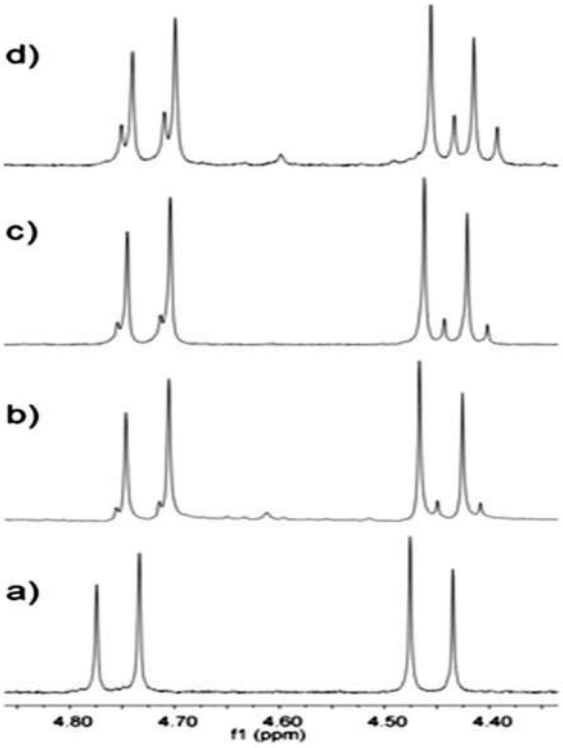

Figura 25. Relación enantiomérica de las reacciones de escalemización del epoxitimol **1** evaluado por la metodología ^{1}H-BINOL-RMN. a) Determinación a las 0 h (100:0), b) 2 h (90:10), c) 4 h (87:13) y d) 6 h (75:25).

Un mecanismo intermolecular concertado fue propuesto para justificar la escalemización del epoxitimol **1** (Figura 26), en el cual se lleva a cabo un ataque nucleofílico del oxígeno O-8 del anillo de epóxido al carbono C–1´´ de carbonilo, que promueve la trasferencia del grupo acilo, con la consecuente ruptura del enlace C-8–O-8 y la formación del enlace O-10–C-8 de manera concertada. Si este mecanismo es reversible el proceso podría generar ambos enantiómeros

hasta alcanzar un equilibrio racémico, pasando a través de proporciones escalémicas durante el tiempo de reacción.

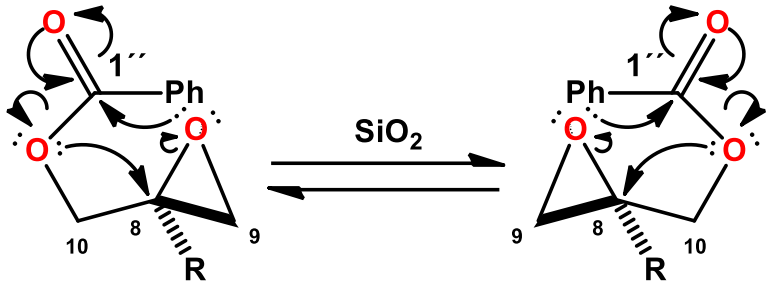

(8*S*)-**1** (8*R*)-**1**

Figura 26. Mecanismo de reacción concertado propuesto para la escalemización del epoxitimol **1**.

8.5 Reacción de transesterificación

En el curso de estos experimentos se detectó un subproducto, este mostró los datos idénticos al isobutirato de 10-benzoiloxi-9-isobutiriloxi-6,8-dihidroxitimol (**37**), descrito previamente por nuestro grupo de trabajo (Arreaga *et al*, 2015). Basados en los datos arrojados por el análisis de RMN de 1D y 2D de este compuesto, por las apreciaciones realizadas recientemente por Bustos-Brito en 2016, se llevó a cabo la revisión de la conectividad de esta estructura y se corrigió como isobutirato de 10-benzoiloxi-9-isobutiriloxi-6,8-dihidroxitimol (**6**) (Figura 27). En este caso, la apertura del anillo puede ser posible por el ataque de una molécula de H_2O al C-8 tras la ruptura concertada del enlace C-8–O-8 y la transesterificación del residuo de isobutirato de O-3 a O-9, como fue sugerida por Bohlmann *et al* en 1969.

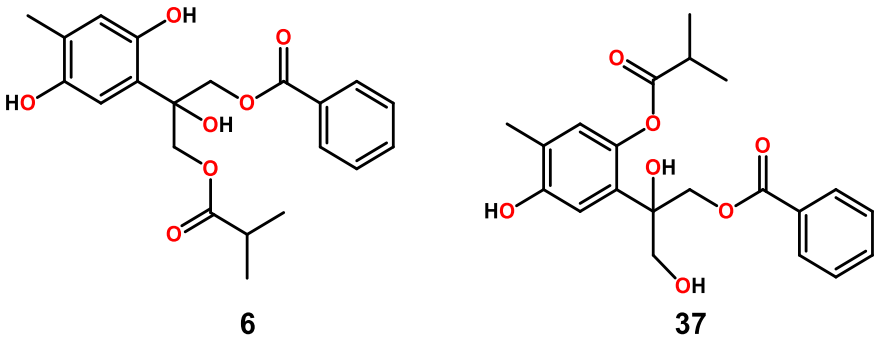

6 **37**

Figura 27. Derivados de timol **6** y **37**.

8.6 Aislamiento del epoxitimol 7 de *Piptotrhrix areolare*

P. areolare se colectó el 14 de octubre de 2017 en el km 32.5 de la carretera Villa Madero-Tacámbaro; posteriormente, se secó a la sombra por dos semanas, se separó en sus diferentes partes (raíces, tallos, hojas y flores), transcurrido este periodo se realizaron macerados de las diferentes partes en disolventes orgánicos en polaridad ascendente (hexanos, acetato de etilo y metanol) por triplicado en periodos de tres días.

Un lote de 520 mg del extracto hexánico de raíces se sometió a cromatografía empleando gel de sílice como fase estacionaria y mezclas de hexanos-AcOEt en polaridad ascendente como fase móvil. Las fracciones obtenidas fueron monitoreadas por cromatografía en capa fina. En la polaridad hexanos- AcOEt (7:3) se obtuvieron 22 mg de una miel amarilla, en su espectro de RMN de ^{1}H (Figura 28) se observó en 9.90 ppm la señal para el hidrógeno H-11 correspondiente a un protón de aldehído, entre 7.8 y 7.50 ppm se observan tres señales de hidrógenos aromáticos cuyas constantes de acoplamiento siguieren la triple sustitución, mientras que entre 7.50 y 7.25 ppm se localizan dos señales múltiples, la integración de estas señales indica la presencia de cinco hidrógenos, además se observaron dos señales dobles en 7.70 y 6.25 ppm entre 4.75 y 1.25 ppm se localizaron las señales típicas de un derivado de timol epoxidado, por lo que el análisis de las señales sugiere la presencia de un éster de cinamato en la posición C-10, un isobutirato en C-3 y un aldehído en C-1. Mientras que en su espectro de RMN de ^{13}C se observan entre 190 y 165 ppm las tres señales correspondientes a los carbonilos C-1´´´, C-1´ y C-1´´, alrededor de 142.5 y 116.0 se ubicaron las señales para los carbonos de doble enlace C-2´´ y C-3´´, lo que confirma la presencia del grupo cinamato, entre 150.0 y 115.0 ppm se localizaron las señales de carbonos aromáticos y finalmente entre 4.7 y 1.0 ppm las señales típicas de la porción alifática. Los experimentos de 2D permitieron corroborar la asignación de esta estructura. Este derivado fue aislado anteriormente de *P. areolare* por Hernández *et al* en 1986, con base en sus desplazamientos de RMN de ^{1}H como isobutirato de 10-cinamoiloxi-7-oxo-8,9-epoxitimol.

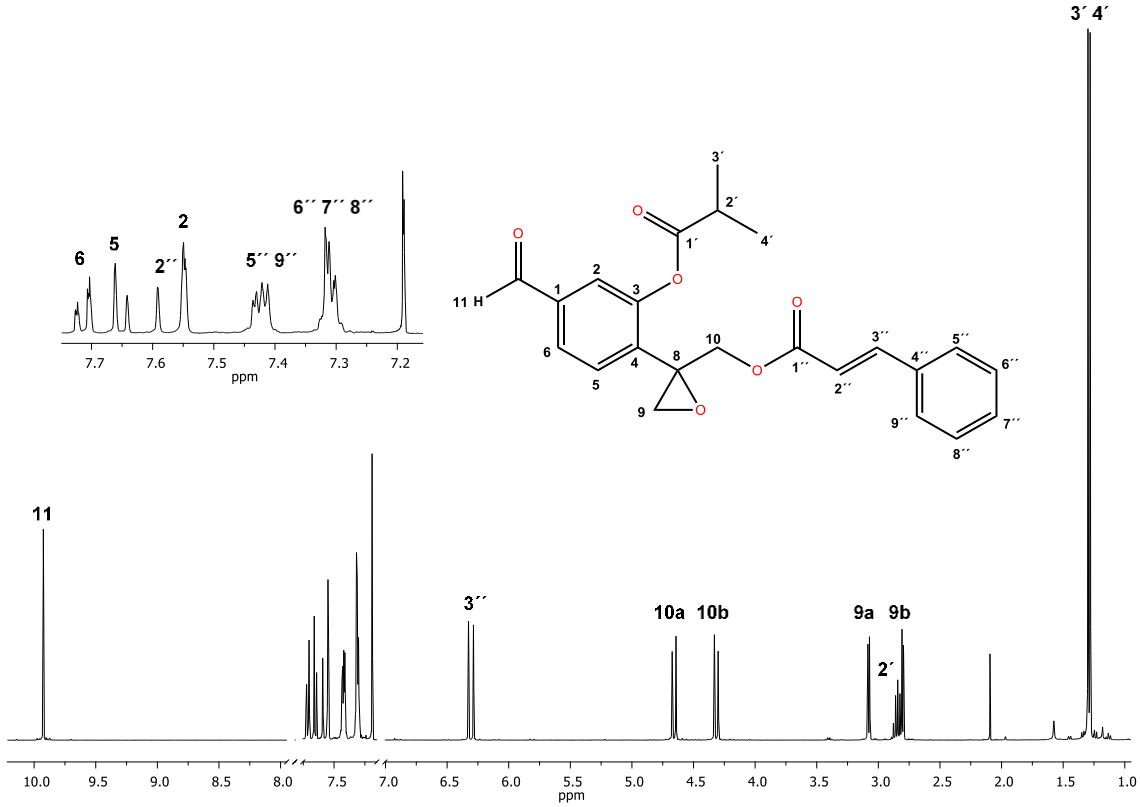

Figura 28. Espectro de RMN de ^{1}H a 400 MHz en $CDCl_3$ del epoxitimol **7**.

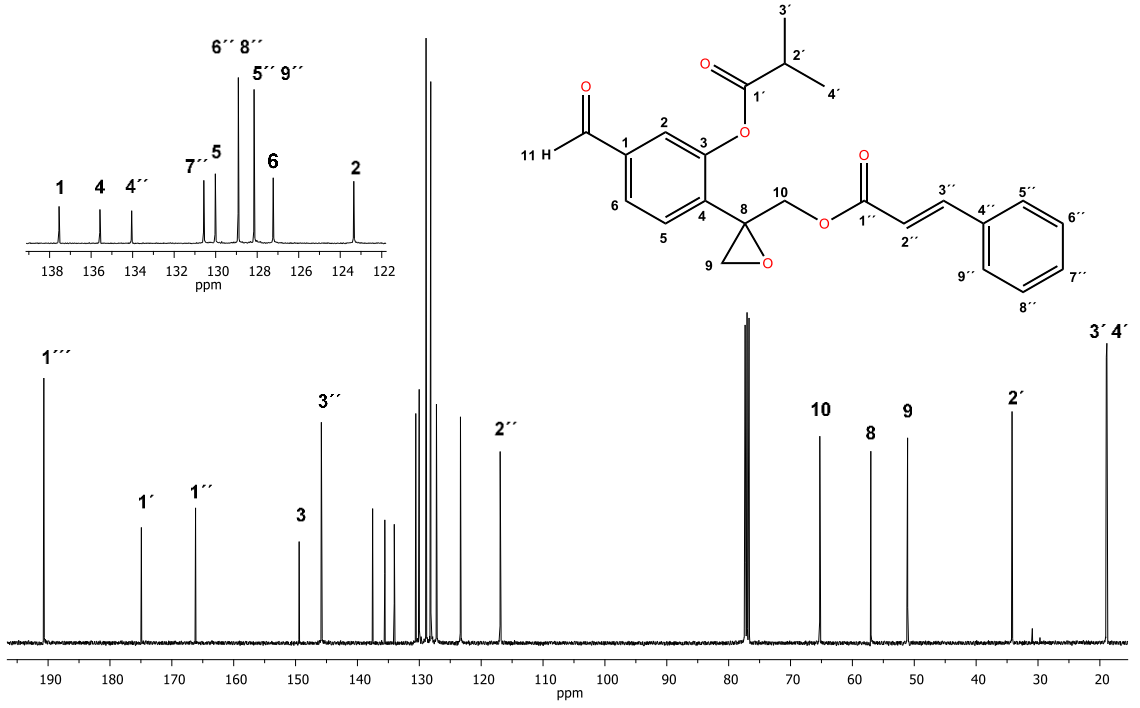

Figura 29. Espectro de RMN de ^{13}C a 100 MHz en $CDCl_3$ del epoxitimol **7**.

8.7 Estudio estacional

El epoxitimol **7** fue reportado previamente por Hernández *et al* en 1986, con nula rotación especifica. Partiendo de este antecedente y de los resultados obtenidos con los epoxitimoles de *A. glabrata*, se decidió valorar el estatus de la pureza óptica susceptibilidad a escalemizarse de forma natural o en los procesos de extracción y almacenaje (Bohlmann, 1966, Tori, 2001). Cabe resaltar que **7** se extrae en buenos rendimientos de las raíces de *P. areolare*.

P. areolare se colectó en periodos de dos semanas del 26 de marzo de 2017 al 26 de junio de 2018 en el kilómetro 32.5 de la carretera Villa Madero-Tacámbaro, como puede apreciarse en la figura 34, *P. areolare* muestra un ciclo anual que coincide con las estaciones anuales ya que en primavera (marzo-junio) el índice de hojas muertas sobrepasa el 50%, mientras que en los meses de verano (junio-septiembre) la defoliación es total con incluso la desaparición total de los tallos, por otro lado, durante el otoño (septiembre- diciembre) los tallos y hojas se desarrollan nuevamente, resaltando que el periodo de floración se da a inicios del mes de noviembre y dura aproximadamente tres semanas, finalmente durante la etapa invernal (diciembre-marzo) la planta muestra un abundante follaje que conserva hasta los inicios del mes de marzo (figura 30).

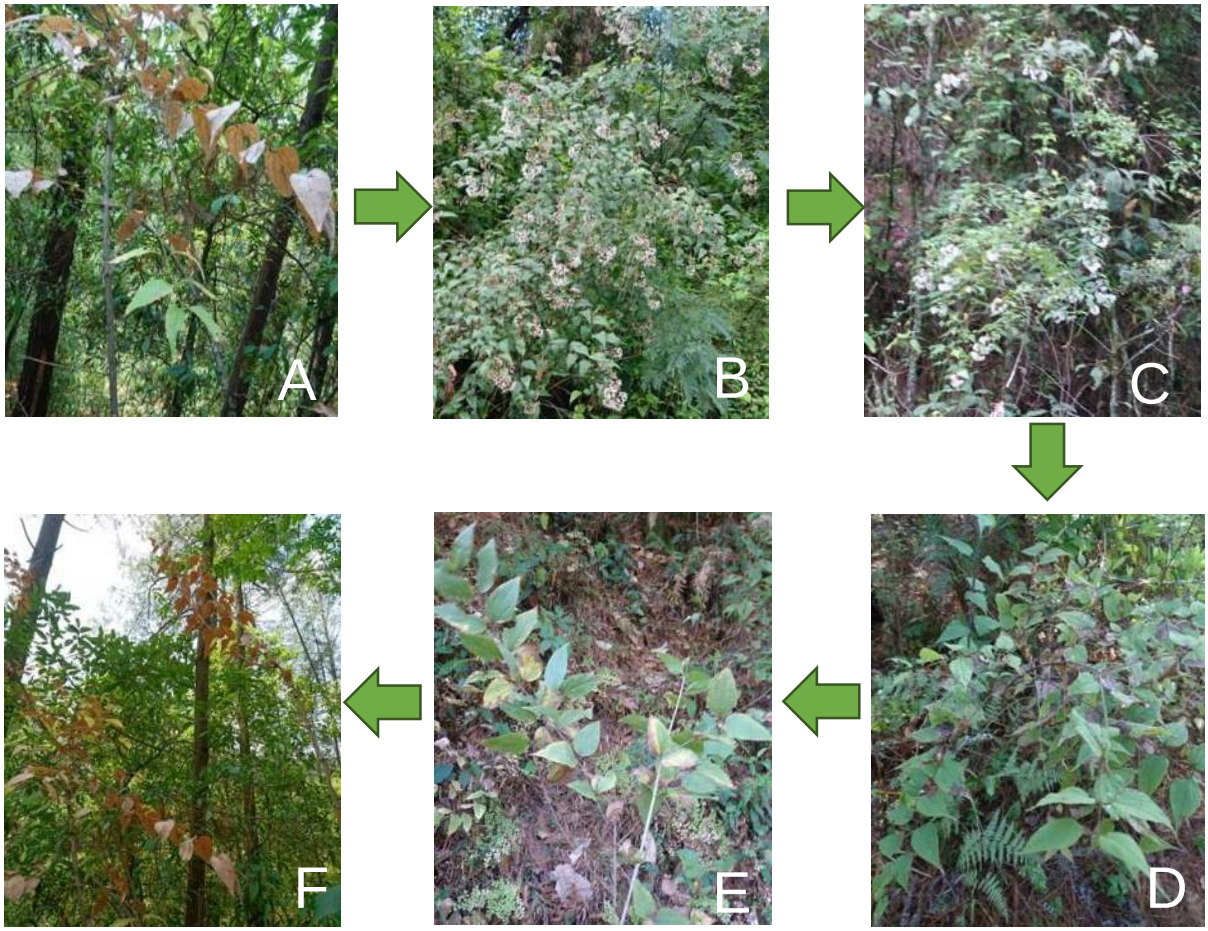

Figura 30. Colectas de *P. areolare* A) mayo de 2017, B) septiembre de 2017, C) noviembre de 2017, D) enero de 2018, E) marzo de 2018, F) mayo de 2018.

En cada periodo se colectaron las raíces de un espécimen, que se dejaron secar a la sombra por tres días, posteriormente se trituraron y se maceraron en hexanos por tres días, el macerado se filtró y se evaporó a presión reducida en rotavapor, el extracto se impregnó en gel de sílice y se sometió a cromatografía en fase directa, se corroboró la purificación del epoxitimol **7** por RMN de ^{1}H, se determinó su grado de escalemización por RMN de ^{1}H y BINOL y se obtuvo su valor de rotación específica en cada muestra colectada, en la tabla 3 se detallan los valores obtenidos. En todos los casos, el método de purificación de **7** fue igual para descartar alteraciones de *e.e*. por metodologías de extracción.

Tabla 3. Valores de rotación específica y exceso enantiomérico de **7**.

Colecta	Fecha	Rotación específica	*e.e.*
1	26/03/17	-3.2	54
2	30/04/17	-2.9	50
3	22/05/17	-1.0	32
4	31/05/17	-3.6	68
5	13/06/17	-1.7	36
6	30/06/17	-3.8	68
7	14/07/17	-3.5	58
8	30/07/17	-3.4	46
9	15/08/17	-5.0	84
10	30/08/17	-5.0	86
11	14/09/17	-4.7	86
12	12/11/17	-5.8	84
13	27/11/17	-4.0	46
14	23/12/17	-1.3	26
15	07/01/18	-3.6	86
16	21/01/18	-4.6	88
17	03/02/18	-1.6	32
18	18/02/18	-2.6	50
19	18/03/18	-4.1	64
20	29/03/18	1.8	-32
21	15/04/18	-1.5	22
22	27/04/18	-5.5	82
23	13/05/18	2.0	84
24	26/05/18	-5.8	84

En la gráfica 31d, se puede observar que la relación enantiomérica no muestra una tendencia a lo largo del año; sin embargo, se puede apreciar que en los meses de agosto a noviembre de 2017 el grado de escalemización alcanza la estabilidad más prolongada observándose una exceso enantiomérico promedio de 86%, este dato coincide con el periodo de floración de la planta, por otro lado la escalemización con un valor más alto se observó en el 21 de enero de 2018 con un exceso enantiomérico de 88%, estos valores tienen concordancia con los valores de rotación especifica de las mismas fechas, mientras que el valor mínimo se observó en la colecta correspondiente al 29 de marzo de 2018 donde la relación enantiomérica es inversa, generándose de forma más abundante el enantiómero opuesto con un exceso enantiomérico del 32%, y en resto del año se observan diferencias significativas en cada periodo de colecta.

Continuando con el análisis estacional, se procedió a realizar una búsqueda de los parámetros climáticos presentes en el municipio de Madero y adyacentes en el periodo 2017- 2018, estos datos fueron obtenidos a través de las normales climatológicas proporcionadas por de Comisión Nacional del Agua (CONAGUA). Cabe resaltar que las estaciones climatológicas más próximas al sitio de colecta no están actualmente en funcionamiento, pero los datos históricos permitieron observar que el clima de la región es igual al de Morelia, los cuales se emplearon para este análisis. Los valores de temperatura máxima en la gráfica 31a se aprecian que el pico más alto se encuentra en el 22 de junio de 2017 con 35.3 °C y el mínimo en el 30 de agosto de 2017 con 25.0 °C, por lo que el promedio de temperatura máxima oscila alrededor de los 30.2 °C. Con base en lo anterior se puede inferir que el clima de la región es templado.

En cuanto a la temperatura mínima se observa en la gráfica 31b que el pico más alto se registró el 22 de junio de 2017 con 17.1 °C, mientras que el mínimo se observó el 21 de enero de 2018 con 5.2 °C, en el resto del año la temperatura mínima oscila en los 11 °C.

Con el análisis de las temperaturas máximas y mínimas se obtuvieron los valores correspondientes a la temperatura media que se observan en la gráfica 31c, estos valores se compararon con los observados en la gráfica 31d que corresponde al exceso enantiomérico, donde se puede observar que si bien existen fluctuaciones a lo largo del año, estás son consistentes en ambas gráficas ya que muestran tendencias semejantes de fluctuación, por lo cual se puede proponer que la escalemización de **7** está estrechamente relacionada con los cambios en la temperatura, ya que se observó que si esta muestra un incremento o disminución, el exceso enantiomérico de **7** puede tender tanto a la pureza enantiomérica como a la racemización; y por otro lado, cuando la temperatura se encuentra en el rango promedio (21 °C) el exceso enantiomérico se mantiene en un promedio del 86%. Con base en estos resultados se puede sugerir que el epoxitimol **7** podría cumplir una función protectora y/o regulatoria en *P. areo*lare frente a los cambios de temperatura.

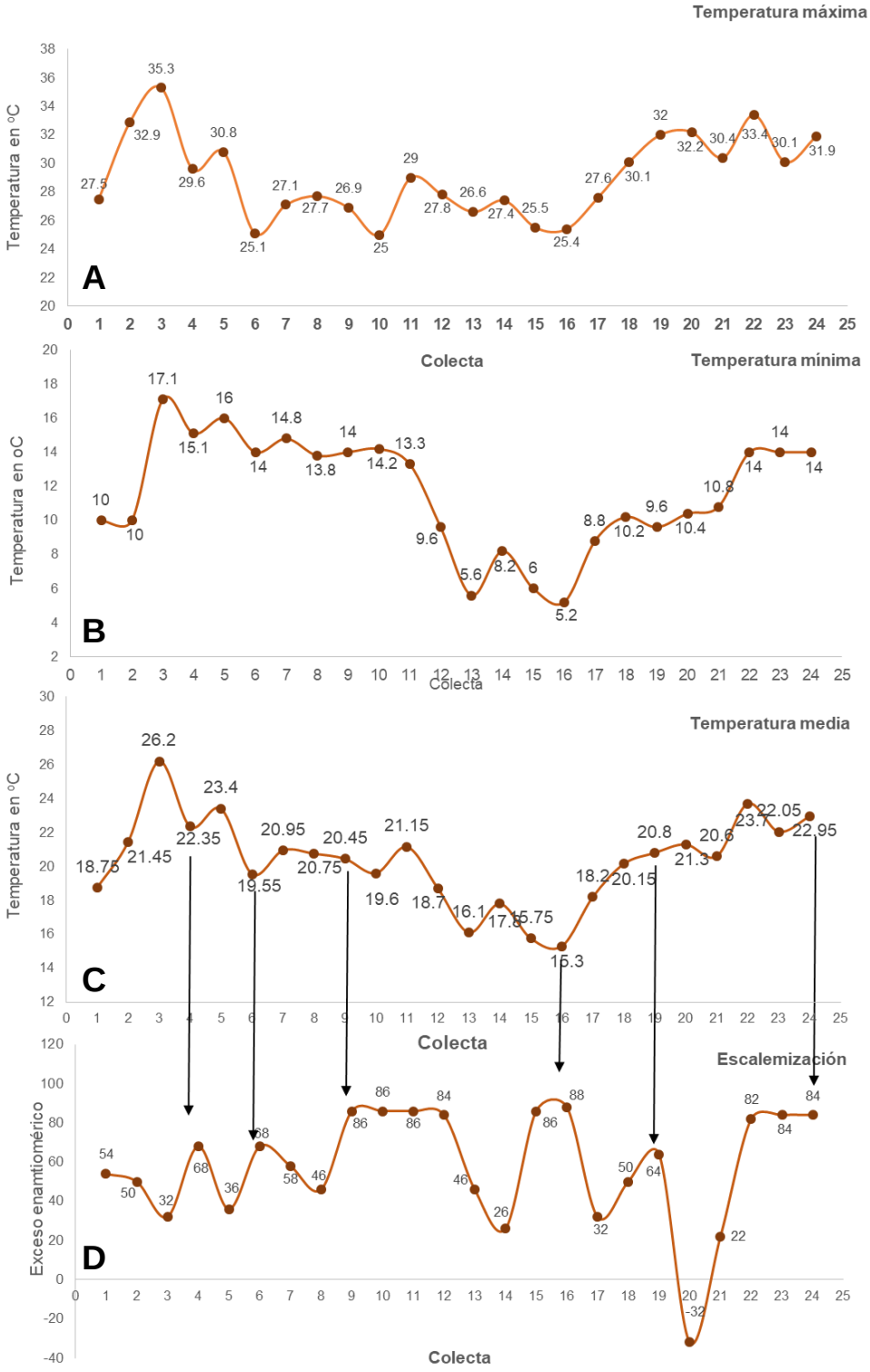

Figura 31. 31a) Valores de temperatura máxima en Morelia de 2017 a 2018, 31b) Valores de temperatura mínima en Morelia de 2017 a 2018, 31c) Valores de temperatura media en Morelia de 2017 a 2018, 31d) Valores de exceso enantiomérico de **7** observados.

8.8 Determinación de la CA de areolal aislado de *Piptothrix areolare*

Basados en la metodología descrita recientemente para la determinación de la CA por DCV (Arreaga *et al*, 2018) donde se dejó de manifiesto que se puede determinar la configuración de un derivado de timol por DCV aun cuando este se presente como mezcla escalémica, se decidió determinar la CA del epoxitimol mayoritario aislado de *P. areolare* **7** partiendo de la muestra que mostró un mayor exceso enantiomérico durante el estudio estacional. Se inició con la construcción de los cuatro modelos de partida; posteriormente, se llevó a cabo el cálculo de distribución conformacional por el método de Monte Carlo. A los confórmeros obtenidos se les optimizó la energía en un nivel de teoría B3LYP-631G(d). De este cálculo, se obtuvieron 83 confórmeros en el rango de 0-2 kcal/mol, los cuales fueron optimizados en energía y geometría a un nivel de teoría DFT PBEPBE/DGDZVP. Con base en la comparación de sus energías y ángulos diedros, fue depurada la lista de confórmeros para obtener una población de 60 confórmeros. Finalmente con las energías y frecuencias de estos se obtuvieron sus espectros teóricos de IR y DCV, los espectros teóricos y experimentales se compararon en el algoritmo compare*VOA*, para esta comparación se aplicó un factor de anharmonicidad de 1.023, el índice de similitud espectral del IR fue del 85.2%, el porcentaje de similitud espectral en DCV para el enantiómero correcto fue de 74.1% mientras que para el enantiómero incorrecto fue del 25.9%, finalmente el nivel de confianza para las asignaciones configuracionales fue del 100%, por lo que se concluyó que la CA del centro estereogénico C-8 es (*S*) y el epoxitimol **7** se define como (-)(8*S*)-isobutirato de 10-cinamoiloxi-7-oxo-8,9-epoxitimol (figura 31), sus datos termoquímicos pueden apreciarse en el anexo 5.

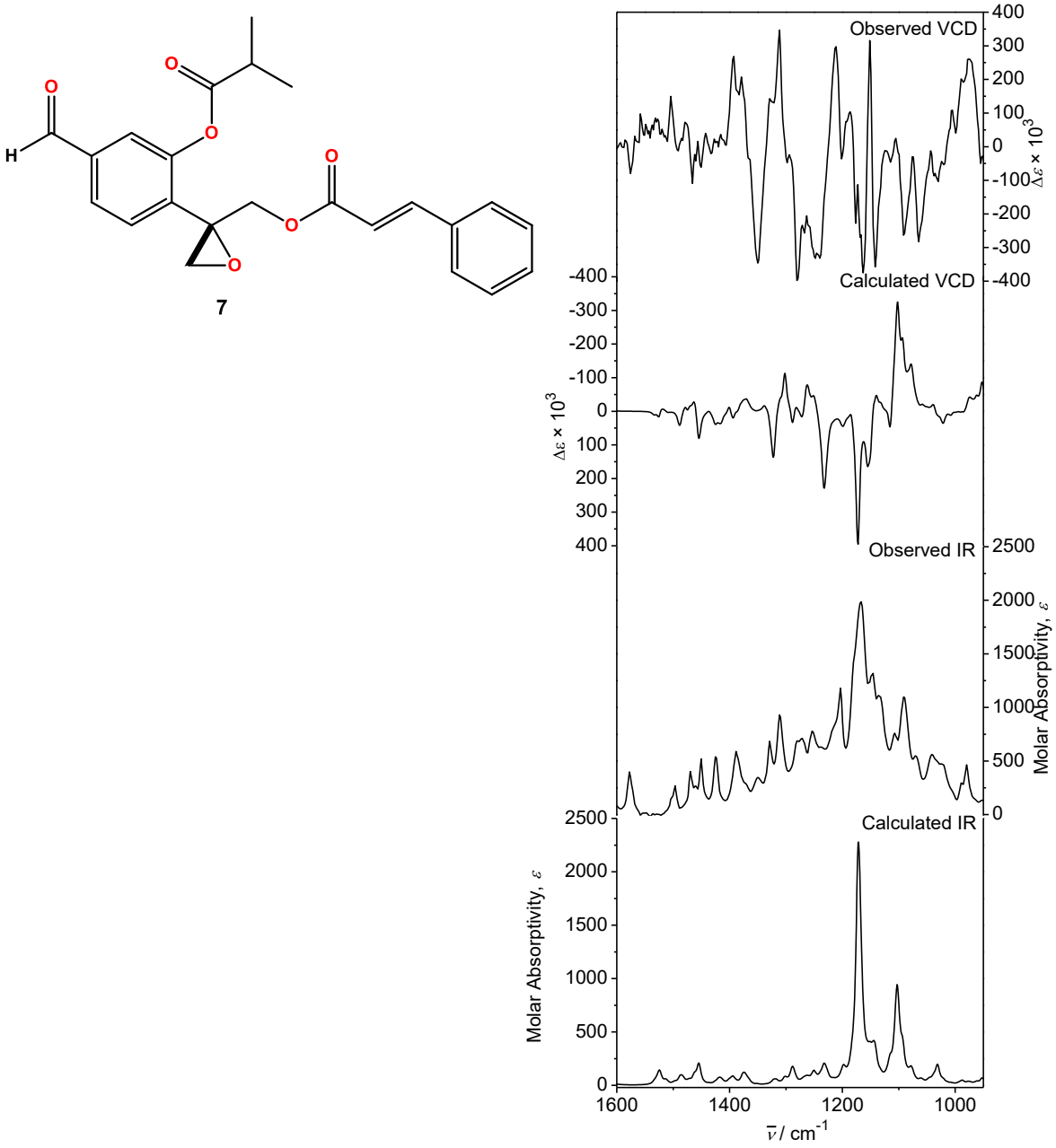

Figura 31. Comparación de los espectros experimentales y calculados de IR y DCV en PBEPBE/DGDZVP para (+)-(8*S*)-Isobutirato de 10-cinamoiloxi-7-oxo-8,9-epoxitimol (**7**).

9 CONCLUSIONES

- La pureza enantiomérica de los epoxitimoles **1**-**5** fue determinada con el uso de (*S*)-BINOL como reactivo de solvatación quiral y RMN de ^{1}H observando que derivados obtenidos de la misma especie vegetal pueden existir como mezclas racémicas y/o escalémicas.
- La capacidad de racemización/escalemización de los epoxitimoles en condiciones de reacción en medios ácidos es posible y puede seguir dos rutas, por un lado, dar lugar a mezclas racémicas y escalémicas y por otro pueden sufrir transesterificaciones como lo reportaron previamente.
- La metodología de análisis en la búsqueda conformacional de epoxitimoles garantiza la inclusión de los confórmeros de mínima energía para el estudio de la CA por el método de DCV, con esta se determinó la CA de los epoxitimoles **1**-**4**, de *A. glabrata*, resaltando que el derivado **2** existe como mezcla escalémica 75:25 (*R**/*S**), este derivado se encuentra presente en 40 especies vegetales, por lo que la CA de los epoxitimoles presentes en estas especies puede ser inferida por correlación química.
- Anteriormente se demostró que los epoxitimoles pueden sufrir escalemización en medio ácido, basados en el reporte de Hernández en 1986, se decidió retomar el estudio de esta especie, por lo que inicialmente se aisló a **7** de las raíces y se llevó a cabo un estudio estacional, que permitió determinar que la escalemización de forma natural de este derivado está estrechamente relacionado con los cambios en la temperatura de la zona de colecta, por lo que se puede sugerir que **7** podría tener una función de protección frente a los cambios de temperatura.
- Para validar la metodología de CA por DCV en una especie diferente, se determinó la misma del derivado **7**, aislado de *P. areolare*, por lo que esta metodología puede ser aplicada a estructuras análogas y a otro tipo de familias estructurales.

10 PARTE EXPERIMENTAL

Procedimientos generales de experimentación

Los puntos de fusión se obtuvieron mediante el instrumento, Fisher-Johns, no están corregidos. Los valores de rotación especifica se determinaron en $CHCl_3$ en un polarimetro Perkin-Elmer341. Los espectros de UV se registraron en un espectrofotometro Perkin-Elmer Lambda 12. Los espectros de RMN de ^{1}H y ^{13}C se midieron en un equipo Varian Mercury 300 ó 400 MHz para ^{1}H, a 75 o 100 MHz para ^{13}C, respectivamente, usando deuterocloroformo ($CDCl_3$) como disolvente y tetrametilsilano (TMS) como referencia interna. Los desplazamientos se reportaron en ppm, las constantes de acoplamiento (*J*) se reportaron en Hertz (Hz). Para las columnas cromatográficas se empleó gel de sílice de malla 230-400 (Merck).

Materia vegetal

A. glabrata se colectó en febrero de 2015 en la carretera Pátzcuaro-Santa Clara del cobre a 1 km de la desviación a Cuanajo.

P. areolare se colectó en dos tiempos por mes, de marzo de 2017 a junio de 2018 en el km 32.5 de la carretera Villa Madero-Tacámbaro.

Extracción y aislamiento

Las hojas de *A. glabrata* se secaron a la sombra por dos semanas. Posteriormente, se maceraron en CH_2Cl_2 por triplicado en periodos de tres días evaporando el disolvente en rotavapor y obteniendo los correspondientes extractos.

Las raíces de *P. areolare* se secaron por tres días, se trituraron y se maceraron en hexanos por tres días, posteriormente se filtraron los macerados y se concentraron en rotavapor a presión reducida.

Reacciones de escalemización

Tres suspensiones de silica gel (1 g) en benceno (60 mL) se reflujaron por 4 h usando una trampa de Dean-Stark para eliminar la humedad. Las muestras del derivado enantioméricamente puro **1** (100 mg) fueron agregadas a cada sistema y se calentaron hasta reflujo por 2, 4 y 6 h, respectivamente. Los

crudos de reacción se filtraron, evaporaron a presión reducida y se purificaron por columna cromatográfica en fase directa usando mezclas de hexanos-AcOEt en polaridad ascendente.

Determinación de las proporciones escalémicas usando (*S*)-BINOL

La pureza enantiomérica de los derivados de timol fue determinada por espectroscopia de RMN de ^{1}H disolviendo las muestras (6 mg) en 0.7 mL de $CDCl_3$ y adicionando (*S*)-BINOL (Aldrich®) como agente de solvatación quiral, la relación enantiomérica de cada muestra fue obtenida con base en la altura de las señales.

Mediciones de dicroísmo circular vibracional

Los espectros de IR_{DCV} y DCV fueron realizados en un espectrofotómetro BioTools dualPEM Chiral*IR* FT. Cada muestra fue disuelta en $CDCl_3$ 100% deuterocloroformo y colocado en una celda de BaF_2 con una ventana de 100 μm. Los datos de **1**,**3**-**5** y **7** fueron adquiridos a una resolución de 4 cm^{-1} por 6 h cada uno, la línea base fue obtenida restando el espectro del disolvente adquirido bajo las mismas condiciones y la estabilidad de las muestras fue monitoreada por RMN de ^{1}H antes y después de cada medición.

Cálculos de dicroísmo circular vibracional

Los protocolos de Monte Carlo se llevaron a cabo usando los campos de fuerza de la mecánica molecular (MMFF94) como un implemento del programa Spartan´04, las barreras rotacionales fueron identificadas usando el programa PCModel 7.0, las búsquedas de Monte Carlo se llevaron a cabo iniciando con cuatro confórmeros de mínima energía, realizando inicialmente cortes a 10 kcal/mol. Todos los confórmeros fueron examinados para descartar los duplicados. La energía en single-point de cada confórmero fue calculada con el nivel de teoría DFT B3LYP/6-31G(d) en el programa Spartan´04. Estas estructuras se sometieron a optimización de la geometría con el nivel de teoría PBEPBE/DGDZVP empleando los programas Gaussian 03W o Gaussian 09. Las estructuras de mínima energía en el rango de 0-2 kcal/mol se usaron para calcular los datos termodinámicos y las frecuencias de IR y DCV a 298 K y 1 atm. De todas las estructuras de mínima energía se verificó la ausencia de

frecuencias imaginarias y sus energías relativas fueron usadas para calcular la población de Boltzmann. Las ponderaciones de Boltzmann de IR y DCV de los compuestos fueron calculadas considerando las bandas Lorentzianas a una anchura media de 6 cm^{-1}. La visualización molecular se llevó a cabo en el programa Gaussian View 3.0. La optimización de la geometría y los cálculos vibracionales requirieron alrededor de 30 h de tiempo computacional por confórmero cuando se usó una computadora operando a 2.20 GHz con 8 Gb de memoria RAM y cerca de 2 h cuando se usó el supercomputador institucional hibrido Xiuhcoatl.

Aislamiento del isobutirato de 10-benzoiloxi-6-metoxi-8,9-epoxitimol (4).

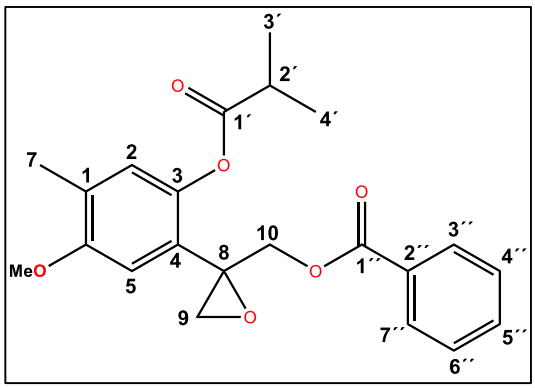

Del extracto hexánico de las hojas, en la polaridad (9:1) hexanos-AcOEt se obtuvieron 30 mg de una miel amarilla. RMN de ^{1}H (400 MHz, $CDCl_3$) δ: 7.99 (2H, m, H-3´´, H-7´´), 7.56 (1H, tt, *J* = 7.4 Hz, H-5´´), 7.42 (2H, t, *J* = 7.4 Hz, H-4´´, H-6´´), 6.96 (1H, s, H-5), 6.82 (1H, s, H-2), 4.79 (1H, d, *J* = 12.2 Hz, H-10a), 4.47 (1H, d, *J* = 12.2 Hz, H-10b), 3.82 (3H, s, H-OMe), 3.13 (1H, d, *J* = 5.2 Hz, H-9a), 2.76 (1H, d, *J* = 5.2 Hz, H-9b), 2.73 (1H, sept, *J* = 7.2 Hz, H-2´), 2.19 (3H, s, H-7), 1.31 (3H, d, *J* = 7.2 Hz, H-3´), 1.31 (3H, d, *J* = 7.2 Hz, H-4´).

Aislamiento del isobutirato de 10-benzoiloxi-8,9-epoxitimol (6).

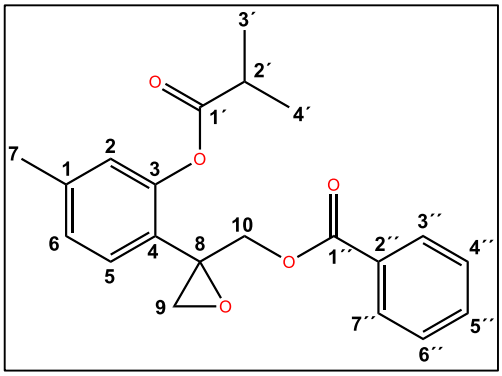

Del extracto hexánico de las hojas, en la polaridad (9:1) hexanos-AcOEt se obtuvieron 16 mg de una miel amarilla. RMN de ^{1}H (400 MHz, $CDCl_3$) δ: 7.96 (2H, dd, *J* = 7.6, 1.8 Hz, H-3´´, H-7´´), 7.54 (1H, tt, *J* = 7.4, 1.8 Hz, H-5´´), 7.40 (2H, t, *J* = 7.6 Hz, H-4´´, H-6´´), 7.44 (1H, d, *J* = 7.6 Hz, H-5), 7.06 (1H, dd, *J* = 7.6, 0.6 Hz, H-6), 6.87 (1H, s, H-2), 4.75 (1H, d, *J* = 12 Hz, H-10a), 4.45 (1H, d, *J* = 12 Hz, H-10b), 3.11 (1H, d, *J* = 5.2 Hz, H-9a), 2.89 (1H, d, *J* = 5.2 Hz, H-9b), 2.84 (1H, sept, *J* = 7.0 Hz, H-2´), 2.34 (3H, s, H-7), 1.30 (3H, d, *J* = 7.0 Hz, H-3´), 1.29 (3H, d, *J* = 7.0 Hz, H-4´).

Aislamiento del isobutirato de 10-cinamoiloxi-7-oxo-8,9-epoxitimol (7).

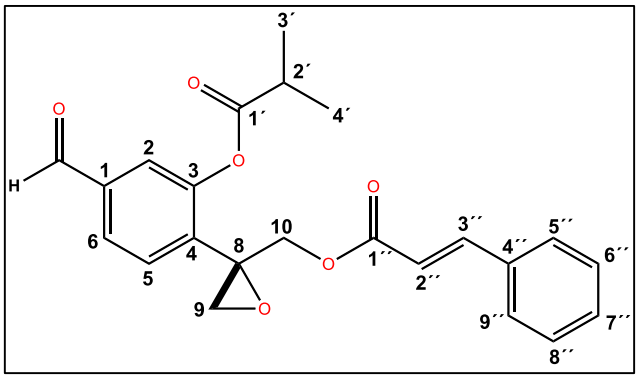

Del extracto hexánico de raíces de *P. areolare*, en la polaridad hexanos-AcOEt (7:3) se obtuvieron 22 mg de una miel amarilla. RMN de ^{1}H (400 MHz, $CDCl_3$) δ: 9.92 (1H, s, H-11), 7.71 (1H, dd, *J* = 7.8, 1.6 Hz, H-6), 7.65 (1H, d, *J* = 7.8 Hz, H-5), 7.57 (1H, d, *J* = 16.4 Hz, H-2´´), 7.54 (1H, d, *J* = 1.6 Hz, H-2), 7.42 (2H, m, H-5´´, H-9´´), 7.38 (3H, m, H-6´´, H-7´´, H-8´´), 6.30 (1H, d, *J* = 16.4 Hz, H-3´´), 4.63 (1H, d, *J* = 12.4 Hz, H-10a), 4.31 (1H, d, *J* = 12.4 Hz H-10b), 3.07 (1H, d, *J* = 5.2 Hz, H-9a), 2.84 (1H, sept, *J* = 7 Hz, H-2´), 2.80 (1H, d, *J* = 5.2 Hz, H-9b), 1.29 (3H, d, *J* = 7.2 Hz, H-3´), 1.28 (3H, d, *J* = 7.2 Hz, H-4´). RMN de ^{13}C (100 MHz, $CDCl_3$) δ: 190.6 (C, C-7), 175.2 (C, C-1´), 166.1 (C, C-1´´), 149.3 (CH, C-3), 116.9 (CH, C-3´´), 137.5 (C, C-1), 135.5 (C, C-4), 134.0 (C, C-4´´), 130.5 (CH, C-7´´), 130.0 (CH, C-5), 128.9 (CH, C-6´´, C-8´´), 128.1 (CH, C-5´´, C-9´´), 127.2 (CH, C-6), 123.6 (CH, C-2), 123.6 (CH, C-2´´), 65.2 (CH_2, C-10), 57.0 (C, C-8), 51.0 (CH_2, C-9), 34.1 (CH, C-2´), 18.9 (CH_3, C-3´), 18.8 (CH_3, C-4´).

12 BIBLIOGRAFÍA

Antkowiak R., Antkowiak W. Z., Nowak-Wydra B., *Heterocycles.* (2002), **58**: 137−146.

Arreaga-González. H. M.*,* Tesis de Maestría, Instituto de Investigaciones Químico Biológicas de la UMSNH, Morelia, Michoacán, México, (2015).

Arreaga-González H. M., Pardo-Novoa J. C., del Río R. E., Rodríguez-García G., Torres-Valencia J. M., Manríquez-Torres J. J., Cerda-García-Rojas C. M., Joseph-Nathan P., Gómez-Hurtado M. A., *Journal of Natural Products.* (2018) **81**: 63-71.

Bello-González M., Salgado G. R., *Revista de la Facultad de Biología de la Universidad Michoacana de San Nicolás de Hidalgo*, (2007), **9**: 126-136.

Bohlmann F., Grenz M., Jakupovic J., King R. M., Robinson H., *Phytochemistry.* (1983), **22**: 1213−1218.

Bohlmann F., Jakupovic J., Lonitz M., *Chemische Berichte*, (1977), **110**: 301-314.

Bohlmann F., Niedballa U., Schulz J., *Chemische Berichte*, (1969), **102**, 864-871.

Bohlmann F., Zdero C., *Phytochemistry.* (1977), **16**: 1854-1855.

Burgueño-Tapia E., Joseph-Nathan P., *Natural Products Communications*. (2015), **10**: 1785−1795.

Bustos-Brito C., Sánchez-Castellanos M., Esquivel B., Calderón J. S., Calzada F., Yépez-Mulia L., Hernández-Barragán A., Joseph-Nathan P., Cuevas G., Quijano L., *Journal of Natural Products.* (2014), **77**: 358−363.

Bustos-Brito C., Vázquez-Heredia V. J., Calzada F., Yépez-Mulia L., Calderón J. S., Hernández-Ortega S., Esquivel B., García-Hernández N., Quijano L., *Molecules.* (2016), **21**: 1132–1145.

Calderón de Rzedowski G., Rzedowski J., Pátzcuaro: Instituto de Ecología A.C. y Comisión Nacional para el Conocimiento y Uso de la Biodiversidad. (2005), 792-794.

Chen L. C., Lee T. H., Sung P. J., Shu C. W., Lim Y. P., Cheng M. J., Kuo W.L., Chen J. J., *Chemisty & Biodiversity*, (2014), **11**: 1374-1380.

Delle Monache G., Delle Monache F., Beccera J., Silva M., Menichini F., *Phytochemistry*. (1984), **23**: 1947-1950.

Dewick P., 3er Ed. Wiley United Kingdom. (2009), 7-33.

Du G., Li Y., Ma S., Wang R., Li B., Guo F., Zhu W., Li Y., *Journal of Natural Products.* (2015), **78**: 2968-2974.

Enciclopedia de los municipios y delegaciones de México, consultado en: http://www.inafed.gob.mx/work/enciclopedia/EMM16michoacan/municipios/16049a.html

Flack. H. D., Bernardinelli G., *Chirality*, (2008), **20**: 681-690.

García P. G., del Río R. E., Guzmán M. R., Martínez G. M. I., Scior, T. R. F., *Revista Mexicana de Ciencias Farmacéuticas*. (2011), **42**: 45-51.

García-Sánchez E., Ramírez-López C. B., Talavera-Alemán A., León-Hernández A., Martínez-Muñoz R. E., Martínez-Pacheco M. M., Gómez- Hurtado M. A., Cerda-García-Rojas C. M., Joseph-Nathan P., *Journal of Natural Products*. (2014), **77**: 1005-1012.

Gómez-Hurtado M. A., Torres-Valencia J. M., Manríquez-Torres J., del Río R. E., Motilva V., García-Mauriño S., Avila J., Talero E., Cerda-García-Rojas C. M., Joseph-Nathan P., *Phytochemistry*. (2011), **72**: 409-414.

Gómez-Hurtado M. A., Álvarez-Esquivel F. E., Rodríguez-García G., Martínez-Pacheco M. M., Espinoza-Madrigal R. M., Pamatz-Bolaños T., Salvador-Hernández J. L., García-Gutiérrez H. A., Cerda-García-Rojas C. M., Joseph-Nathan P., del Río R. E., *Phytochemistry*. (2013), **96**: 397-403.

Hernández J. D., Román M. L. U., Rodríguez M., Espiñeira J., Joseph-Nathan P., *Phytochemistry*. (1986), **7**: 1743-1744.

Herz W., Sosa V. E., *Phytochemistry*. (1988), **27**: 155−159.

Hu X., Yang Y., Shi S., Shan Z., *Chirality.* (2016), **28**: 784–788.

Jiang H. X., Li Y., Pan J., Gao K., *Helvetica Chimica Acta*. (2006), **89**: 558-566.

Joseph-Nathan P., Gordillo-Roman B. In Progress in the Chemistry of Organic Natural Products; Kinghorn, A. D., Falk, H., Kobayashi, J., Eds.; Springer International Publishing: Cham, Switzerland, 2015; Vol. 100, pp 311−451.

Juaristi E., Introducción a la estereoquímica y el anális coformacional, El Colegio nacional, México DF. (2010), 2-10.

King R. M., Rob H., *Phytologia*. (1970), **19**: 426.

King M. R., Robinson H., *Phytologia*. (1978), **38**: 323-355.

Kos O., Lindenmeyer M. T, Tubaro A., Sosa S., Merfort I., *Planta Medica.* (2005), **71**: 1044-1052.

Liang H., Bao F., Dong X., Tan R., Zhang C., Lu Q., Cheng Y., *Molecules*. (2007), **12**: 1606-1613.

Maldonado E, Márquez C. L., Ortega A., *Phytochemistry*. (1992), **31**: 2527-2528.

Marco J. A., Sanz-Cervera J. F., Manglano E. *Phytochemistry.* (1993), **33**: 875−878.

Muñoz M. A., Chamy C., Bucio M. A., Hernández-Barragán A., Joseph-Nathan P., *Tetrahedron Letters*. (2014), **55** 4274-4277.

Pardo-Novoa J. C., Arreaga-González H. M., Gómez-Hurtado M. A., Rodríguez García G., Cerda-García-Rojas C. M., Joseph-Nathan P., del Río R. E., *Journal Natural Prod*ucts. (2016), **79**: 2570-2579.

Sánchez-González A., Granados-Sánchez D., *Revista Chapingo Serie Horticultura*. (2008), **14**: 271-279.

Redondo J., Capdevila A., Ciudad S. *Chirality.* (2013), **25**: 780-786.

Redondo J., Capdevila A., Latorre I., *Chirality.* (2010), **22**: 472-478.

Talavera-Alemán A., Rodríguez-García G., López Y., García-Gutiérrez H. A., Torres-Valencia J. M., del Río R. E., Cerda-García-Rojas C. M., Joseph-Nathan P., Gómez-Hurtado M. A., *Phytochemical review*. (2016), **15**: 251-277.

Tamayo-Castillo G., Jaupovic J., Bolhmann F., Rojas A., Castro V. King M., *Phytochemistry.* (**1988**), 27: 2893-2897.

Thompson A. L., Watkin D. J., Chemical crystallographyc, departament of inorganic chemistry. Oxford, (2009).

Tori M., Ohara Y., Nakashima K., Sono M., *Journal of Natural Products*. (2001), **64**: 1048-1051.

Trang N. D., Wanner M. J., Koomen G. J., Dung N. X., *Planta Medica*. (1993), **59**: 480−481.

Villaseñor J. L., Ortiz E., *Acta Botánica Mexicana*. (2012), **100**: 259-291.

Wang Y., Li J., Wang H., Jin D. Q., Chen H., Xu J., Ohizumi Y., Guo Y-., *Phytochemistry Letter.* (2014), **7**:190-193.

Yi J., Du G., Yang Y., Li Y., Li Y., Guo F., *Tetrahedron: Asymmetry.* (2016), **27**: 1153–1159.

Zhao J., Li Y., Liu Q., Gao K., *Food Chemistry*. (2010), **120**: 512-516.

Zhou Z. Y., Liu W. X., Pei G., Ren H., Wang J., Xu Q. L., Xie H. H., Wan F. H., Tan J. W., *Journal of Agricultural Food and Chemistry*. (2003), **61**:11792-11799.

ANEXOS

Anexo 1. Datos termoquímicos y estructuras calculadas para el (+)-(8*S*)-isobutirato de10-benzoiloxi-6-hidroxi-8,9-epoxitimol (**1**).

Tabla A1.1. Análisis termoquímico de (+)-(*8S*)-isobutirato de-10-benzoiloxi-6-hidroxi-8,9-epoxitimol (**1**).

Confórmero	ΔE_{MMFF}[a]	$\%_{MMFF}$[b]	ΔE_{DFT}[c]	$\%_{DFT}$[d]	ΔG_{opt}[e]	$\%_{opt}$[f,g]
1a	4.50	0.04	5.76	0.0045	**0.00**	14.84
1b	2.79	0.80	4.17	0.0652	0.05	13.58
1c	3.20	0.40	5.38	0.0086	0.07	13.12
1d	3.71	0.17	**0.00**	70.9743	0.26	9.62
1e	3.01	0.54	6.15	0.0024	0.32	8.62
1f	4.12	0.08	7.44	0.0003	0.77	4.10
1g	2.51	1.26	4.46	0.0398	0.82	3.78
1h	2.61	1.07	6.19	0.0022	0.82	3.75
1i	3.53	0.23	6.14	0.0024	0.89	3.33
1j	5.02	0.02	6.88	0.0007	0.96	2.98
1k	2.38	1.57	5.22	0.0112	1.03	2.63
1l	2.71	0.91	6.26	0.0020	1.22	1.91
1m	4.46	0.05	1.14	10.5207	1.37	1.50
1n	3.41	0.28	7.55	0.0002	1.38	1.46
1o	3.17	0.42	5.02	0.0157	1.45	1.29
1p	3.67	0.18	6.55	0.0012	1.50	1.20
1q	3.59	0.21	5.75	0.0046	1.60	1.01
1r	2.61	1.08	5.59	0.0060	1.62	0.98
1s	3.91	0.12	6.42	0.0015	1.63	0.96
1t	3.50	0.24	5.82	0.0041	1.69	0.85
1u	3.54	0.22	0.81	18.1275	1.69	0.87
1v	3.93	0.12	6.48	0.0013	1.69	0.86
1w	1.90	3.56	5.49	0.0071	1.75	0.79
1x	3.71	0.17	5.20	0.0115	1.76	0.77
1y	4.08	0.09	5.93	0.0034	1.82	0.70
1z	3.94	0.11	7.08	0.0005	1.87	0.64
1a´	**0.00**	85.49	3.60	0.1698	1.88	0.63
1b´	3.22	0.39	5.90	0.0036	1.88	0.63
1c´	4.67	0.03	6.25	0.0020	1.88	0.63
1d´	4.73	0.03	6.25	0.0020	1.92	0.60
1e´	4.01	0.10	7.15	0.0004	1.92	0.59

[a]Energía relativa en Mecánica Molecular respecto a **1a´**, E_{MMFF} = 53.533 kcal/mol. [b]Población en % calculada de las energías de MMFF de acuerdo a $\Delta E_{MMFF} \approx -RT \ln K$. [c]Energía relativa en single-point B3LYP/6-31G(d) respecto a **1d**, $E_{6\text{-}31G(d)}$ = −793707.737 kcal/mol. [d]Población en % calculada de B3LYP/6-31G(d) energía respecto a $\Delta E_{6\text{-}31G(d)} \approx -RT \ln K$. [e] Energía relativa libre de Gibbs respecto a **1a**, $G_{PBEPBE/DGDZVP}$ = −792638.484 kcal/mol. [f]Población en % calculada de la energía libre Gibbs de acuerdo a $\Delta G = -RT \ln K$.

δ

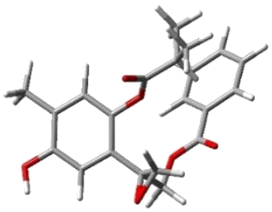

1a
14.8411%

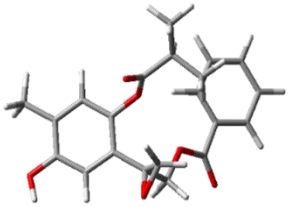

1b
13.5852%

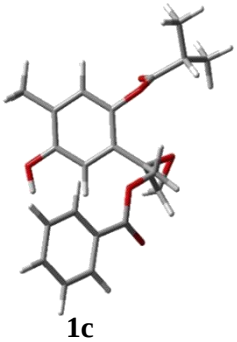

1c
13.1214%

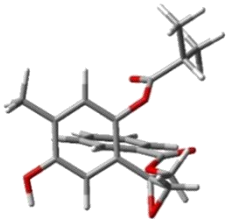

1d
9.6189%

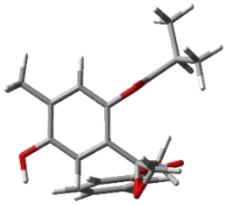

1e
8.6215%

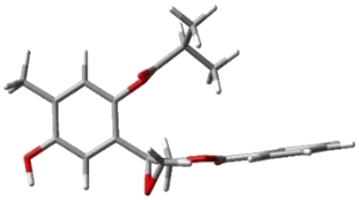

1f
4.1006%

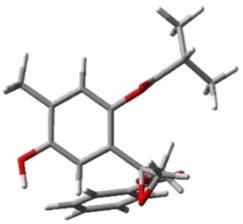

1g
3.7774%

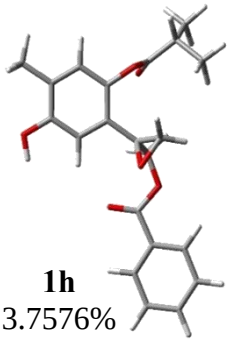

1h
3.7576%

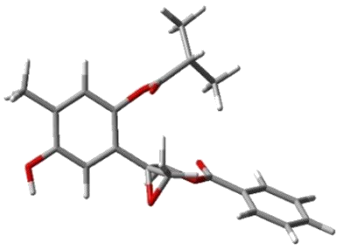

1i
3.3362%

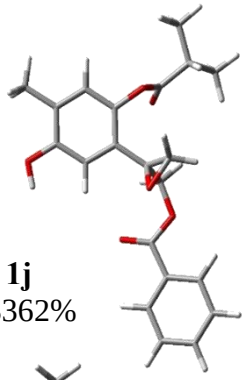

1j
3.3362%

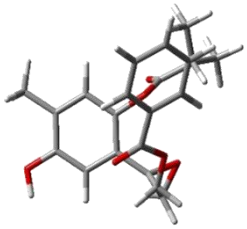

1k
2.6327%

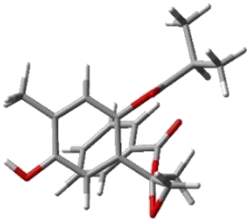

1l
1.9138%

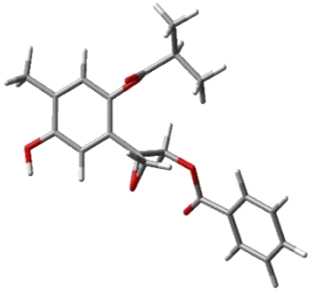

1m
1.50071%

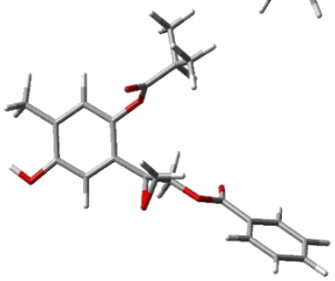

1n
1.4571%

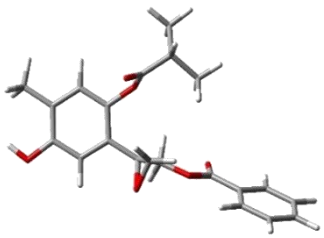

1o
1.2896%

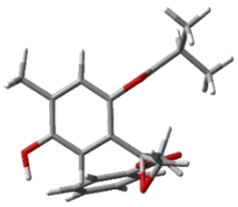

1p
1.1980%

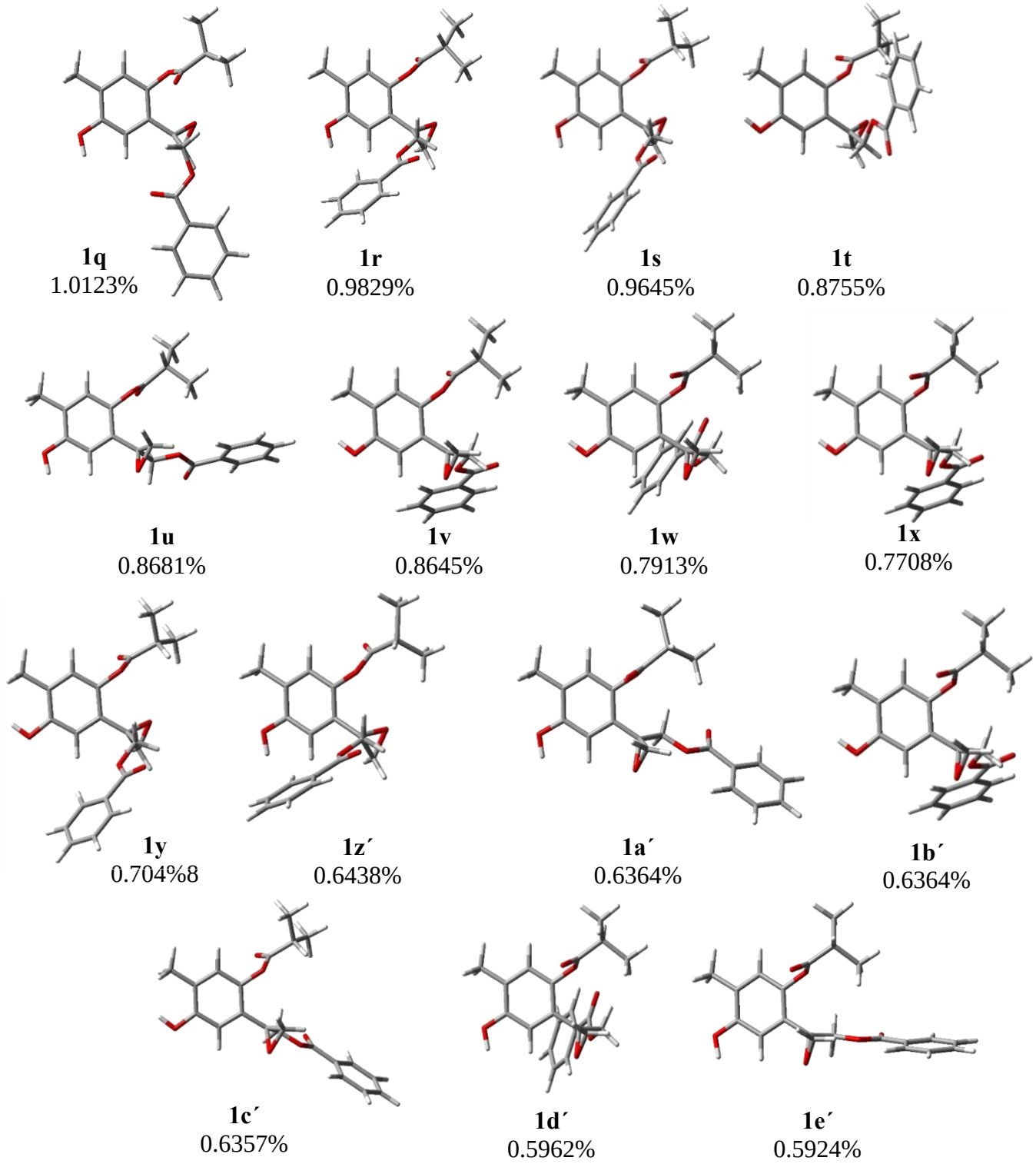

Figura A1.1. Confórmeros del (+)-(8*S*)-isobutirato de10-benzoiloxi-6-hidroxi-8,9-epoxitimol (**1**) que representan el 100% de la población conformacional.

Anexo 2. Datos termoquímicos y estructuras calculadas para el (+)-(8*S*)-isobutirato de 10-isobutiriloxi-8,9-epoxitimol (**2**).

Tabla A2.1. Análisis termoquímico de (+)-(8*S*)-isobutirato de 10-isobutiriloxi-8,9-epoxitimol (**2**).

Confórmero	ΔE_{MMFF}[a]	$\%_{MMFF}$[b]	ΔE_{DFT}[c]	$\%_{DFT}$[d]	ΔG_{opt}[e]	$\%_{opt}$[f,g]
2a	1.66	1.11	0.21	7.66	**0.00**	10.84
2b	1.34	1.89	1.56	0.80	0.22	7.49
2c	1.49	1.47	0.50	4.72	0.28	6.80
2d	1.59	1.26	2.03	0.36	0.51	4.61
2e	1.05	3.11	1.25	1.35	0.51	4.61
2f	1.86	0.80	0.99	2.07	0.56	4.22
2g	1.91	0.73	1.03	1.94	0.63	3.80
2h	3.69	0.04	0.70	3.39	0.69	3.42
2i	2.19	0.46	2.23	0.26	0.74	3.13
2j	1.73	0.99	0.29	6.72	0.75	3.08
2k	1.99	0.64	2.46	0.18	0.76	3.02
2l	2.71	0.19	0.78	2.95	0.79	2.88
2m	2.27	0.40	2.30	0.23	0.85	2.62
2n	1.41	1.70	0.94	2.28	0.87	2.52
2o	1.40	1.71	0.14	8.67	0.87	2.51
2p	3.59	0.04	0.80	2.86	0.88	2.49
2q	1.56	1.32	1.10	1.75	0.89	2.45
2r	2.05	0.58	0.63	3.82	0.99	2.08
2s	1.21	2.35	0.13	8.77	1.00	2.01
2t	2.98	0.12	2.38	0.20	1.03	1.92
2u	1.55	1.34	1.36	1.12	1.04	1.88
2v	3.38	0.06	2.14	0.30	1.19	1.47
2w	4.21	0.02	1.43	1.00	1.22	1.40
2x	2.07	0.56	0.92	2.34	1.23	1.37
2y	3.72	0.04	1.02	1.98	1.24	1.35
2z	2.77	0.17	1.53	0.84	1.28	1.28
2a´	0.62	6.32	2.14	0.30	1.41	1.02
2b´	3.33	0.07	1.68	0.65	1.43	0.99
2c´	2.45	0.30	1.53	0.84	1.45	0.95
2d´	1.97	0.66	1.57	0.79	1.48	0.91
2e´	1.60	1.23	1.70	0.64	1.49	0.90
2f´	3.10	0.10	1.44	0.98	1.50	0.88
2g´	3.42	0.06	2.44	0.18	1.58	0.77
2h´	1.85	0.81	1.82	0.52	1.60	0.75
2i´	3.29	0.07	2.20	0.28	1.60	0.74
2j´	3.17	0.09	1.34	1.17	1.60	0.74
2k´	2.57	0.24	1.15	1.58	1.60	0.74
2l´	2.89	0.14	2.35	0.21	1.72	0.61
2m´	0.94	3.70	2.70	0.12	1.77	0.56
2n´	3.73	0.03	2.74	0.11	1.79	0.53

2o´	1.59	1.25	2.11	0.32	1.80	0.53
2p´	0.09	15.38	1.28	1.29	1.83	0.50
2q´	4.57	0.01	2.04	0.36	1.85	0.49
2r´	0.33	10.39	1.43	0.99	1.87	0.47
2s´	0.04	16.95	**0.00**	10.96	1.90	0.45
2t´	**0.00**	18.01	0.83	2.72	1.93	0.43
2u´	3.68	0.04	2.38	0.20	1.93	0.42
2v´	1.69	1.06	0.34	6.23	2.00	0.38

[a]Energía relativa en Mecánica Molecular respecto a **2t´**, E_{MMFF} = 37.735 kcal/mol. [b]Población en % calculada de las energías de MMFF de acuerdo a $\Delta E_{MMFF} \approx -RT \ln K$. [c]Energía relativa en single-point B3LYP/6-31G(d) respecto a **2s´**, $E_{6\text{-}31G(d)}$ = −675524.785 kcal/mol. [d]Población en % calculada de B3LYP/6-31G(d) energía respecto a $\Delta E_{6\text{-}31G(d)} \approx -RT \ln K$. [e] Energía relativa libre de Gibbs respecto a **2a**, $G_{PBEPBE/DGDZVP}$ = −674566.684 kcal/mol. [f]Población en % calculada de la energía libre Gibbs de acuerdo a $\Delta G = -RT \ln K$.

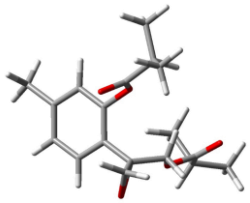

2a
10.84%

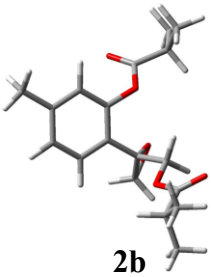

2b
7.49%

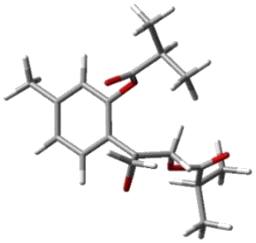

2c
6.80%

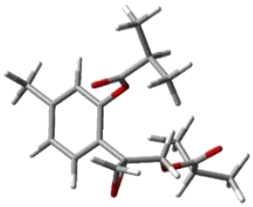

2d
4.61%

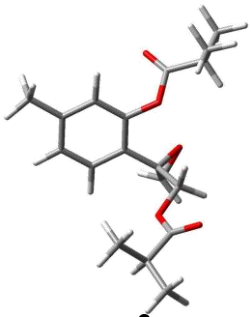

2e
4.61%

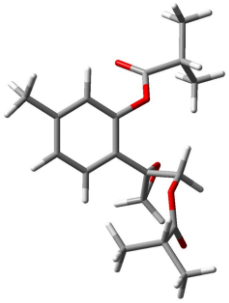

2f
4.22%

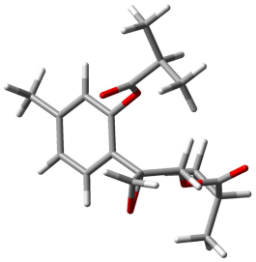

2g
3.80%

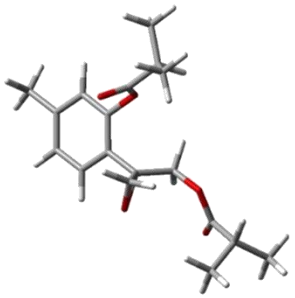

2h
3.42%

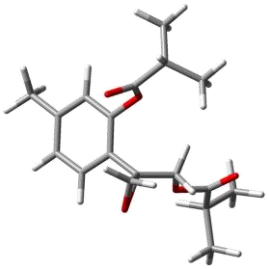

2i
3.13%

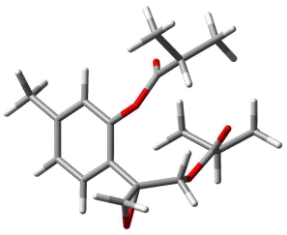

2j
3.08%

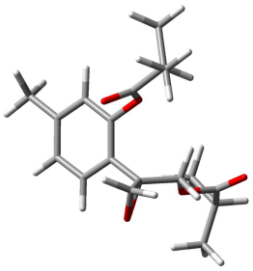

2k
3.02%

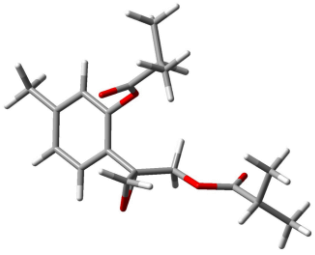

2l
2.88%

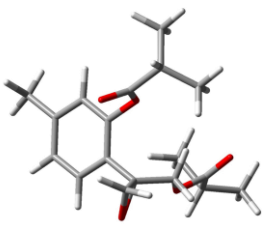

2m
2.62%

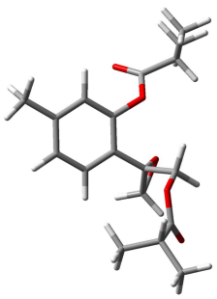

2n
2.52%

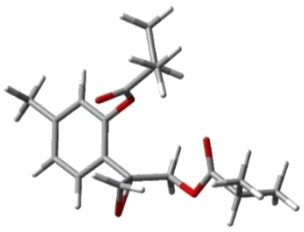

2o
2.51%

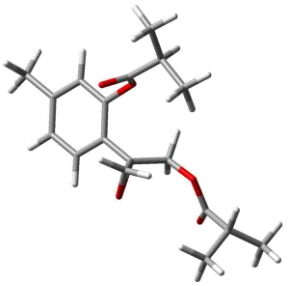

2p
2.49%

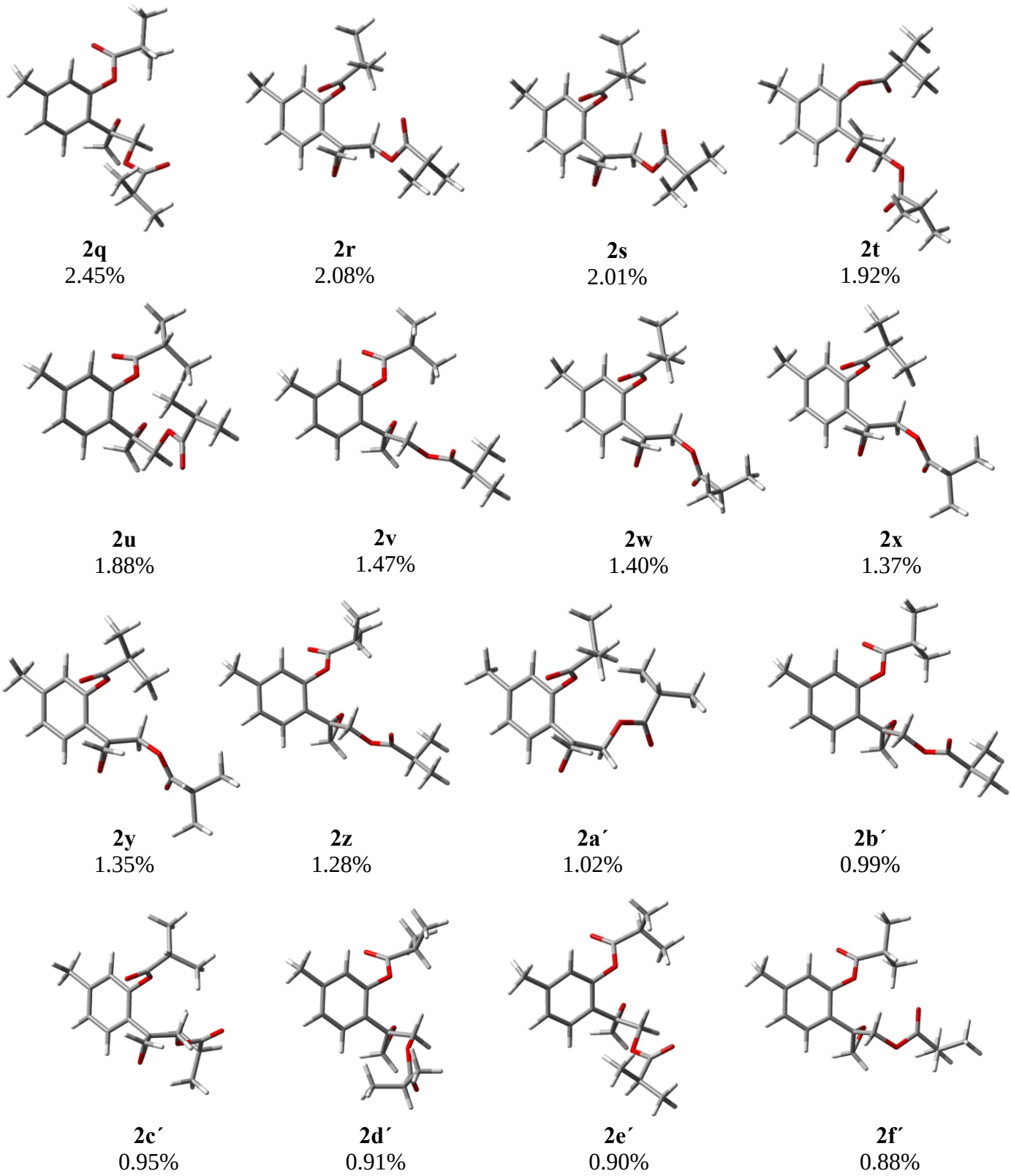

Figura A2.1. Conformeros de (+)-(8*S*)-Isobutirato de 10-isobutiriloxi-8,9-epoxitimol (**2**) que representan el 100% de la población conformacional.

Anexo 3. Datos termoquímicos y estructuras calculadas para el (+)-(8*S*)-isobutirato de 10-acetoxi-6-metoxi-8,9-epoxitimol (**3**)

Tabla A3.1. Análisis termoquímico de (+)-(8*S*)-isobutirato de 10-acetoxi-6-metoxi-8,9-epoxitimol (**3**)

Confórmero	ΔE_{MMFF}[a]	$\%_{MMFF}$[b]	ΔE_{DFT}[c]	$\%_{DFT}$[d]	ΔG_{opt}[e]	$\%_{opt}$[f,g]
3a	0.64	7.22	1.540	2.33	**0.00**	19.24
3b	0.52	8.79	1.746	1.64	0.05	17.63
3c	0.53	8.66	**0.000**	30.77	0.38	10.17
3d	0.54	8.53	0.003	30.62	0.52	8.07
3e	0.61	7.50	2.622	0.38	0.77	5.26
3f	1.55	1.58	1.328	3.32	0.78	5.20
3g	2.63	0.25	0.873	7.11	0.86	4.55
3h	1.85	0.94	1.539	2.33	0.87	4.47
3i	2.57	0.28	0.916	6.62	0.98	3.71
3j	2.27	0.47	1.945	1.18	1.09	3.07
3k	0.10	4.00	2.193	0.78	1.17	2.72
3l	0.25	13.90	3.258	0.13	1.22	2.48
3m	2.35	0.41	1.543	2.31	1.25	2.38
3n	0.37	11.29	1.021	5.55	1.30	2.18
3o	1.02	3.80	2.204	0.76	1.31	2.13
3p	**0.00**	21.10	2.661	0.35	1.32	2.11
3q	2.14	0.58	2.041	1.00	1.42	1.77
3r	2.97	0.14	1.508	2.45	1.61	1.29
3s	2.73	0.21	3.015	0.20	1.87	0.83
3t	2.46	0.33	3.165	0.15	1.97	0.70

[a]Energía relativa en Mecánica Molecular respecto a **3p**, E_{MMFF} = 39.603 kcal/mol. [b]Población en % calculada de las energías de MMFF de acuerdo a $\Delta E_{MMFF} \approx -RT \ln K$. [c]Energía relativa en single-point B3LYP/6-31G(d) respecto a **3c**, $E_{6\text{-}31G(d)}$ = −698051.239 kcal/mol. [d]Población en % calculada de B3LYP/6-31G(d) energía respecto a $\Delta E_{6\text{-}31G(d)} \approx -RT \ln K$. [e] Energía relativa libre de Gibbs respecto a **3a**, $G_{PBEPBE/DGDZVP}$ = −697105.530 kcal/mol. [f]Población en % calculada de la energía libre Gibbs de acuerdo a $\Delta G = -RT \ln K$.

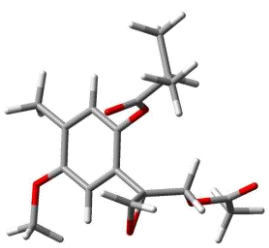

3a
16.658%

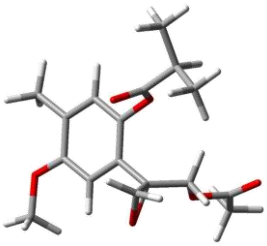

3b
15.265%

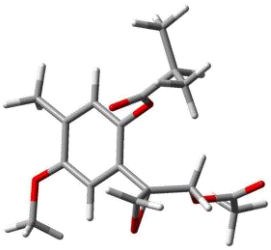

3c
13.439%

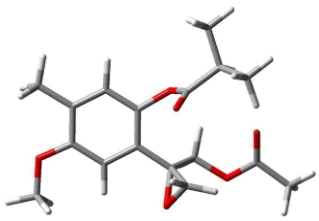

3d
8.803%

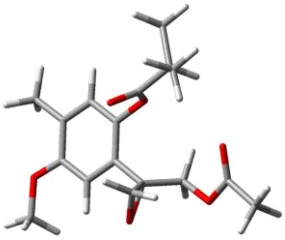

3e
6.990%

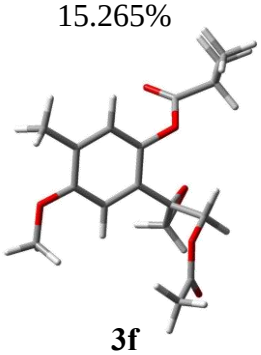

3f
4.559%

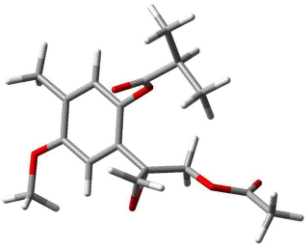

3g
4.507%

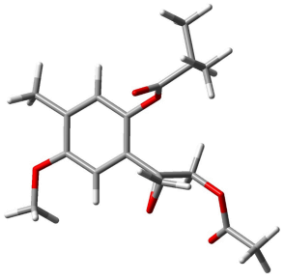

3h
3.943%

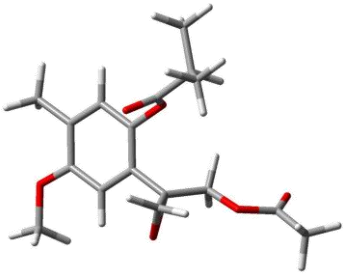

3i
3.873%

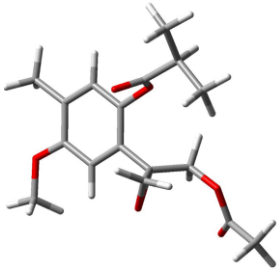

3j
3.211%

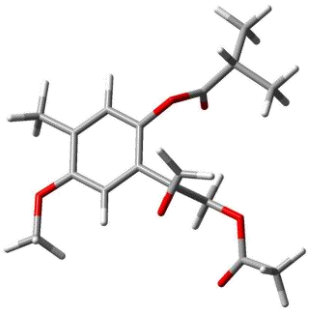

3k
2.663%

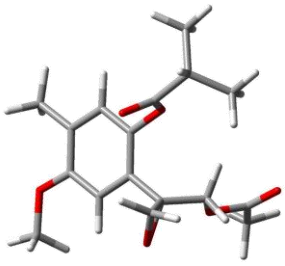

3l
2.352%

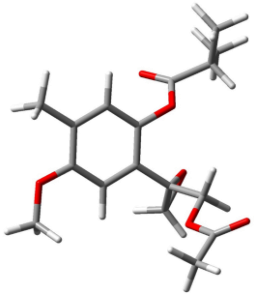

3m
2.150%

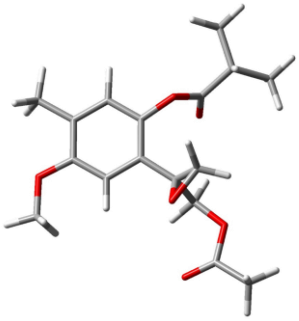

3n
2.057%

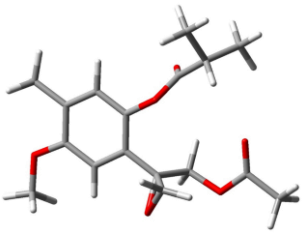

3o
1.883%

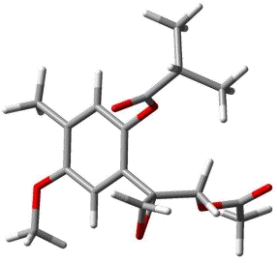

3p
1.848%

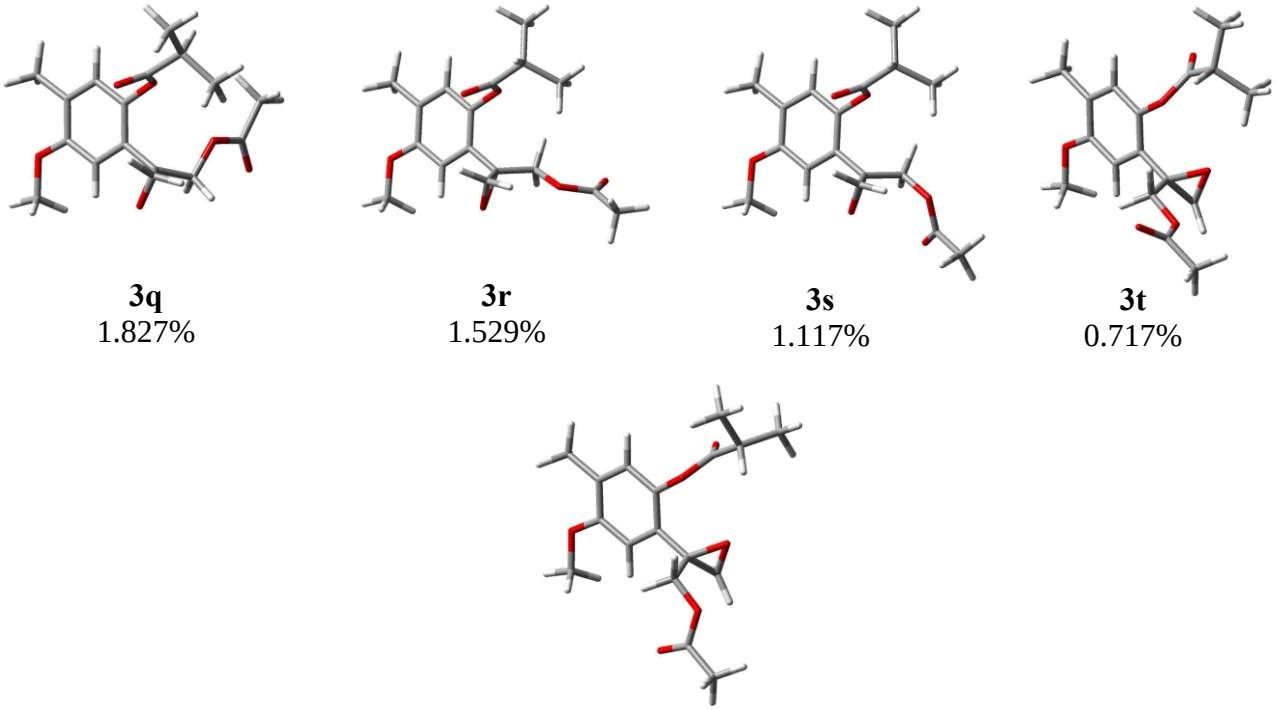

Figura A3.1. conformeros del (+)-(8*S*)-isobutirato de 10-acetoxi-6-metoxi-8,9-epoxitimol (**3**) que representan el 100% de la población conformacional.

Anexo 4. Datos termoquímicos y estructuras calculadas para el (+)-(8*S*)-isobutirato de-10-benzoiloxi-6-metoxi-8,9-epoxitimol (**4**).

Tabla A4.1. Análisis termoquímico de (+)-(8*S*)-isobutirato de-10-benzoiloxi-6-metoxi-8,9-epoxitimol (**4**).

Confórmero	ΔE_{MMFF}[a]	$\%_{MMFF}$[b]	ΔE_{DFT}[c]	$\%_{DFT}$[d]	ΔG_{opt}[e]	$\%_{opt}$[f,g]
4a	3.14	0.2183	1.32	4.3953	**0.00**	9.51
4b	3.10	0.2327	5.40	0.0046	0.28	5.87
4c	3.58	0.1056	1.56	2.9191	0.30	5.76
4d	2.01	1.4642	0.91	8.6994	0.43	4.63
4e	3.09	0.2413	1.69	2.3590	0.46	4.37
4f	1.83	1.9826	2.34	0.7836	0.51	4.06
4g	3.07	0.2458	3.46	0.1213	0.53	3.94
4h	2.61	0.5338	1.70	2.3081	0.58	3.59
4i	4.92	0.0110	5.34	0.0051	0.70	2.90
4j	4.11	0.0431	2.23	0.9424	0.74	2.75
4k	4.58	0.0197	3.54	0.1049	0.77	2.62
4l	4.11	0.0431	6.89	0.0004	0.78	2.55
4m	3.06	0.2487	3.03	0.2484	0.82	2.41
4n	5.26	0.0063	2.00	1.4048	0.87	2.21
4o	4.60	0.0193	1.36	4.0690	0.88	2.19
4p	3.50	0.1201	3.26	0.1697	0.90	2.10
4q	**0.00**	42.7159	1.14	5.9446	0.91	2.05
4r	1.98	1.5336	**0.00**	40.0322	0.96	1.90
4s	3.37	0.1485	1.42	3.6979	0.98	1.83
4t	4.22	0.0357	2.97	0.2761	1.02	1.72
4u	0.42	20.9333	1.28	4.6925	1.02	1.71
4v	1.84	1.9285	1.98	1.4528	1.08	1.56
4w	4.50	0.0222	3.14	0.2055	1.12	1.47
4x	3.62	0.0989	3.65	0.0879	1.12	1.45
4y	1.52	3.3253	1.81	1.9160	1.13	1.42
4z	2.44	0.7067	1.78	2.0183	1.16	1.35
4a'	4.01	0.0512	2.90	0.3099	1.17	1.33
4b'	2.17	1.1207	2.60	0.5143	1.17	1.32
4c'	2.06	1.3512	2.59	0.5161	1.18	1.32
4d'	3.88	0.0636	2.70	0.4284	1.18	1.30
4e'	1.91	1.7261	2.37	0.7552	1.19	1.29
4f'	3.56	0.1084	3.41	0.1313	1.20	1.26
4g'	3.09	0.2373	2.03	1.3203	1.20	1.26
4h'	3.72	0.0825	3.94	0.0540	1.22	1.22
4i'	3.56	0.1084	3.13	0.2097	1.22	1.21

4j'	2.49	0.6488	3.00	0.2621	1.23	1.20
4k'	4.69	0.0163	2.34	0.7863	1.38	0.94
4l'	3.74	0.0799	2.15	1.0796	1.41	0.89
4m'	0.83	10.4671	2.20	0.9927	1.45	0.83
4n'	3.33	0.1589	2.22	0.9616	1.50	0.77
4o'	1.50	3.4123	2.99	0.2665	1.50	0.77
4p'	2.56	0.5787	3.47	0.1185	1.54	0.72
4q'	2.15	1.1675	2.44	0.6693	1.54	0.72
4r'	4.05	0.0476	2.87	0.3232	1.58	0.67
4s'	2.32	0.8709	3.16	0.2007	1.60	0.65
4t'	2.74	0.4272	2.54	0.5650	1.61	0.64
4u'	3.96	0.0558	3.83	0.0650	1.65	0.59
4v'	5.02	0.0094	2.62	0.4932	1.66	0.58
4w'	3.12	0.2258	3.47	0.1183	1.71	0.54

[a]Energía relativa en Mecánica Molecular respecto a **4q**, E_{MMFF} = 71.178 kcal/mol. [b]Población en % calculada de las energías de MMFF de acuerdo a $\Delta E_{MMFF} \approx -RT \ln K$. [c]Energía relativa en single-point B3LYP/6-31G(d) respecto a **4r**, $E_{6\text{-}31G(d)}$ = −343187.213 kcal/mol. [d]Población en % calculada de B3LYP/6-31G(d) energía respecto a $\Delta E_{6\text{-}31G(d)} \approx -RT \ln K$. [e] Energía relativa libre de Gibbs respecto a **4a**, $G_{PBEPBE/DGDZVP}$ = −343188.127 kcal/mol. [f]población en % calculada de la energía libre Gibbs de acuerdo a $\Delta G = -RT \ln K$.

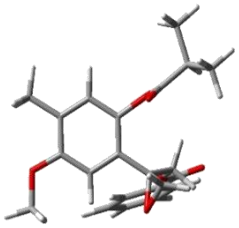

4a
9.5 %

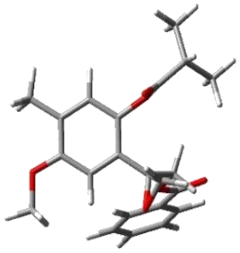

4b
5.9%

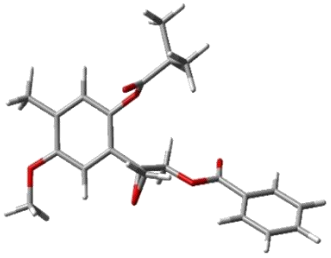

4c
5.8%

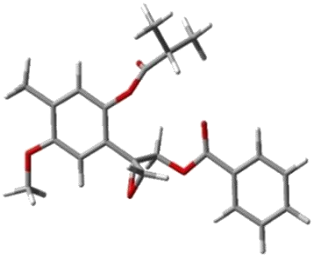

4d
4.6 %

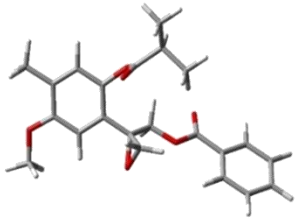

4e
4.3%

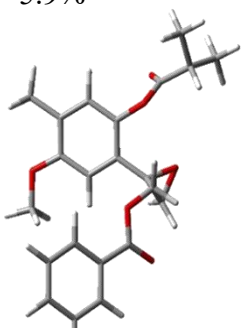

4f
4.0%

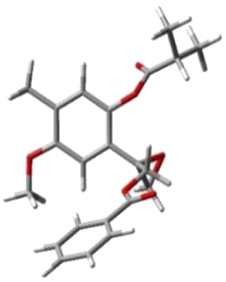

4g
3.9 %

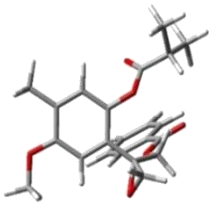

4h
3.6%

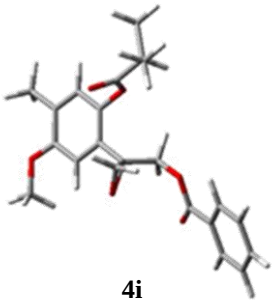

4i
2.9%

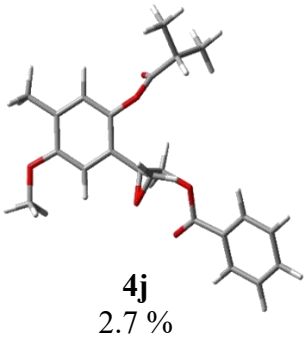

4j
2.7 %

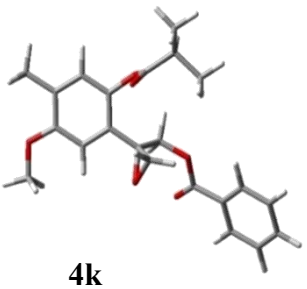

4k
2.6%

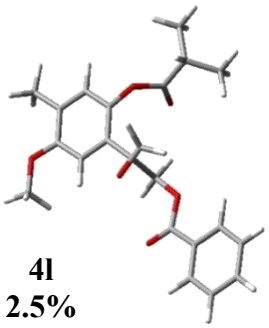

4l
2.5%

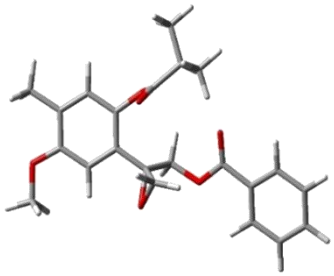

4m
2.4%

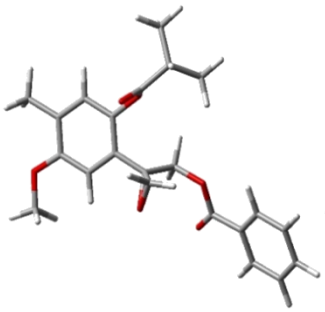

4n
2.2 **%**

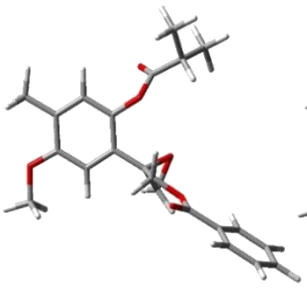

4o
2.2%

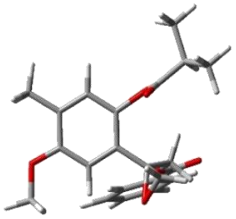

4p
2.1%

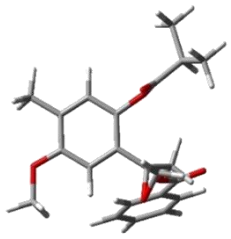

4q
2.0%

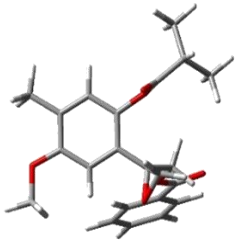

4r
1.9%

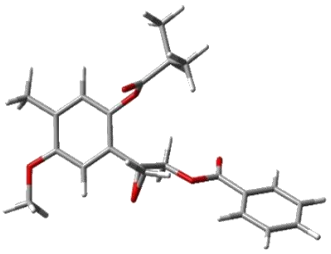

4s
1.8%

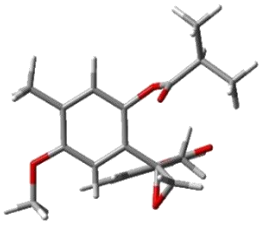

4t
1.7%

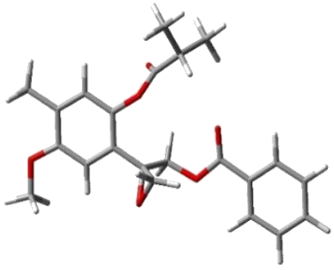

4u
1.7%

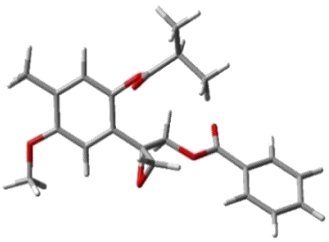

4v
1.5%

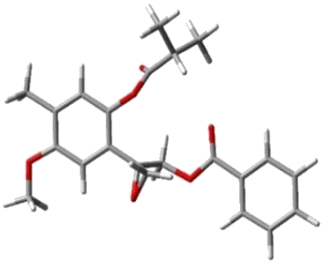

4w
1.5%

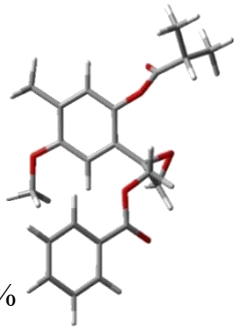

4x
1.4%

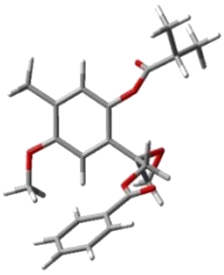

4y
1.4%

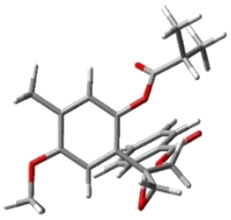

4z
1.3%

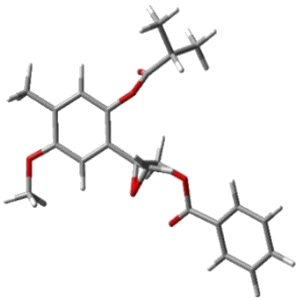

4a´
1.3%

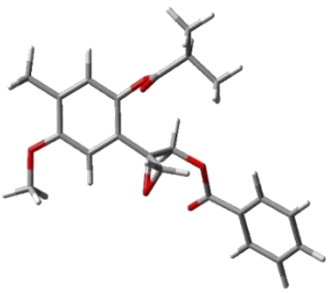

4b´
1.3%

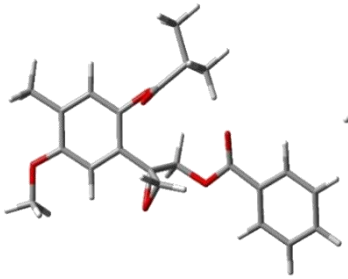

4c´
1.3%

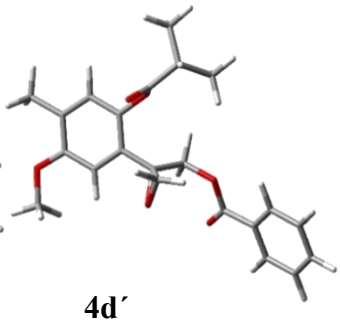

4d´
1.3%

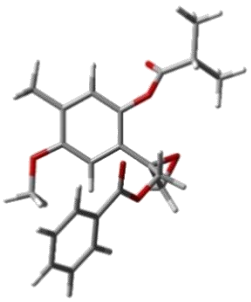

4e´
2.3%

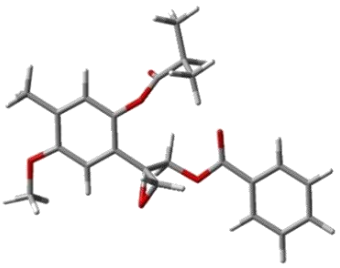

4f´
1.3%

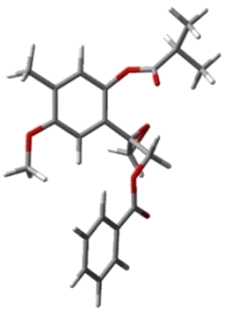

4g´
1.2%

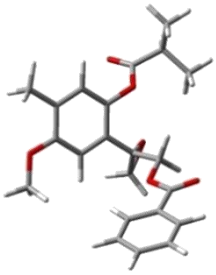

4h´
1.2%

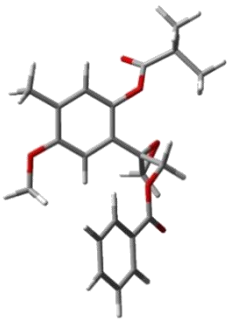

4i´
1.2%

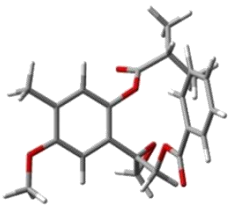

4j´
1.2%

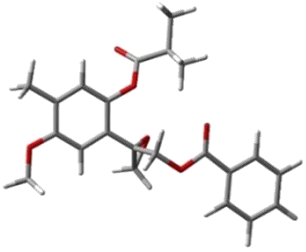

4k´
0.9%

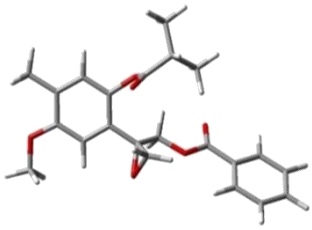

4l´
0.9%

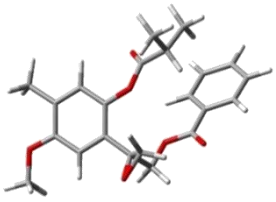

4m´
0.8%

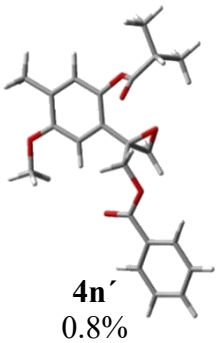

4n´
0.8%

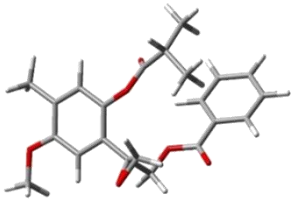

4o´
0.8 %

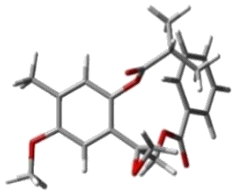

4p´
0.7%

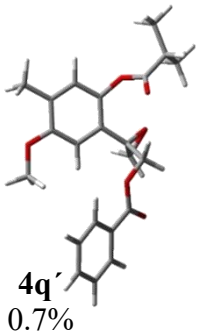

4q´
0.7%

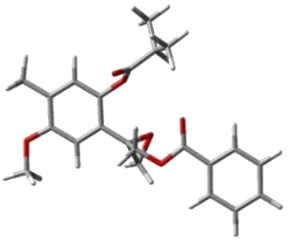

4r´
0.7%

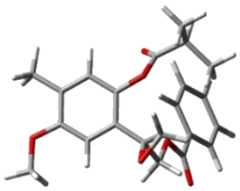

4s´
0.6%

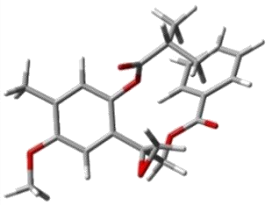

4t´
0.6%

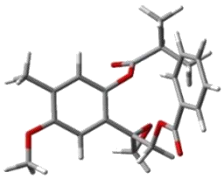

4u´
0.6%

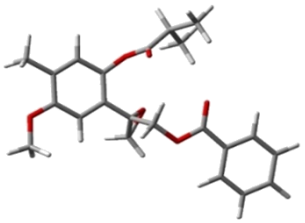

4v´
0.6%

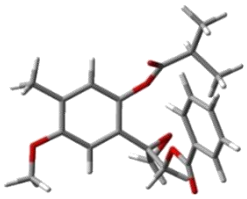

4w´
0.5%**%**

Figura A4.1. Conformeros de (+)-(8*S*)-isobutirato de-10-benzoiloxi-6-metoxi-8,9-epoxitimol (**4**) que representan el 100% de la población conformacional.

Anexo 5. Datos termoquímicos y estructuras calculadas para el (+)-(8*S*) isobutirato de 10-cinamoiloxi-7-oxo-8,9-epoxitimol (**7**).

Tabla A5.1. Análisis termoquímico de (+)-(8*S*) isobutirato de 10-cinamoiloxi-7-oxo-8,9-epoxitimol (**7**).

Confórmero	ΔE_{MMFF}[a]	$\%_{MMFF}$[b]	ΔE_{DFT}[c]	$\%_{DFT}$[d]	ΔG_{opt}[e]	$\%_{opt}$[f,g]
7a	4.56	0.0114	5.82	0.0025	**0.00**	9.16
7b	3.47	0.0710	0.85	10.6354	0.08	7.93
7c	4.68	0.0092	6.89	0.0004	0.34	5.11
7d	3.21	0.1090	6.15	0.0014	0.43	4.41
7e	3.60	0.0568	1.55	3.2651	0.44	4.38
7f	4.44	0.0140	0.53	17.9792	0.50	3.98
7g	4.10	0.0245	6.97	0.0003	0.50	3.94
7h	2.08	0.7288	4.61	0.0191	0.51	3.83
7i	2.02	0.8019	4.54	0.0217	0.54	3.67
7j	2.34	0.4746	5.25	0.0065	0.64	3.13
7k	5.37	0.0029	6.39	0.0009	0.72	2.71
7l	3.31	0.0933	6.63	0.0006	0.79	2.46
7m	4.21	0.0206	6.49	0.0008	0.80	2.40
7n	2.48	0.3734	6.24	0.0012	0.81	2.34
7o	2.27	0.5290	5.51	0.0042	0.83	2.29
7p	3.51	0.0663	6.27	0.0011	0.84	2.23
7q	2.75	0.2390	5.90	0.0022	0.86	2.16
7r	2.88	0.1892	5.27	0.0063	0.87	2.12
7s	3.42	0.0772	5.84	0.0024	0.95	1.87
7t	3.04	0.1450	5.17	0.00750	0.98	1.75
7u	3.77	0.0430	6.07	0.00167	1.05	1.56
7v	2.62	0.2932	6.15	0.0014	1.11	1.41
7w	4.99	0.0055	6.56	0.0007	1.12	1.40
7x	3.28	0.0982	**0.00**	43.9596	1.13	1.37
7y	2.13	0.6683	5.69	0.0031	1.21	1.20
7z	4.19	0.0213	6.83	0.0004	1.29	1.05
7a´	2.97	0.1638	5.17	0.0075	1.33	0.97
7b´	3.96	0.0309	7.18	0.0002	1.39	0.89
7c´	4.88	0.0066	7.12	0.0002	1.39	0.89
7d´	4.81	0.0074	2.64	0.5246	1.40	0.87
7e´	3.02	0.1497	6.88	0.0004	1.46	0.79
7f´	3.28	0.0982	6.40	0.0009	1.46	0.78
7g´	2.67	0.2699	5.78	0.0027	1.48	0.77
7h´	2.94	0.1732	6.29	0.0011	1.51	0.73
7i´	0.27	15.131	4.31	0.0317	1.57	0.73
7j´	2.98	0.1624	7.18	0.0002	1.53	0.70
7k´	4.48	0.0131	7.15	0.0002	1.53	0.70
7l´	3.89	0.0350	1.97	1.6222	1.54	0.69
7m´	5.71	0.0016	7.11	0.0002	1.55	0.68
7n´	0.19	17.2954	4.20	0.0381	1.57	0.65
7o´	3.88	0.0353	7.04	0.0003	1.60	0.63
7p´	0.78	6.4513	4.88	0.0121	1.64	0.58
7q´	4.03	0.0278	6.09	0.0016	1.65	0.57
7r´	3.25	0.1023	6.64	0.0006	1.68	0.54

7s´	2.98	0.1600	6.99	0.0003	1.73	0.49
7t´	0.55	9.5766	0.47	19.8495	1.74	0.49
7u´	0.65	7.9857	4.53	0.0219	1.74	0.49
7v´	4.37	0.0156	6.86	0.0004	1.75	0.48
7w´	4.94	0.0060	7.12	0.0002	1.77	0.47
7x´	3.31	0.0933	3.39	0.1488	1.79	0.45
7y´	2.99	0.1590	6.80	0.0004	1.79	0.45
7z´	0.73	7.0075	4.56	0.0210	1.81	0.43
7a´´	2.90	0.1842	5.99	0.0018	1.82	0.43
7b´´	3.98	0.0299	7.20	0.0002	1.85	0.41
7c´´	4.78	0.0078	6.61	0.0006	1.90	0.37
7d´´	2.65	0.2801	6.39	0.0009	1.91	0.37
7e´´	3.93	0.0330	7.04	0.0003	1.94	0.35
7f´´	0.92	5.1328	4.43	0.0261	1.95	0.34
7g´´	**0.00**	23.89	4.95	0.0108	1.95	0.34
4h´´	3.21	0.1089	1.92	1.7435	1.96	0.34

[a]Energía relativa en Mecánica Molecular respecto a **7g´´**, E_{MMFF} = 55.1418 kcal/mol. [b]Población en % calculada de las energías de MMFF de acuerdo a $\Delta E_{MMFF} \approx -RT \ln K$. [c]Energía relativa en single-point B3LYP/6-31G(d) respecto a **7x**, $E_{6\text{-}31G(d)}$ = -840374.333 kcal/mol. [d]Población en % calculada de B3LYP/6-31G(d) energía respecto a $\Delta E_{6\text{-}31G(d)} \approx -RT \ln K$. [e] Energía relativa libre de Gibbs respecto a **7a**, $G_{PBEPBE/DGDZVP}$ = -840375.318 kcal/mol. [f]población en % calculada de la energía libre Gibbs de acuerdo a $\Delta G = -RT \ln K$.

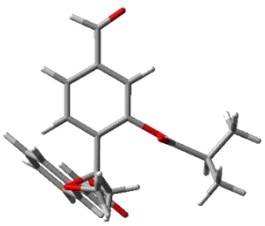

7a
9.16%

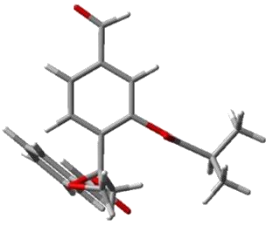

7b
7.93%

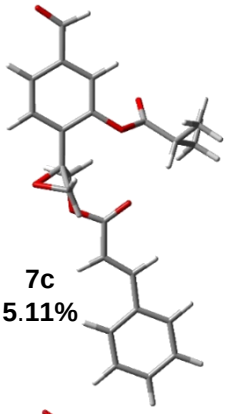

7c
5.11%

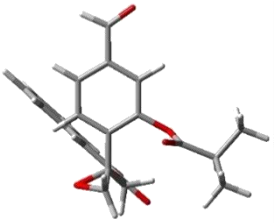

7d
4.41%

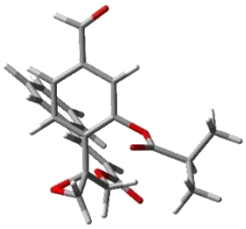

7e
4.38%

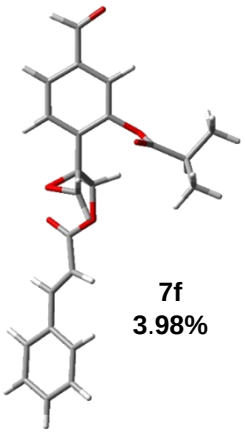

7f
3.98%

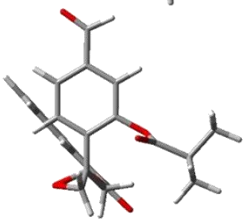

7g
3.94%

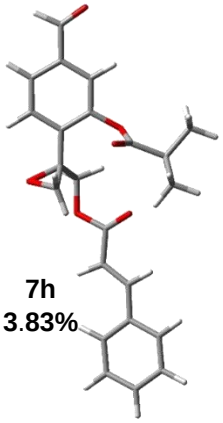

7h
3.83%

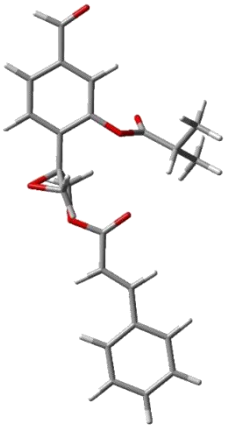

7i
3.67%

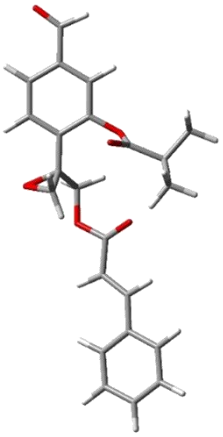

7j
3.13%

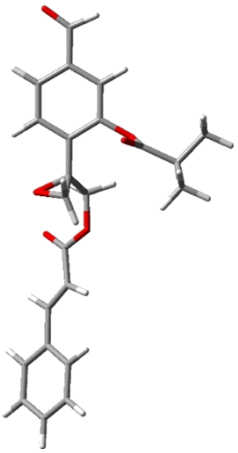

7k
2.71
%

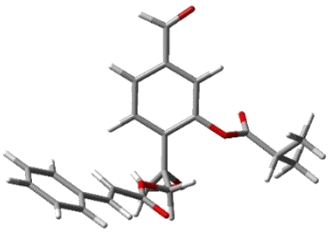

7l
2.46
%

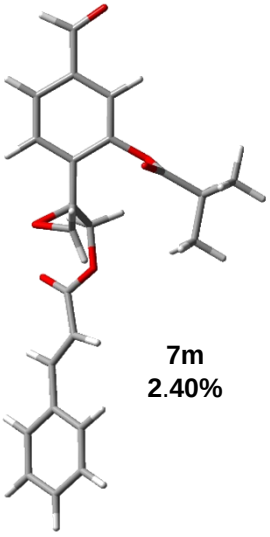

7m
2.40%

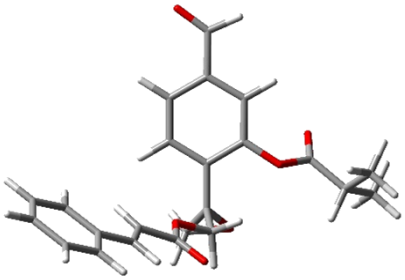

7n
2.34%

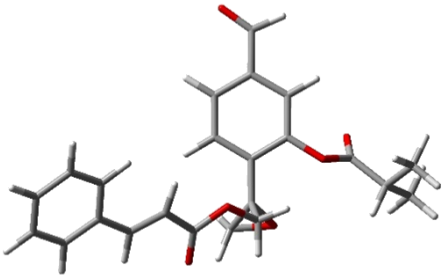

7o
2.29%

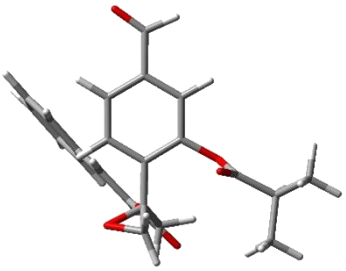

7p
2.23%

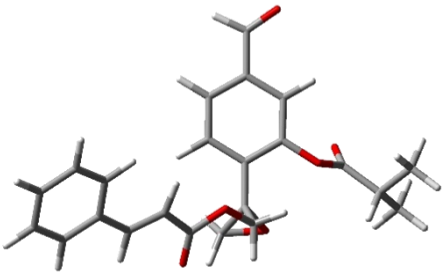

7q
2.16%

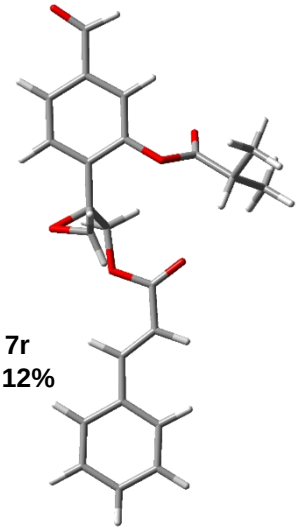

7r
2.12%

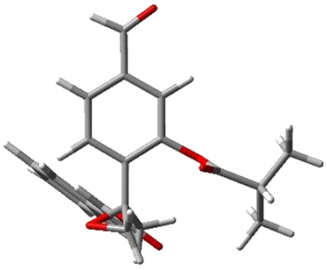

7s
1.87%

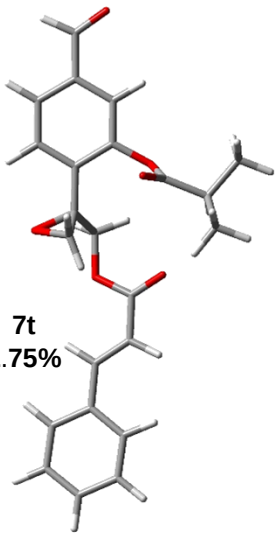

7t
1.75%

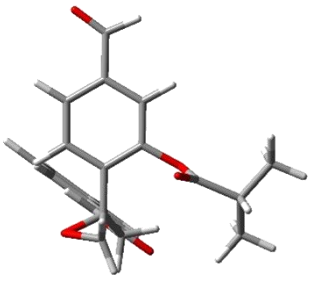

7u
1.56%

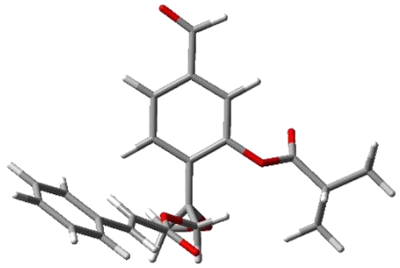

7v
1.41%

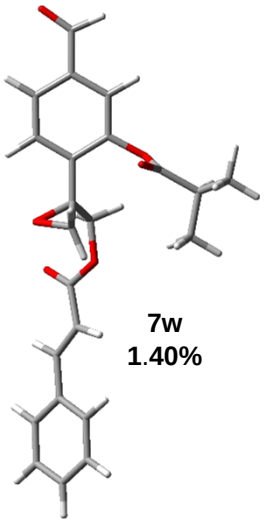

7w
1.40%

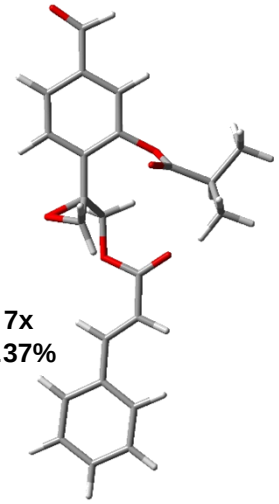

7x
1.37%

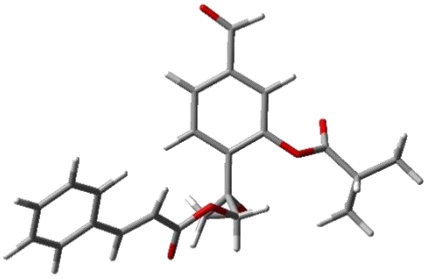

7y
1.20%

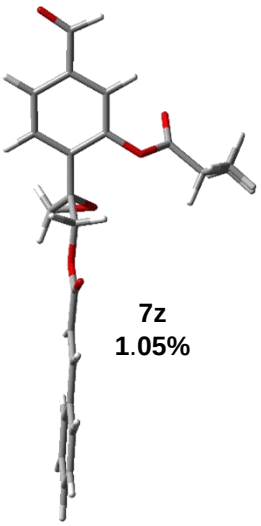

7z
1.05%

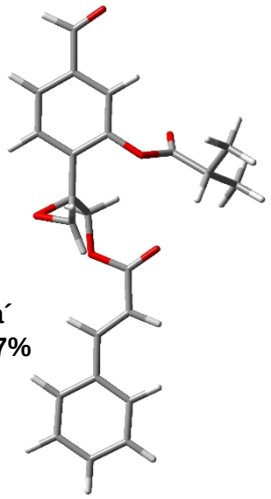

7a´
0.97%

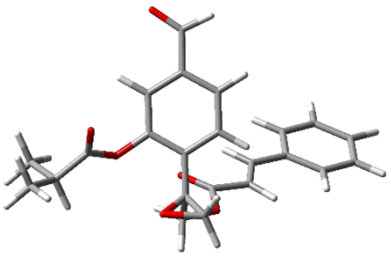

7b´
0.89%

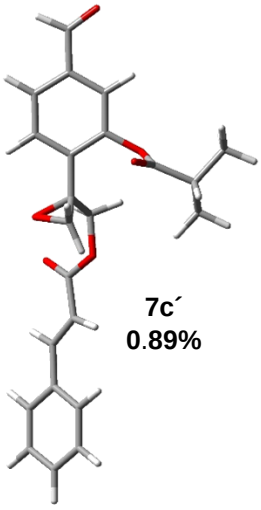

7c´
0.89%

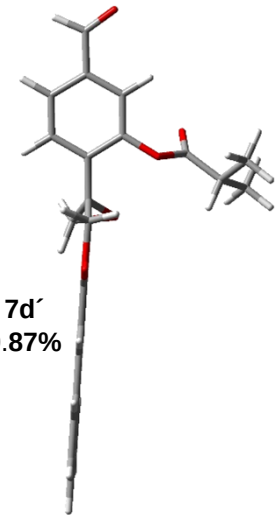

7d´
0.87%

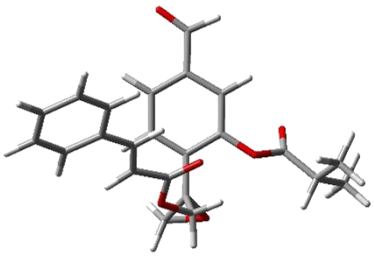

1e´
0.79%

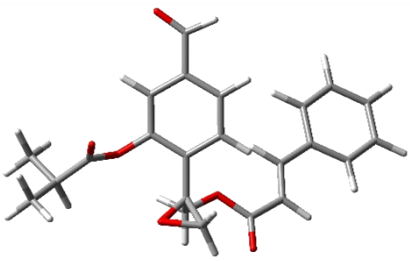

7f´
0.78%

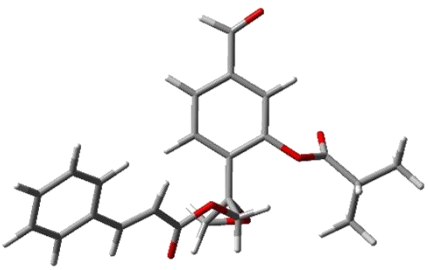

7g´
0.77%

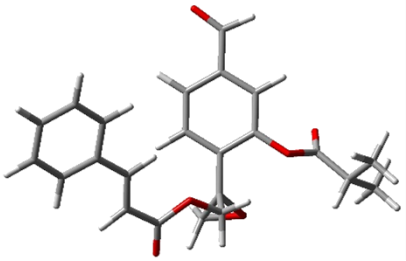

7h´
0.73%

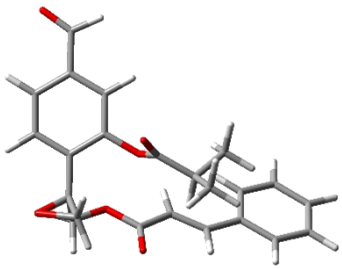

7i´
0.73%

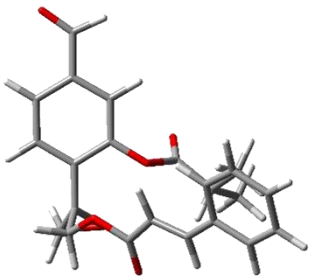

7j´
0.70%

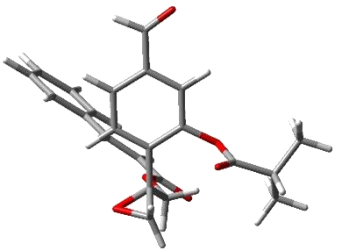

7k´
0.70%

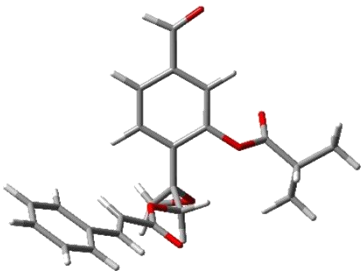

7l´
0.69%

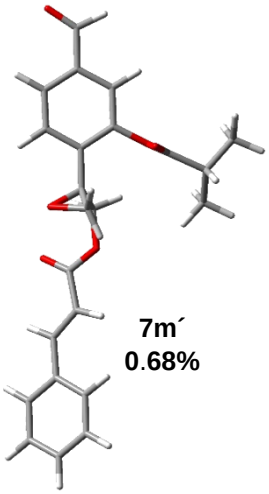

7m´
0.68%

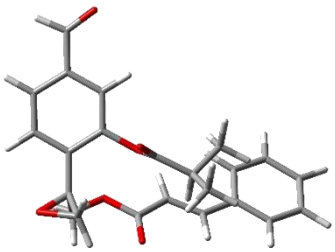

7n´
0.65%

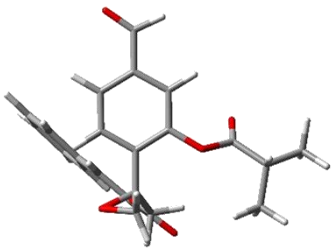

7o´
0.63%

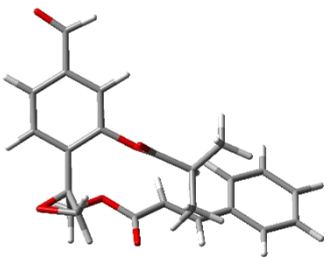

7p´
0.58%

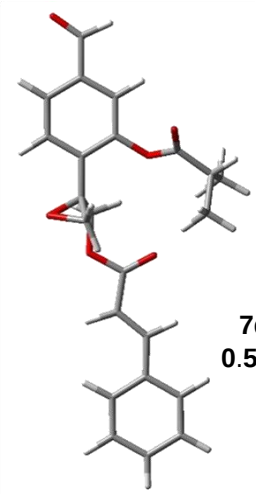

7q´
0.57%

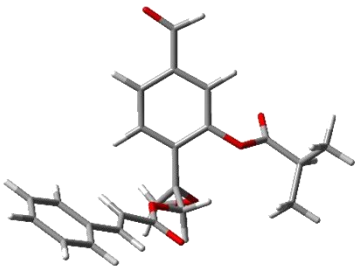

7r´
0.54%

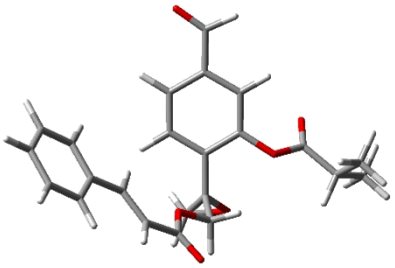

7s´
0.49%

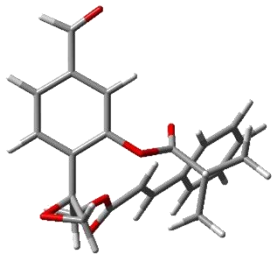

7t´
0.49%

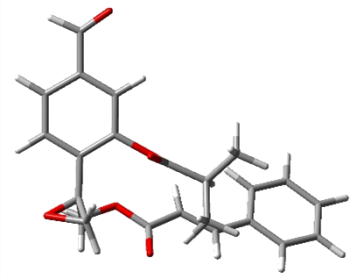

7u´
0.49%

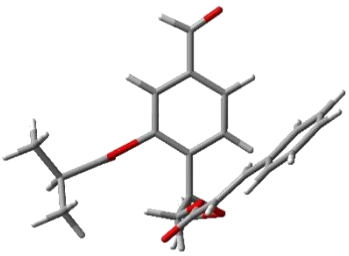

7v´
0.48%

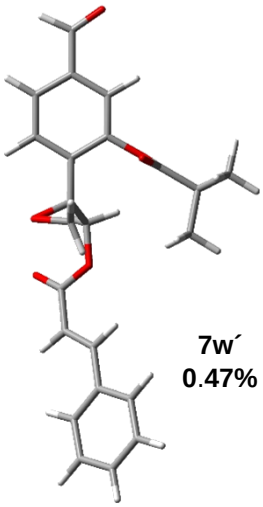

7w´
0.47%

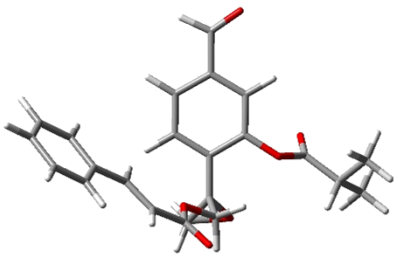

7x´
0.45%

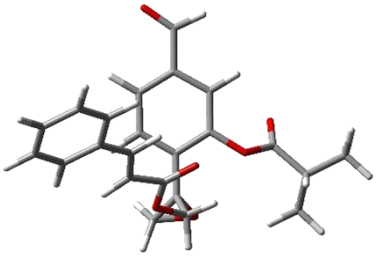

7y´
0.45%

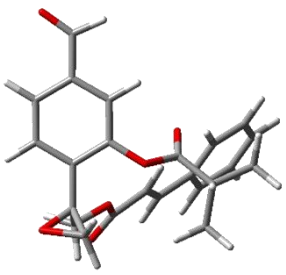

7z´
0.43%

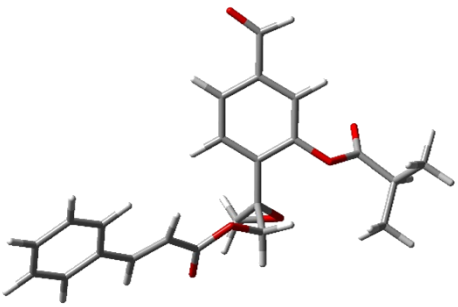

7a´´
0.43%

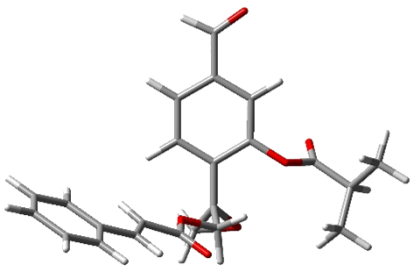

7b´´
0.41%

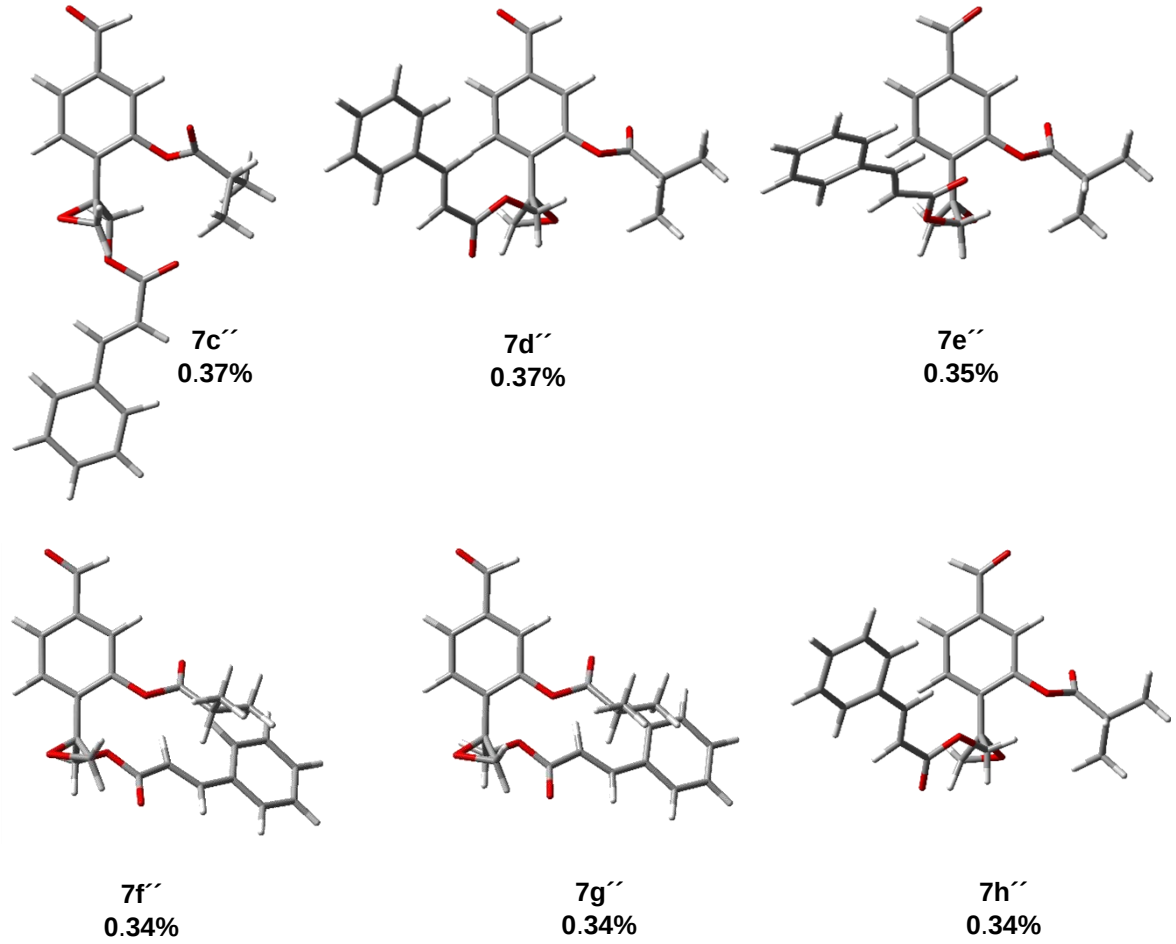

Figura A5.1. Conformeros de (+)-(8*S*) isobutirato de 10-cinamoiloxi-7-oxo-8,9-epoxitimol (**7**). que representan el 100% de la población conformacional.

ANEXO 6. **Generalidades del municipio de Villa Madero**, **Michoacán**

El municipio de Villa Madero, se localiza al este del estado de Michoacán en las coordenadas 19º23´ de latitud norte y 101º17´ de longitud oeste, a una altura de 2180 metros sobre el nivel del mar. Limita al norte con Morelia, al este con Tzitzio y Tiquicheo, al sur con Carácuaro y al oeste con Tacámbaro y Acuitzio (figura A6.1). Su relieve lo constituyen el sistema volcánico transversal; las sierras de Curupatzeo y Nocupetaro; y los Cerros de Porúa, Caracol, Moreno y Verde. Su hidrografía se constituye por el río Carácuaro y los arroyos de Porúa, Zirapio y por Juntas. El clima es templado, con lluvias en verano y en algunas partes tropical. Tiene una precipitación pluvial anual de 1654.5 mm y temperaturas que oscilan de 7.5ºC a 23.9ºC. En el municipio predominan los bosques: bosque mixto, con pino, encino y cedro; bosque tropical decíduo, con ceiba, parota, tepeguaje, zapote y mango. Los suelos del municipio datan de los periodos cenozoico, terciarios y paloceno; corresponden principalmente a los de tipo podzólico y chernozem (Enciclopedia de los municipios y delegaciones de México).

Figura A6.1 Municipio de Villa Madero Michoacán.

Anexo 7. Articulos publicados

JOURNAL OF NATURAL PRODUCTS

Article

pubs.acs.org/jnp

Absolute Configuration of Menthene Derivatives by Vibrational Circular Dichroism

Julio C. Pardo-Novoa,[†] Héctor M. Arreaga-González,[†] Mario A. Gómez-Hurtado,[†] Gabriela Rodríguez-García,[†] Carlos M. Cerda-García-Rojas,[*,‡] Pedro Joseph-Nathan,[‡] and Rosa E. del Río[*,†]

[†]Instituto de Investigaciones Químico Biológicas, Universidad Michoacana de San Nicolás de Hidalgo, Ciudad Universitaria, Morelia, Michoacán 58030, Mexico

[‡]Departamento de Química, Centro de Investigación y de Estudios Avanzados del Instituto Politécnico Nacional, Apartado 14-740, Mexico City 07000, Mexico

Supporting Information

ABSTRACT: The aerial parts of *Ageratina glabrata* afforded (−)-(3*S*,4*R*,5*R*,6*S*)-3,5,6-trihydroxy-1-menthene 3-*O*-β-D-glucopyranoside (**1**) and (−)-(3*S*,4*S*,6*R*)-3,6-dihydroxy-1-menthene 3-*O*-β-D-glucopyranoside (**3**). Acid hydrolysis of **1** yielded (+)-(1*R*,4*S*,5*R*,6*R*)-1,5,6-trihydroxy-2-menthene (**5**) and (+)-(1*S*,4*S*,5*R*,6*R*)-1,5,6-trihydroxy-2-menthene (**6**), while hydrolysis of **3** yielded (+)-(3*S*,4*S*,6*R*)-3,6-dihydroxy-1-menthene (**10**), (+)-(1*R*,4*S*,6*R*)-1,6-dihydroxy-2-menthene (**11**), and (+)-(1*S*,4*S*,6*R*)-1,6-dihydroxy-2-menthene (**12**). The structures of the new compounds **1**, **2**, **5**−**9**, and **11** were defined by 1D and 2D NMR experiments, while the absolute configurations of the series of compounds were determined by comparison of the experimental vibrational circular dichroism (VCD) spectra of the 1,6-acetonide 5-acetate derived from **6** and of the 1,6-acetonide derived from **12** with their DFT-calculated spectra. In addition, Flack and Hooft X-ray parameters of **10** permitted the same conclusion. The results further led to the absolute configuration reassignment of **10** isolated from *Brickellia rosmarinifolia*, *Mikania saltensis*, *Ligularia muliensis*, *L. sagitta*, and *Lindera strychnifolia*, as well as of **11** from *Cacalia tangutica*, as *ent*-**11**.

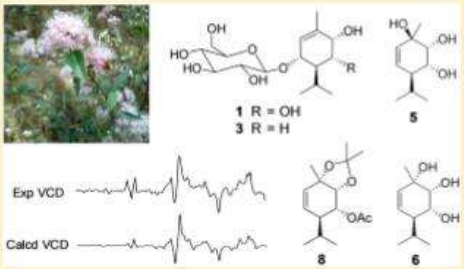

The Astereaceae family occupies an important niche in the Mexican flora since many of its species are listed in Mexican traditional medicine. This is the case for *Ageratina glabrata* (Kunth) R.M.King & H.Rob. (Asteraceae), popularly known as "chamizo blanco" (white greasewood), which is used as an analgesic. Such biological activity was established using the CH_2Cl_2 extract of the leaves.[1] In previous chemical studies of the nonpolar extracts from the aerial parts of *A. glabrata*, the presence of thymol derivatives, as main constituents, was evidenced,[2−5] while to date chemical studies of the polar extracts from this species have not been reported. In the present paper, the structure elucidation of the new (−)-(3*S*,4*R*,5*R*,6*S*)-3,5,6-trihydroxy-1-menthene 3-*O*-β-D-glucopyranoside (**1**) and the isolation of the known (−)-(3*S*,4*S*,6*R*)-3,6-dihydroxy-1-menthene 3-*O*-β-D-glucopyranoside (**3**) are reported. Full characterization of **1** and **3** was supported by derivatization and subsequent spectroscopic studies of **2** and **4**−**13**, while the absolute configuration (AC) for the whole series was established by comparison of the experimental and calculated vibrational circular dichroism (VCD) spectra of **8** and **13**, as well as by the Flack and Hooft X-ray parameters of **10**. Likewise, this study permitted the reassignment of the AC of **10** isolated from *Brickellia rosmarinifolia*,[6] *Mikania saltensis*,[7] *Ligularia muliensis*,[8] *Ligularia sagitta*,[9] and *Lindera strychnifolia*[10] and **11** from *Cacalia tangutica*.[11]

RESULTS AND DISCUSSION

Successive column chromatography of the methanol extract from the aerial parts of *A. glabrata* afforded (−)-(3*S*,4*R*,5*R*,6*S*)-3,5,6-trihydroxy-1-menthene 3-*O*-β-D-glucopyranoside (**1**) and (−)-(3*S*,4*S*,6*R*)-3,6-dihydroxy-1-menthene 3-*O*-β-D-glucopyranoside (**3**). The molecular formula of **1** was established as $C_{16}H_{28}O_8$ by HRESI/APCIMS, showing a sodium adduct molecular ion at *m*/*z* 371.1678 (calcd as 371.1676 for $C_{16}H_{28}O_8Na^+$). It showed a specific rotation value of −39 in MeOH. Its ^{1}H NMR data (400 MHz, methanol-d_4, Table 1) indicated H-2 as a multiplet at δ_H 5.69; the H-3, H-6, and H-5 signals appearing at δ_H 4.19 (br d, J = 7.9 Hz), 3.81 (d, J = 3.8 Hz), and 3.55 (dd, J = 10.5, 3.8 Hz), respectively; an isopropyl group at δ_H 2.17 (septd, J = 7.0, 3.3 Hz, H-8), 1.06 (d, J = 7.0 Hz, CH_3-9), and 1.05 (d, J = 7.0 Hz, CH_3-10); and a vinylic methyl group at δ_H 1.82 (br t, J = 1.4 Hz, CH_3-7). In addition, the seven

Received: May 28, 2016
Published: October 11, 2016

DOI: 10.1021/acs.jnatprod.6b00491
J. Nat. Prod. 2016, 79, 2570−2579

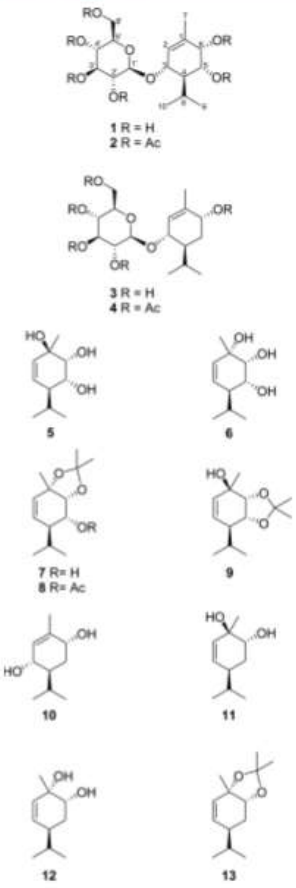

Figure 1. Menthene glucopyranosides **1** and **3**, isolated from *Ageratina glabrata*, and their derivatives **2** and **4**–**13**.

characteristic proton chemical shifts for a β-D-glucopyranosyl moiety were observed (Table 1). Its ^{13}C NMR spectrum showed 16 signals: the C-1 and C-2 vinylic carbon signals at δ_C 137.7 and 125.7, respectively; three oxymethines at δ_C 75.0 (C-3), 71.6 (C-6), and 70.8 (C-5); and the five remaining carbon signals of the aglycone portion within the δ_C 46.5–19.3 range. The typical chemical shifts for the carbons of the β-D-glucopyranosyl moiety resonated in the δ_C 101.6–63.0 region (Table 1). In the COSY spectrum of **1**, H-3 (δ_H 4.19) displayed correlations with H-2 (δ_H 5.69) and H-4 (δ_H 1.84), while H-5 (δ_H 3.55) showed a correlation with H-6 (δ_H 3.81) (Figure S2, Supporting Information). The HSQC spectrum allowed the unambiguous assignment of all the protonated carbons as listed in Table 1. The HMBC spectrum established the positional assignment since H-6 correlated with C-1, C-2, C-5, and C-7, while H-3 correlated with C-2, C-4, and the anomeric carbon (C-1′). This analysis indicated the presence of a trihydroxylated menthene skeleton bearing a glucopyranosyloxy unit at C-3. The relative configuration of **1** was deduced from the vicinal coupling constant values $J_{3,4}$ = 7.9 Hz, $J_{4,5}$ = 10.5 Hz, and $J_{5,6}$ = 3.8 Hz, as well as from the NOESY correlations of H-3 with H-5 and H-6. The ^{1}H and ^{13}C NMR spectra were also measured in DMSO-d_6 and in pyridine-d_5 in order to increase the pool of available data for future comparative purposes (Table 2). In order to confirm the presence of the hydroxy groups in **1**, it was peracetylated to afford compound **2**. The HRESI/APCIMS spectrum showed an $[M + Na]^+$ ion at m/z 623.2322 (calcd as 623.2310 for $C_{28}H_{40}O_{14}Na^+$), in agreement with the molecular formula $C_{28}H_{40}O_{14}$. The ^{1}H NMR data (Table 1) showed six methyl singlets within the δ_H 2.12–2.01 range, and the ^{13}C NMR spectrum displayed six carbonyl signals (δ_C 170.9–169.3) and six methyl signals (δ_C 21.0–20.6), reminiscent of the incorporation of six *O*-acetyl groups.

The molecular formula of **3** was determined as $C_{16}H_{28}O_7$ by HRESI/APCIMS, showing an $[M + Na]^+$ molecular ion at m/z 355.1735 (calcd as 355.1727 for $C_{16}H_{28}O_7Na^+$). Its ^{1}H NMR (400 MHz, methanol-d_4) spectrum showed the characteristic signals for a disubstituted menthene having one glucopyranosyl unit. Compound **3** was previously reported from *Ageratina anisochroma*[12] and *Telekia speciosa*;[13] however, the structure elucidation was based only on the ^{1}H NMR data in methanol-d_4.[12] Herein, the ^{1}H NMR data were also recorded in DMSO-d_6 and pyridine-d_5, while the ^{13}C and 2D NMR spectra were also measured in methanol-d_4, DMSO-d_6, and pyridine-d_5 (Tables 1 and 2). These spectra were useful to confirm the connectivity and the relative configuration of the molecule. Its ^{13}C NMR (100 MHz, methanol-d_4) spectrum showed 16 signals, including the C-1 and C-2 vinylic carbons at δ_C 138.5 and 127.1, respectively, and two oxymethine carbon atoms at δ_C 76.4 (C-3) and 68.2 (C-6). The typical carbon signals of the β-D-glucopyranosyl unit were observed in the δ_C 102.1–62.9 range. Analysis of the HSQC and HMBC spectra allowed the unambiguous assignment of the ^{13}C NMR data for **3** (Table 1 and Figures S29 and S30, Supporting Information). Peracetylation of **3** afforded **4**,[12] which confirmed the presence of the five hydroxy groups. The HRESI/APCIMS spectrum showed an $[M + Na]^+$ ion at m/z 565.2267 (calcd as 565.2255 for $C_{26}H_{38}O_{12}Na^+$) consistent with the molecular formula, $C_{26}H_{38}O_{12}$. The ^{1}H NMR spectrum in $CDCl_3$ was in agreement with that reported,[12] and the ^{13}C NMR spectrum, which displayed five carbonyl signals (δ_C 171.0–169.3) and five methyl signals (δ_C 21.2–20.7), is fully assigned in Table 1.

In order to determine the AC of **1** and **3** using the versatile VCD methodology of the corresponding aglycones, these compounds were subjected to acid hydrolysis.[14] The specific rotation and NMR spectra of the sugars arising from these reactions established the D-glucopyranosyl moieties in **1** and **3**, as carried out for the glycosylated compounds of *Ageratina cylindrica*.[29] Acid hydrolysis of **1** gave the menthene triol derivatives **5** and **6** (Scheme 1), while none of the expected 3,5,6-triol derivatives could be detected. This transformation can take place if, after hydrolysis of the glucose moiety (Scheme 1a), the protonated hydroxy group at C-3 acts as a leaving group, generating an allylic carbocation[15] at C-3, which can migrate to C-1 with the simultaneous shift of the double bond from the C-1=C-2 to the C-2=C-3 position. Finally, a H_2O molecule may stabilize the carbocation at C-1 to yield **5** or **6**, depending on the face of the attack. Alternatively, a concerted mechanism could also be possible, as depicted in Scheme 1b, in which the attack at C-1 of a H_2O molecule promotes the shift of the double bond from the C-1=C-2 to the C-2=C-3 position with the simultaneous departure of the protonated glucose moiety.

DOI: 10.1021/acs.jnatprod.6b00491
J. Nat. Prod. 2016, 79, 2570–2579

Table 1. NMR Data for Menthene Glucopyranosides 1 and 3 in Methanol-d_4 and 2 and 4 in $CDCl_3$ (δ in ppm)

	1[a]			2[b]			3[a]	4[b]
position	δ_C	δ_H, mult (J in Hz)	HMBC (H→C)	δ_C	δ_H, mult (J in Hz)	HMBC (H→C)	δ_C	δ_C
1	137.7			132.6			138.5	134.9
2	125.7	5.69, m	4, 6, 10	127.1	5.64, m	4, 6, 10	127.1	127.8
3	75.0	4.19, br d (7.9)	1, 2, 4, 7, 1′	74.8	4.10, br d (9.4)	1, 2, 4, 7, 1′	76.4	75.9
4	46.5	1.84, m	3, 8	42.8	2.03, m	3, 6, 7	40.8	40.0
5	70.8	3.55, dd (10.5, 3.8)	3, 4, 6	69.4	4.89, dd (11.4, 4.1)	3, 4, 6, Ac-5	30.5	26.4
6	71.6	3.81, d (3.8)	1, 2, 4, 10	68.7	5.39, br d (4.1)	1, 2, 4, 5, 10, Ac-6	68.2	69.4
7	20.8	1.82, br t (1.4)	1, 2, 6	20.2	1.71, br s	1, 2, 6	20.7	20.3
8	27.0	2.17, septd (7.0, 3.3)	3, 4, 5, 8, 9	25.2	2.10, m	4, 8, 9	26.3	25.0
9	21.4	1.06, d (7.0)	4, 7, 9	20.78	0.98, d (6.8)	4, 7, 9	21.4	20.64
10	19.3	1.05, d (7.0)	4, 7, 8	17.7	0.89, d (6.8)	4, 7, 8	17.1	16.4
1′	101.6	4.43, d (8.0)	3, 5′	98.6	4.64, d (8.2)	3, 3′, 5′	102.1	98.8
2′	75.1	3.15, dd (9.0, 8.0)	1′, 3′	71.5	4.96, dd (9.4, 8.2)	1′, 3′, Ac-2′	75.0	71.5
3′	78.1	3.37, dd (9.0, 8.0)	2′, 4′	73.0	5.22, t (9.4)	2′, 4′, Ac-3′	78.2	73.0
4′	71.9	3.31, m	5′, 6′	68.6	5.05, dd (10.0, 9.4)	3′, 5′, 6′, Ac-4′	71.8	68.7
5′	77.8	3.26, m		71.8	3.68, m	1′, 3′, 4′,	77.7	71.7
6′a	63.0	3.86, dd (11.7, 2.2)	4′, 5′	62.4	4.16, m	4′, 5′, Ac-6′	62.9	62.4
6′b		3.68, dd (11.7, 5.3)	4′, 5′		4.15, m	4′, 5′, Ac-6′		
Ac-5				170.2				170.4
				20.60	2.01, s	Ac-5		20.60
Ac-6				170.9				
				20.97	2.12, s	Ac-6		
Ac-2′				169.3				169.3
				20.60	2.00, s	Ac-2′		20.68
Ac-3′				170.3				170.6
				20.94	2.06, s	Ac-3′		20.71
Ac-4′				169.4				169.4
				20.72	2.04, s	Ac-4′		20.62
Ac-6′				170.6				171.0
				20.67	2.03, s	Ac-6′		21.24

[a]Measured at 400 MHz for ^1H and 100 MHz for ^{13}C using TMS as the internal reference. [b]Measured at 300 MHz for ^1H and 75.4 MHz for ^{13}C.

Table 2. NMR Data for Menthene Glucopyranosides 1 and 3 in DMSO-d_6 and in Pyridine-d_5 (δ in ppm)[a]

	1[b]		1[c]		3[b]		3[c]	
position	δ_C	δ_H, mult (J in Hz)	δ_C	δ_H, mult (J in Hz)	δ_C	δ_H, mult (J in Hz)	δ_C	δ_H, mult (J in Hz)
1	135.1		137.1		137.1		138.9	
2	125.1	5.52, br s	126.4	6.03, br s	125.5	5.49, br s	126.6	6.01, br s
3	73.4	3.98, br d (9.4)	75.1	4.54, br d (9.1)	74.4	3.93, br d (9.3)	75.9	4.44, br d (9.0)
4	44.1	1.64, ddd (11.3, 9.4, 1.8)	46.4	2.44, ddd (10.7, 9.1, 1.9)	39.0	1.64, m	40.7	2.32, m
5β	68.9	3.27, dd (11.3, 3.8)	70.7	3.86, br d (10.7)	29.6	1.26, td (13.3, 4.1)	31.1	1.55, td (13.3, 4.1)
5α						1.57, dt (13.3, 2.6)		2.05, dt (13.3, 2.8)
6	69.9	3.60, d (3.8)	71.6	4.22, br s	65.7	3.76, br s	67.5	4.25, br s
7	20.6	1.68, br s	21.6	1.91, br s	20.5	1.67, br s	21.4	1.92, br s
8	24.7	2.15, m	26.5	2.80, septd (7.0, 1.9)	24.7	2.08, septd (6.9, 3.1)	26.1	2.54, septd (6.9, 3.0)
9	20.9	0.96, d (7.2)	22.3	1.32, d (7.0)	20.9	0.84, d (6.9)	21.6	0.94, d (6.9)
10	18.3	0.93, d (7.2)	19.3	1.32, d (7.0)	16.5	0.73, d (6.9)	17.4	0.93, d (6.9)
1′	100.3	4.24, d (8.5)	102.5	5.09, d (8.5)	100.9	4.22, d (8.3)	103.0	5.07, d (8.0)
2′	73.5	2.89, t (8.5)	75.7	4.04, t (8.5)	73.5	2.90, t (8.3)	75.6	4.05, t (8.0)
3′	77.1	3.13, t (8.5)	79.2	4.32, t (8.5)	77.1	3.13, t (8.3)	79.2	4.33, t (8.0)
4′	70.5	3.03, dd (9.6, 8.5)	72.7	4.23, t (8.5)	70.4	3.03, m	72.5	4.30, t (8.0)
5′	76.7	3.07, m	78.9	4.00, m	76.7	3.06, m	78.7	3.98, m
6′a	61.5	3.63, dd (11.5, 1.6)	63.8	4.59, br d (11.7)	61.4	3.64, br d (11.2)	63.6	4.57, br d (11.0)
6′b		3.38, dd (11.5, 5.8)		4.40, dd (11.7, 4.4)		3.39, br d (11.2)[d]		4.41, br d (11.0)

[a]Measured at 300 MHz for ^1H and 75.4 MHz for ^{13}C using TMS as the internal reference. [b]In DMSO-d_6. [c]In pyridine-d_5. [d]Partially overlapped with the HOD signal.

The molecular formula of **5** was established as $C_{10}H_{18}O_3$ by HRESI/APCIMS, displaying a molecular ion at m/z 186.1256 (calcd as 186.1251 for $C_{10}H_{18}O_3^+$). Its ^1H NMR (400 MHz, $CDCl_3$) spectrum displayed two vinylic proton signals at δ_H 5.62 (ddd, J = 10.1, 2.2, 1.4 Hz, H-2) and 5.68 (dd, J = 10.1, 2.1 Hz, H-3), the signals for the oxymethine hydrogens appeared at δ_H 3.97

DOI: 10.1021/acs.jnatprod.6b00491
J. Nat. Prod. 2016, 79, 2570−2579

Scheme 1. Putative Reaction Mechanisms for the Hydrolysis of 1 To Yield Trihydroxymenthene Derivatives 5 and 6: (a) Stepwise Mechanism Involving Allylic Carbocations and (b) Concerted Mechanism

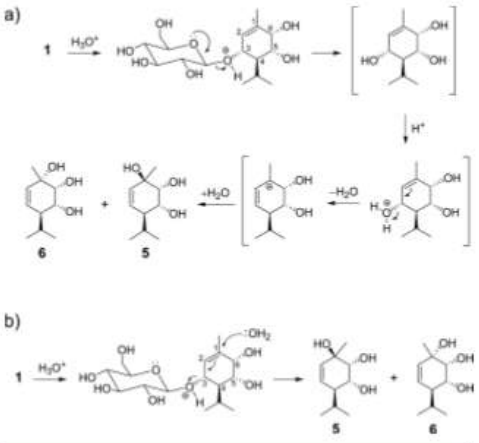

(dd, J = 8.4, 2.7 Hz, H-5) and 3.73 (dd, J = 2.6, 1.3 Hz, H-6), the H-4 methine showed a mutliplet at δ_H 2.16, the isopropyl group showed characteristic signals at δ_H 2.11 (m, H-8), 1.04 (d, J = 6.8 Hz, H-9), and 0.85 (d, J = 6.8 Hz, H-10), and the 7-methyl group was observed as a sharp singlet at δ_H 1.40 (Table 3). Its ^{13}C NMR (100 MHz, $CDCl_3$) spectrum showed 10 signals (Table 4), of which the two vinyl carbon signals appeared at δ_C 131.0 (C-2) and 129.4 (C-3), and the signals for three oxymethine carbon atoms resonated at δ_C 77.1 (C-6), 68.4 (C-5), and 71.3 (C-1). The COSY spectrum confirmed the vicinity of H-5 (δ_H 3.97) with H-6 (δ_H 3.73) and H-4 (δ_H 2.16). The unambiguous assignment of the ^{13}C NMR spectrum was done via the HETCOR and HMBC spectra, which also established the positions of the functional groups in the menthene skeleton. The NOESY data confirmed the relative configuration through correlations between H-5 and H-6, as well as between H-4 and CH_3-7, indicating the *cis* relationship between the hydroxy groups at C-5 and C-6 and between H-4 and CH_3-7 (Figure S51, Supporting Information).

In turn, **6** displayed an $[M + Na]^+$ ion at m/z 209.1156 (calcd as 209.1148 for $C_{10}H_{18}O_3Na^+$), in agreement with the molecular formula, $C_{10}H_{18}O_3$. Although the ^1H and ^{13}C NMR spectra resembled those of **5** (Tables 3 and 4), there were evident changes in the chemical shifts of the H-4 (δ_H 2.19), H-7 (δ_H 1.29), and H-8 (δ_H 1.83) signals. The COSY spectrum confirmed the vicinity of H-5 (δ_H 3.92) to H-4 (δ_H 2.19) and H-6 (δ_H 3.66), while the ^{13}C NMR (100 MHz, $CDCl_3$) spectrum exhibited 10 signals, of which the chemical shifts at δ_C 132.4 (C-2), 127.1 (C-3), 75.0 (C-6), 71.0 (C-5), and 71.1 (C-1) showed clear differences when compared with those observed for **5**. The HETCOR and HMBC spectroscopic data were sufficient to allow the full assignment of all ^{13}C NMR signals. The HMBC spectrum displayed correlations of H-6 (δ_H 3.66) with C-1 (δ_C 71.1), C-2 (δ_C 132.4), and C-4 (δ_C 47.4), while H-5 (δ_H 3.92) showed correlations with C-3 (δ_C 127.1) and C-4 (δ_C 47.4). The relative configuration was established using the NOESY correlations of H-6 with H-5 and H-7 indicative of the all-*cis*

Table 3. ^1H NMR Data for Menthene Derivatives 5–13 in $CDCl_3$ (δ in ppm, J in Hz)

position	5[a]	6[a]	7[a]	8[b]	9[b]	11[b]	12[a]	13[b]
2	5.62, ddd (10.1, 2.2, 1.4)	5.65, dd (10.4, 1.2)	5.51, dd (10.4, 1.4)	5.53, m	5.79, dd (10.0, 3.6)	5.62, ddd (10.0, 2.4, 0.8)	5.55, ddd (10.4, 2.8, 1.6)	5.48, ddd (10.4, 2.7, 1.7)
3	5.68, dd (10.1, 2.1)	5.62, dd (10.4, 2.8)	5.47, br d (10.4)	5.48, dd (10.5, 1.1)	5.57, dd (10.0, 2.6)	5.71, dd (10.0, 3.0)	5.65, ddd (10.4, 2.8, 1.0)	5.58, dt (10.4, 1.6)
4	2.16, m	2.19, m	2.28, br d (9.9)	2.60, br d (10.5)	2.11, m	2.14, ddt (12.4, 6.8, 3.0)	2.19, ddt (14.4, 5.6, 2.8)	2.23, m
5α						1.83, ddd (13.6, 6.8, 3.2)	1.88, dtd (14.2, 5.8, 1.0)	2.07, dddd (14.0, 5.1, 3.7, 2.0)
5β	3.97, dd (8.4, 2.7)	3.92, dd (5.6, 2.4)	3.58, br d (9.9)	4.99, dd (10.4, 2.2)	4.13, dd (7.6, 5.5)	1.73, td (13.6, 7.6)	1.63, t (14.2)	1.42, ddd (14.0, 11.4, 2.0)
6	3.73, dd (2.6, 1.3)	3.66, br d (2.4)	4.12, br t (1.6)	4.06, br t (2.2)	4.03, d (7.6)	3.80, dd (7.6, 3.2)	3.76, dt (5.6, 1.6)	4.05, dt (3.7, 2.0)
7	1.40, s	1.29, s	1.36, s	1.38, s	1.26, s	1.30, s	1.26, s	1.29, s
8	2.11, m	1.83, septd (6.8, 1.2)	2.20, septd (7.0, 2.5)	1.83, septd (7.0, 2.8)	1.88, m	1.70, m	1.62, m	1.66, septd (6.7, 1.8)
9	1.04, d (6.8)	1.00, d (6.8)	1.05, d (7.0)	1.00, d (7.0)	1.00, d (6.8)	0.93, d (7.0)	0.88, d (6.8)	0.90, d (6.7)
10	0.85, d (6.8)	0.89, d (6.8)	0.83, d (7.0)	0.78, d (7.0)	0.95, d (6.8)	0.92, d (7.0)	0.87, d (6.8)	0.88, d (6.7)
12			1.41, s	1.40, s	1.48, d (0.6)			1.38, br s (0.4)
13			1.38, s	1.39, s	1.38, d (0.6)			1.36, br s (0.4)
Ac-5				2.16, s				

[a]Measured at 400 MHz using TMS as the internal reference. [b]Measured at 300 MHz.

DOI: 10.1021/acs.jnatprod.6b00491
J. Nat. Prod. 2016, 79, 2570−2579

Table 4. ^{13}C NMR Data for Menthene Derivatives 5−13 in $CDCl_3$ (δ in ppm)

position	5[a]	6[a]	7[a]	8[b]	9[b]	11[b]	12[a]	13[b]
1	71.3	71.1	80.0	109.0	71.9	70.9	70.2	77.5
2	131.0	132.4	131.3	131.6	134.9	131.9	131.9	130.9
3	129.4	127.1	125.0	124.7	127.7	132.1	131.1	130.2
4	44.6	47.4	43.7	40.3	45.1	38.4	37.5	35.6
5	68.4	71.0	69.3	70.6	74.4	28.7	29.3	26.6
6	77.1	75.0	82.4	80.0	82.3	73.4	72.7	78.5
7	25.5	26.6	24.9	24.4	23.5	23.5	27.0	24.8
8	27.0	28.6	25.9	26.1	30.6	31.8	31.5	31.2
9	20.8	21.2	20.8	20.5	20.1	19.9	19.6	19.3
10	17.7	19.0	17.0	17.0	19.0	19.8	19.4	19.0
11			108.6	80.2	108.3			107.3
12			27.7	27.7	26.8			27.6
13			27.5	27.5	25.0			27.5
Ac-5				170.8				
				21.3				

[a]Measured at 100 MHz. [b]Measured at 75.4 MHz using TMS as the internal reference.

orientations of the hydroxy groups at C-1, C-5, and C-6 (Figure S57, Supporting Information).

To gain chemical support for the positional assignment of the hydroxy groups at C-1 in **5** and **6**, the corresponding acetonide derivatives were prepared. Thus, triol **6** afforded acetonide **7**, established as $C_{13}H_{22}O_3$ by HRESI/APCIMS, displaying an $[M + NH_4]^+$ ion at m/z 244.1908 (calcd as 244.1907 for $C_{13}H_{22}O_3 + NH_4^+$). Its ^1H NMR (400 MHz, $CDCl_3$) spectrum displayed a significant low-field shift of H-6 (δ_H 4.12) and showed two methyl signals at δ_H 1.41 and 1.38 arising from the acetonide moiety. The signal for H-5 was observed at δ_H 3.58 as a broad doublet (J = 9.9 Hz) (Table 3), while the COSY spectrum showed correlations of H-5 (δ_H 3.58) with H-6 (δ_H 4.12) and H-4 (δ_H 2.28). The ^{13}C NMR (100 MHz, $CDCl_3$) spectrum displayed the three signals at δ_C 108.6 (C), 27.7 (CH_3), and 27.5 (CH_3) of the acetonide moiety. Significant differences in the C-1 and C-6 chemical shifts of **7** with respect to **6** were observed, confirming that the acetonide group was located at C-1 and C-6 and not at C-5 and C-6 (Table 4). The HETCOR and HMBC spectra facilitated the unequivocal assignment of the carbon signals of the menthene skeleton of **7** (Figures S65 and S66, Supporting Information), while the presence of the C-5 hydroxy group was chemically confirmed by formation of the corresponding acetylated acetonide menthene derivative **8** (Tables 3 and 4). In turn, menthene triol **5** gave acetonide **9**. Its ^1H NMR spectrum (300 MHz, $CDCl_3$) showed significant differences in the chemical shifts in comparison with **5**. Both H-2 and H-3 appeared as double doublets at δ_H 5.79 (1H, dd, J = 10.0, 3.6 Hz), and 5.57 (1H, dd, J = 10.0, 2.6 Hz). The oxymethine hydrogen atoms resonated at δ_H 4.13 (1H, dd, J = 7.6, 5.5 Hz, H-5) and 4.03 (1H, d, J = 7.6 Hz, H-6), which indicated the presence of the acetonide group at OH-5 and OH-6. The two signals for the acetonide methyl groups were observed at δ_H 1.48 (d, J = 0.6 Hz) and 1.38 (d, J = 0.6 Hz) (Table 3). The ^{13}C NMR spectrum (75.4 MHz, $CDCl_3$) showed 13 signals, including the carbon signals for the acetonide group at δ_C 108.3 (C), 26.8 (CH_3), and 25.0 (CH_3). Significant differences for C-5 (δ_C 74.4) and C-6 (δ_C 82.3) were observed in comparison with those of **5**, suggesting the formation of the C-5/C-6 acetonide (Table 4).

In contrast to compound **1**, acid hydrolysis of menthene glucoside **3** gave the expected menthenediol **10**, together with epimeric compounds **11** and **12**. Diol **10** was obtained as colorless needles (mp 166−168 °C) and had a specific rotation of +10 (c 0.54, MeOH). The ^1H and ^{13}C NMR data were identical to those obtained for the compound isolated from *Ligularia sagitta*,[9] although no specific rotation values were reported. Comparison of the AC and the specific rotation data of **10** and *ent*-**10** with reported data showed some inconsistencies. The first report of the AC determination of **10** (lit.[16] $[\alpha]_D$ +28) referred to its preparation by reduction of 3,6-endoperoxide-1-menthene isolated from *Chenopodium multifidum*.[16] The authors assumed the (+)-(3*S*,4*S*,6*R*)-3,6-dihydroxy-1-menthene (**10**) structure by comparison of the specific rotation with that of (−)-*ent*-**10**, which was prepared from (−)-(*R*)-α-phellandrene.[17] The same reaction sequence was also used to define the configuration of several menthene derivatives.[18−20] Nonetheless, in a chemical study of *Mikania saltensis*,[7] *ent*-**10** was reported with a dextrorotatory specific rotation of +114 (at unspecified wavelength), contrasting with the results from the study of **10** from *Chenopodium multifidum*.[16] In more recent papers on the medicinal plants *Brickellia rosmarinifolia*,[6] *Ligularia muliensis*,[8] *Ligularia sagitta*,[9] and *Lindera strychnifolia*[10] and on the mixture of *Amomum tsao-ko*, *Artemisia scoparia*, *Chrysanthemum indicum*, *Eupatorium fortunei*, and *Houttuynia cordata* contained in a Chinese multiherb remedy,[21] the AC of the 3,6-dihydroxy-1-menthene **10** was defined on the basis of the data given in the chemical study of *Mikania saltensis*.[7]

Compound **11** was obtained as colorless oil, whose molecular formula was confirmed as $C_{10}H_{18}O_2$ by HRESI/APCIMS displaying an $[M + NH_4]^+$ ion at m/z 188.1637 (calcd as 188.1645 for $C_{10}H_{18}O_2 + NH_4^+$). This compound had a specific rotation of +58 (c 0.9, $CHCl_3$). Its structure was supported by the ^1H, ^{13}C, and 2D NMR data. In particular, the NOESY spectrum showed a cross-peak between H-4 and CH_3-7, which accounted for their *cis* relationship. The ^1H and ^{13}C NMR spectroscopic data of **11** (Tables 3 and 4) were similar to those of *ent*-**11** (lit.[22] $[\alpha]_D$ −46, c 1.0, $CHCl_3$), which was obtained by microbial transformation of (−)-(*R*)-α-phellandrene.[22] However, in the chemical study of *Cacalia tangutica*,[11] **11** is reported to possess a levorotatory specific rotation of −24 (c 1.38, $CHCl_3$), which is in disagreement with the current results.

The menthenediol **12** was obtained as colorless oil with a specific rotation of +43 (c 0.65, $CHCl_3$). The NMR spectroscopic data (Tables 3 and 4) were similar to those of an isolate from the essential oil of *Chenopodium multifidum* (lit.[23] $[\alpha]_D$ +40, c 0.92, $CHCl_3$). The relative configuration of **12** was confirmed

DOI: 10.1021/acs.jnatprod.6b00491
J. Nat. Prod. 2016, 79, 2570−2579

by NOESY (Figure S93, Supporting Information) data, since a cross-peak was observed between H-6 and CH_3-7. Also, the corresponding acetonide **13** showed $[\alpha]_D$ +13 (*c* 0.57, $CHCl_3$). This derivative was also prepared in the *C. multifidum* study; however, surprisingly the specific rotation was very different (lit.[23] $[\alpha]_D$ −143, *c* 0.25, $CHCl_3$) from that of our compound.

Because of all these discrepancies, the AC of natural and prepared menthene derivatives **1**−**13** needed more scrutiny, and therefore the determination of the AC by VCD of selected derivatives was undertaken. This spectroscopic technique requires a comparison of both the experimental and calculated VCD and IR spectra and has been successfully employed in the AC determination of many monoterpenes.[24,25] Molecular models of (1*S*,4*S*,5*R*,6*R*)-**8** and (1*S*,4*S*,6*R*)-**13** were built, and their conformer distribution was explored with the Monte Carlo protocol using the Merck Molecular Force Field.[26] An energy window of 10 kcal/mol produced nine conformers for **8** and six for **13**. Those conformations within a 5 kcal/mol energy range, three for **8** and five for **13**, were subjected to single-point DFT energy calculation at the B3LYP/6-31G(d) level of theory, followed by geometry optimization at the B3LYP/DGDZVP level[27] for those structures within an energy range of 3 kcal/mol. This procedure yielded three conformers for both **8** and **13**, corresponding to the three rotamers of the isopropyl group, as depicted in Figures 2 and 3, where it can be visualized that

8a (*P* = 94.7%)

8b (*P* = 4.7%)

8c (*P* = 0.4%)

Figure 2. Most relevant conformers of (+)-(1*S*,4*S*,5*R*,6*R*)-5-acetyloxy-1,6-dihydroxy-2-menthene 1,6-acetonide (**8**), accounting for 99.8% of the conformational population.

the cyclohexene ring exists in a single conformation. Table 5 summarizes the thermochemical data for the **8a**−**c** and **13a**−**c** conformers, respectively. The IR/VCD frequencies were calculated for the three rotamers, and the conformational populations were obtained by means of the $\Delta G = -RT \ln K$ equation to generate the Boltzmann-averaged IR and VCD spectra. Figures 2 and 3 show the minimum energy structures of the conformers

13a (*P* = 50.1%)

13b (*P* = 32.4%)

13c (*P* = 17.4%)

Figure 3. Most relevant conformers of (+)-(1*S*,4*S*,6*R*)-1,6-dihydroxy-2-menthene 1,6-acetonide (**13**), accounting for 99.9% of the conformational population.

Table 5. Thermochemical Analysis of (+)-(1*S*,4*S*,5*R*,6*R*)-5-Acetyloxy-1,6-dihydroxy-2-menthene 1,6-Acetonide (8) and (+)-(1*S*,4*S*,6*R*)-1,6-Dihydroxy-2-menthene 1,6-Acetonide (13)

conformer	ΔE_{MMFF} [a]	$\%_{MMFF}$ [b]	ΔE_{DFT} [c]	ΔE_{OPT} [d]	ΔG_{OPT} [e]	$\%_{OPT}$ [f]
8a	0.00	80.6	0.00	88.6	0.00	94.7
8b	0.89	17.8	1.26	10.4	1.76	4.7
8c	2.35	1.5	2.70	0.9	3.19	0.4
13a	0.00	47.1	0.00	42.3	0.00	50.1
13b	0.07	41.2	0.05	38.4	0.25	32.4
13c	0.85	11.2	0.47	19.0	0.62	17.4

[a]Molecular mechanics energies relative to **8a**, E_{MMFF} = 42.183 kcal/mol, and to **13a**, E_{MMFF} = 37.924 kcal/mol. [b]Population in % calculated from the MMFF energies according to $\Delta E_{MMFF} \approx -RT \ln K$. [c]Single-point B3LYP/6-31G(d) energies relative to **8a**, $E_{6\text{-}31G(d)}$ = −556 589.884 kcal/mol, and to **13a**, $E_{6\text{-}31G(d)}$ = −413 573.847 kcal/mol. [d]Population in % calculated from B3LYP/6-31G(d) energies according to $\Delta E_{6\text{-}31G(d)} \approx -RT \ln K$. [e]Gibbs free energies relative to **8a**, G_{DGDZVP} = −556 438.652 kcal/mol, and to **13a**, G_{DGDZVP} = −413 441.275 kcal/mol. [f]Population in % calculated from Gibbs free energies according to $\Delta G = -RT \ln K$.

of **8** and **13**, respectively, while Figures 4 and 5 demonstrate the good agreement of the experimental and calculated VCD and IR spectra for **8** and **13**, respectively.

Visual comparison of experimental and calculated VCD spectra is in general sufficient to decide if the calculated enantiomer is the correct one, although statistical methods are helpful to quantitatively evaluate the agreement. The quantitative approximation of the spectral similarity was accomplished by using the CompareVOA algorithm[28] (BioTools Inc., Jupiter, FL, USA), which compares the integrated overlap of the experimental and calculated data. The optimal anharmonicity factors (anH)

DOI: 10.1021/acs.jnatprod.6b00491
J. Nat. Prod. 2016, 79, 2570−2579

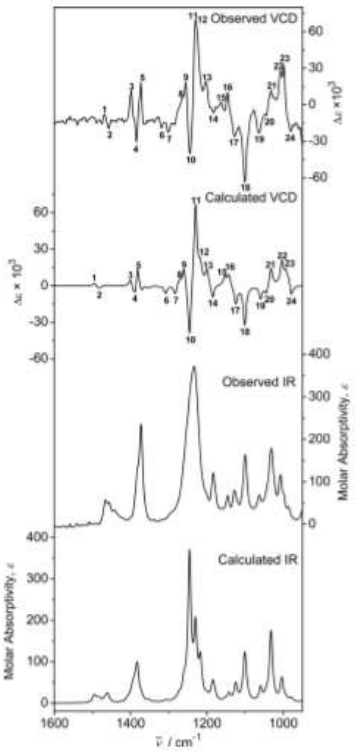

Figure 4. Comparison of the experimental and B3LYP/DGDZVP-calculated VCD and IR spectra of (+)-(1*S*,4*S*,5*R*,6*R*)-5-acetyloxy-1,6-dihydroxy-2-menthene 1,6-acetonide (**8**).

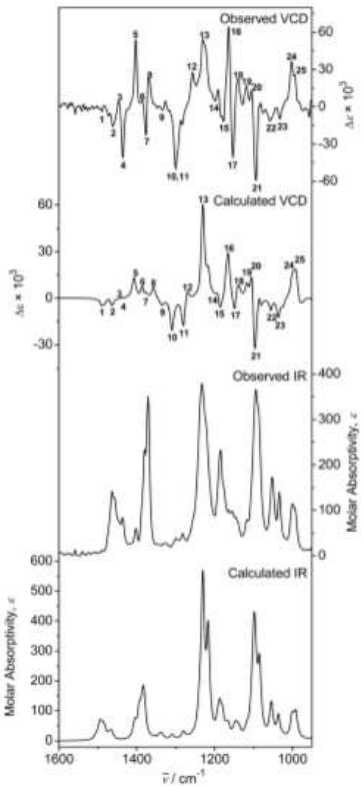

Figure 5. Comparison of the experimental and B3LYP/DGDZVP-calculated VCD and IR spectra of (+)-(1*S*,4*S*,6*R*)-1,6-dihydroxy-2-menthene 1,6-acetonide (**13**).

and the VCD spectroscopic similarities for the correct (S_E) and the incorrect enantiomers (S_{-E}) of each compound are listed in Table 6, together with the enantiomer similarity index (ESI) values, indicating that the structures of (1*S*,4*S*,5*R*,6*R*)-**8** and (1*S*,4*S*,6*R*)-**13** have the correct AC [100% confidence (*C*)] according to the employed algorithm.[28]

During the exploration of VCD spectroscopy of natural products we have found that a specific spectrum is not straightforwardly comparable to others, especially if there are changes in one stereogenic center or when an additional stereogenic center is added. These differences are valuable because the method, besides distinguishing between enantiomers, is also capable of differentiating among stereoisomers, as has been done for monoterpenes,[29] sesquiterpenoids,[30,31] diterpenoids,[32] and a triterpenoid,[33] or between closely related compounds as in the present study. The normal modes of vibration of the calculated VCD bands for **8** and **13** were contrasted with those found in their respective experimental spectra. Also, the main differences between the experimental spectra of **8** and **13** were in good agreement with the expected vibrational changes when going from one compound to the other. The negative band labeled as 10 in compound **8** (Figure 4) is due to the O−CO stretching of the acetyl group, which is absent in **13** (Figure 5). In compound **13**, negative bands 4 and 10, 11 (Figure 5) are mainly due to bending of the C-5 methylene (scissoring and wagging, respectively), while the positive band 16 arises from the twisting vibration of this same methylene group. In addition, the negative band labeled as 17 in **13** originates from vibrations associated with the C-4−C-5 and C-5−C-6 stretching motions, which are modified in **8**. The positive bands labeled as 11 in **8** and 13 in **13** are due to the O−C−O stretching of the acetonide groups present in both compounds. To facilitate this comparison,

Table 6. Confidence Level Data for the IR and VCD Spectra of 8 and Two Epimers of 13, Calculated at the B3LYP/DGDZVP Level of Theory

compound	anH[a]	S_{IR}[b]	S_E[c]	S_{-E}[d]	ESI[e]	C[f] (%)
(1*S*,4*S*,5*R*,6*R*)-**8**	0.98	96.5	81.7	11.9	69.8	100
(1*S*,4*S*,6*R*)-**13**	0.98	92.6	85.4	8.0	77.4	100
(1*R*,4*S*,6*R*)-**13**	0.98	72.6	20.2	47.1	−26.9[g]	44[g]

[a]Anharmonicity factor. [b]IR spectra similarty. [c]VCD spectra similarity for the correct enantiomer. [d]VCD spectra similarity for the incorrect enantiomer. [e]Enantiomer similarity index calculated as $S_E - S_{-E}$. [f]Confidence level for the configurational assignments. [g]These values indicate that the (1*R*,4*S*,6*R*)-stereoisomer is not the correct one for **13** and that its experimental and calculated VCD spectra do not match.

DOI: 10.1021/acs.jnatprod.6b00491
J. Nat. Prod. 2016, 79, 2570−2579

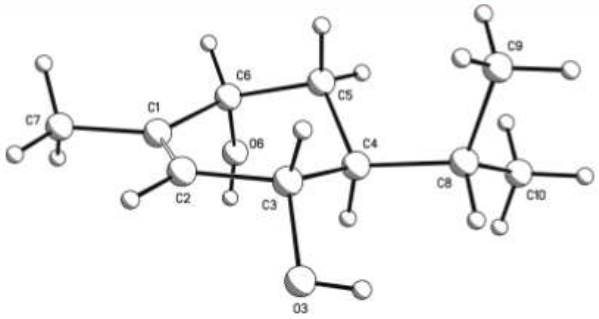

Figure 6. X-ray crystal structure of (+)-(3*S*,4*S*,6*R*)-3,6-dihydroxy-1-menthene (**10**).

overlays of the calculated and experimental VCD spectra of compounds **8** and **13**, as well as superimposition of both experimental spectra, are included in the Supporting Information (Figures S103–S105, respectively). The VCD methodology is sensitive enough to differentiate between epimers because the change in one stereogenic center is immediately reflected by the CompareVOA values.[29−33] This was tested again for **13** by calculating the VCD spectrum of its C-1 epimer since this stereogenic center was created from C-1 in **10**. The results were conclusive, as can be observed in Table 6 when comparing the correct (1*S*,4*S*,6*R*)-**13** vs the incorrect (1*R*,4*S*,6*R*)-**13** diastereoisomer.

In addition, a single crystal of **10** was obtained by recrystallization in acetone and was measured on an X-ray diffractometer equipped with Cu Kα monochromated radiation and collecting one-half of the data sphere. The structure was solved by direct methods and refined to a discrepancy index of 3.3%. The data set was also used to calculate the Flack parameter,[34] which for the enantiomer shown in Figure 6 was $x = 0.0(3)$, and the Hooft parameter,[35] which was $y = 0.09(10)$. For the inverted structure, these parameters were $x = 1.0(3)$ and $y = 0.91(10)$, respectively, confirming that the correct enantiomer is the one depicted in Figure 6. In a previous study, the X-ray diffraction analysis of **10** was undertaken, but its AC was not determined.[36]

In summary, the AC of the new compounds **1**, **2**, **5**−**9**, and **11** was defined by the VCD methodology and X-ray diffraction analysis. The data provided herein for the AC of (+)-(3*S*,4*S*,6*R*)-3,6-dihydroxy-1-menthene (**10**) indicate that this substance, previously isolated from *Brickellia rosmarinifolia*,[6] *Ligularia muliensis*,[8] *Ligularia sagitta*,[9] *Lindera strychnifolia*,[10] and *Mikania saltensis*,[7] as well as from the Chinese multiherb remedy,[21] needs AC reassignment according to its specific rotation data to agree with either (+)-(3*S*,4*S*,6*R*)-**10** or (−)-(3*R*,4*R*,6*S*)-**10**. Also, the AC of **11**, isolated from *Cacalia tangutica*,[11] is reassigned as (−)-(1*S*,4*R*,6*S*), while **11** from the present study corresponds to the (+)-(1*R*,4*S*,6*R*) enantiomer. The AC of **13** was established as (+)-(1*S*,4*S*,6*R*) from its dextrorotatory specific rotation. The present results are useful to assign the AC for menthene derivatives since the employed methods have been proved to be accurate.

■ EXPERIMENTAL SECTION

General Experimental Procedures. Melting points were determined on a Fisher-Johns apparatus and are uncorrected. Optical rotations were recorded in $CHCl_3$ or MeOH solutions on a PerkinElmer 341 polarimeter. 1D and 2D NMR spectra were measured at 300 or 400 MHz for ^{1}H and at 75.4 or 100 MHz for ^{13}C on a Varian Mercury 300 or 400 spectrometer, respectively, from $CDCl_3$, methanol-d_4, DMSO-d_6, or pyridine-d_5 solutions using tetramethylsilane (TMS) as internal reference. Chemical shift values are reported in ppm, and coupling constants (J) are in Hz. HRESIMS data were acquired on an Agilent LCTOF instrument at the UCR Mass Spectrometry Facility, University of California, Riverside. Silica gel 230−400 mesh (Merck) was used for column chromatography.

Plant Material. *Ageratina glabrata* (Kunth) R.M.King & H.Rob. specimens were collected during the flowering stage, on February 28, 2012, near km 4.5 of the Pátzcuaro−Santa Clara del Cobre federal road no. 200, N 19°29.516′ W 101°35.273′ at 2285 m above sea level. A voucher specimen (No. 226133) was deposited at the Herbarium of Instituto de Ecología, A. C., Centro Regional del Bajío, Pátzcuaro, Michoacán, Mexico, where Prof. Jerzy Rzedowski identified the plant material.

Extraction and Isolation. Leaves (500 g), flowers (460 g), and stems (470 g) from *A. glabrata* were individually macerated with hexanes (3 × 2 L), CH_2Cl_2 (3 × 2 L), and MeOH (3 × 2 L) at room temperature for 3 days each. Filtration and evaporation of the MeOH extracts yielded 80 g (16%) from leaves, 83 g (18%) from flowers, and 38 g (8%) from stems. Aliquots of extracts from leaves (40 g), flowers (20 g), and stems (35 g) were column-chromatographed using EtOAc−MeOH mixtures in ascending polarity, affording **3** (100 mg, 0.25%) at 4:1 EtOAc−MeOH and **1** (40 mg, 0.1%) at 7:3 EtOAc−MeOH. An additional purification of **1** employing alumina as the support and acetone as the eluent was required.

Acetylation Reactions. Aliquots of **1** (20 mg) or **3** (50 mg) were dissolved in pyridine (1 mL), and Ac_2O (1 mL) was added. Each reaction mixture was heated at 45 °C for 4 h. In turn, a solution of **7** (20 mg) in pyridine (1 mL) was mixed with Ac_2O (1 mL) and left at room temperature for 3 h. Each reaction mixture was poured over ice−H_2O and extracted with CH_2Cl_2, and the organic layer was washed with aqueous 10% HCl, H_2O, aqueous $NaHCO_3$, and H_2O, dried, filtered, and evaporated. The crude reaction products from **2** (17 mg) or **4** (45 mg) were column-chromatographed using silica gel. Elution with hexanes−EtOAc (4:1) afforded **2** (15 mg, 44%), while elution with hexanes−EtOAc (9:1) afforded **4** (40 mg, 44%). The residue from the acetylation of **7** was filtered and evaporated to yield **8** (11 mg, 46%).

(−)-(3S,4R,5R,6S)-3,5,6-Trihydroxy-1-menthene 3-O-β-D-glucopyranoside (1): colorless oil; $[\alpha]_{589}$ −39, $[\alpha]_{578}$ −41, $[\alpha]_{546}$ −49 (*c* 0.9, MeOH); IR ν_{max} 3372, 2922, 1652 cm^{-1}; ^{1}H NMR (400 MHz, methanol-d_4) and ^{13}C NMR (100 MHz, methanol-d_4) data, see Table 1; NMR data in pyridine-d_5 and DMSO-d_6, see Table 2; HRESI/APCIMS m/z 371.1678 $[M + Na]^+$ (calcd for $C_{16}H_{28}O_8$ + Na$^+$, 371.1676).

(−)-(3S,4S,5R,6S)-5,6-Diacetyloxy-3-hydroxy-1-menthene 3-O-(2′,3′,4′,6′-tetra-O-acetyl)-β-D-glucopyranoside (2): colorless oil; $[\alpha]_{589}$ −9, $[\alpha]_{578}$ −9, $[\alpha]_{546}$ −10, $[\alpha]_{436}$ −16, $[\alpha]_{365}$ −20 (*c* 0.6, $CHCl_3$); IR ν_{max} 1754 (OAc) cm^{-1}; ^{1}H NMR (300 MHz, $CDCl_3$) and ^{13}C NMR (75.4 MHz, $CDCl_3$) data, see Table 1; HRESI/APCIMS m/z 623.2322 $[M + Na]^+$ (calcd for $C_{28}H_{40}O_{14}$ + Na$^+$, 623.2310).

DOI: 10.1021/acs.jnatprod.6b00491
J. Nat. Prod. 2016, 79, 2570−2579

(−)-(3S,4S,6R)-3,6-Dihydroxy-1-menthene 3-O-β-D-glucopyranoside (3): colorless oil; $[\alpha]_{589}$ −58, $[\alpha]_{578}$ −61, $[\alpha]_{546}$ −69 (*c* 1.6, MeOH); IR ν_{max} 3383, 2953, 1646 cm^{-1}; ^1H NMR (400 MHz, methanol-d_4) and ^{13}C NMR (100 MHz, methanol-d_4) data, see Table 1; NMR data in pyridine-d_5 and DMSO-d_6 see Table 2; HRESI/APCIMS *m/z* 355.1735 $[M + Na]^+$ (calcd for $C_{16}H_{28}O_7 + Na^+$, 355.1727).

(−)-(3S,4S,6R)-6-Acetyloxy-3-hydroxy-1-menthene 3-O-(2′,3′,4′,6′-tetra-O-acetyl)-β-D-glucopyranoside (4): amorphous powder; mp 108−110 °C; $[\alpha]_{589}$ −35, $[\alpha]_{578}$ −48, $[\alpha]_{546}$ −56, $[\alpha]_{436}$ −90, $[\alpha]_{365}$ −133 (*c* 0.6, $CHCl_3$); IR ν_{max} 1752 (OAc) cm^{-1}; ^1H NMR (300 MHz, $CDCl_3$) and ^{13}C NMR (75.4 MHz, $CDCl_3$) data, see Table 1; HRESI/APCIMS *m/z* 565.2267 $[M + Na]^+$ (calcd for $C_{26}H_{38}O_{12} + Na^+$, 565.2255).

Acid Hydrolysis of 1. A solution of **1** (45 mg) in aqueous 2% HCl (3 mL) was stirred at room temperature during 30 min. The reaction mixture was extracted with EtOAc, and the organic layer was washed with H_2O, aqueous $NaHCO_3$, and H_2O, dried, filtered, and evaporated. The residue was column-chromatographed using silica gel and hexanes−EtOAc mixtures as the eluent. Fractions 5−8 (hexanes−EtOAc, 1:4) afforded **6** (10 mg, 41%), and fractions 10−13 (hexanes−EtOAc, 1:4) gave **5** (9 mg, 37%). To recover the sugar fraction, the aqueous layer was neutralized with 10% KOH, extracted with *n*-BuOH, and washed with H_2O. The solvent was removed under reduced pressure to yield a mixture of α- and β-D-glucopyranose in a 36:64 ratio (^1H NMR), which was purified by column chromatography using silica gel and eluting with AcOEt−MeOH, 1:1. The residue was dissolved in H_2O and filtered throughout a 0.2 μm nylon membrane. The sugar identity was verified by ^1H NMR in D_2O and a specific rotation of +48 (*c* 0.4, H_2O) in comparison with an authentic sample.

Acid Hydrolysis of 3. A solution of **3** (60 mg) in 2% HCl (3 mL) was treated as done for **1**. The reaction residue was column-chromatographed with silica gel and hexanes−EtOAc mixtures. Fractions 4−9 (hexanes−EtOAc, 3:2) afforded **12** (8 mg, 26%), fractions 11−14 (hexanes−EtOAc, 1:1) yielded **11** (7 mg, 23%), and fractions 16−19 (hexanes−EtOAc, 2:3) gave **10** (15 mg, 49%). The sugar identity was established as D-glucose following the same procedure, as described above, for the acid hydrolysis of **1**.

Preparation of Acetonide Derivatives. Solutions of **5** (25 mg), **6** (25 mg), or **12** (20 mg) in acetone (2 mL) were treated with *p*-toluenesulfonic acid (8 mg). The reaction mixtures were stirred for 2 h at room temperature and subsequently extracted with CH_2Cl_2. The organic layers were washed with H_2O, dried, filtered, and evaporated to yield **7** (20 mg, 65%), **9** (19 mg, 62%), and **13** (11 mg, 45%).

(+)-(1R,4S,5R,6R)-1,5,6-Trihydroxy-2-menthene (5): colorless oil; $[\alpha]_{589}$ +33, $[\alpha]_{578}$ +34, $[\alpha]_{546}$ +38, $[\alpha]_{436}$ + 64 (*c* 0.3, $CHCl_3$); IR ν_{max} 3605, 2964, 2875, 1635, 1051 cm^{-1}; ^1H NMR (400 MHz, $CDCl_3$) and ^{13}C NMR (100 MHz, $CDCl_3$) data, see Tables 3 and 4; HRESIMS *m/z* 186.1256 $[M]^+$ (calcd for $C_{10}H_{18}O_3^+$, 186.1251).

(+)-(1S,4S,5R,6R)-1,5,6-Trihydroxy-2-menthene (6): colorless oil; $[\alpha]_{589}$ +64, $[\alpha]_{578}$ +66, $[\alpha]_{546}$ +75 (*c* 0.7, $CHCl_3$); IR ν_{max} 3416, 2963, 2875, 1625 cm^{-1}; ^1H NMR (400 MHz, $CDCl_3$) and ^{13}C NMR (100 MHz, $CDCl_3$) data, see Tables 3 and 4; HRESI/APCIMS *m/z* 209.1156 $[M + Na]^+$ (calcd for $C_{10}H_{18}O_3 + Na^+$, 209.1148).

(+)-(1S,4S,5R,6R)-1,5,6-Trihydroxy-2-menthene 1,6-acetonide (7): colorless oil; $[\alpha]_{589}$ +34, $[\alpha]_{578}$ +35, $[\alpha]_{546}$ +38, $[\alpha]_{436}$ +69 (*c* 0.1, $CHCl_3$); IR ν_{max} 3585, 2958, 2854, 1098, 1003 cm^{-1}; ^1H NMR (400 MHz, $CDCl_3$) and ^{13}C NMR (100 MHz, $CDCl_3$) data, see Tables 3 and 4; HRESIMS *m/z* 244.1908 $[M + NH_4]^+$ (calcd for $C_{13}H_{22}O_3 + NH_4^+$, 244.1907).

(+)-(1S,4S,5R,6R)-5-Acetyloxy-1,6-dihydroxy-2-menthene 1,6-acetonide (8): colorless oil; $[\alpha]_{589}$ +62, $[\alpha]_{578}$ +64, $[\alpha]_{546}$ +73, $[\alpha]_{436}$ +124 (*c* 0.6, $CHCl_3$); IR ν_{max} 2958, 2925, 2869, 2851, 1730, 1465 cm^{-1}; ^1H NMR (300 MHz, $CDCl_3$) and ^{13}C NMR (75.4 MHz, $CDCl_3$) data, see Tables 3 and 4; HRESI/APCIMS *m/z* 286.2001 $[M + NH_4]^+$ (calcd for $C_{15}H_{24}O_4 + NH_4^+$, 286.2013).

(+)-(1R,4S,5R,6R)-1,5,6-Trihydroxy-2-menthene 5,6-acetonide (9): colorless oil; $[\alpha]_{589}$ +15, $[\alpha]_{578}$ +16, $[\alpha]_{546}$ +18 (*c* 0.3, $CHCl_3$); IR ν_{max} 3596, 2962, 2876, 1655, 1060 cm^{-1}; ^1H NMR (300 MHz, $CDCl_3$) and ^{13}C NMR (75.4 MHz, $CDCl_3$) data, see Tables 3 and 4; HRESI/APCIMS *m/z* 233.1733 $[M + Li]^+$ (calcd for $C_{13}H_{22}O_3 + Li^+$, 233.1723).

(+)-(3S,4S,6R)-3,6-Dihydroxy-1-menthene (10): colorless needles; mp 166−168 °C (MeOH); $[\alpha]_D$ = +10 (*c* 0.5, MeOH). ^1H and ^{13}C NMR data were identical to those reported.[8]

(+)-(1R,4S,6R)-1,6-Dihydroxy-2-menthene (11): colorless oil; $[\alpha]_{589}$ +58, $[\alpha]_{578}$ +61, $[\alpha]_{546}$ +69, $[\alpha]_{436}$ +122 (*c* 0.9, $CHCl_3$); IR ν_{max} 3600, 2961, 2874 cm^{-1}; ^1H NMR (300 MHz, $CDCl_3$) and ^{13}C NMR (75.4 MHz, $CDCl_3$) data, see Tables 3 and 4; HRESI/APCIMS *m/z* 188.1637 $[M + NH_4]^+$ (calcd for $C_{10}H_{18}O_2 + NH_4^+$, 188.1645).

(+)-(1S,4S,6R)-1,6-Dihydroxy-2-menthene (12): $[\alpha]_D$ +40 (*c* 0.92, $CHCl_3$) and ^1H NMR (60 MHz, CCl_4) data as per ref 23; colorless oil; $[\alpha]_{589}$ +43, $[\alpha]_{578}$ +45, $[\alpha]_{546}$ +52 (*c* 0.7, $CHCl_3$); ^1H NMR (300 MHz, $CDCl_3$) and ^{13}C NMR (75.4 MHz, $CDCl_3$) data, see Tables 3 and 4.

(+)-(1S,4S,6R)-1,6-Dihydroxy-2-menthene 1,6-acetonide (13): colorless oil; $[\alpha]_{589}$ +13, $[\alpha]_{578}$ +14, $[\alpha]_{546}$ +16, $[\alpha]_{436}$ +31 (*c* 0.6, $CHCl_3$); ^1H NMR (300 MHz, $CDCl_3$) and ^{13}C NMR (75.4 MHz, $CDCl_3$) data, see Tables 3 and 4; HREIMS *m/z* 195.1387 $[M - CH_3]^+$ (calcd for $C_{12}H_{19}O_2^+$, 195.1380).

X-ray Diffraction Analysis of 10. The data were collected on a Bruker-Nonius CAD4 diffractometer using Cu Kα monochromated radiation (λ = 1.541 84 Å) at 293(2) K in the $\omega/2\theta$ scan mode. Crystal data were $C_{10}H_{18}O_3$, *M* = 170.24, monoclinic, space group C2, *a* = 17.843(4) Å, *b* = 7.112(1) Å, *c* = 8.102(2) Å, β = 102.17(3) deg, *V* = 1005.1(3) $Å^3$, *Z* = 4, ρ = 1.125 mg/mm^3, μ = 0.604 mm^{-1}, total reflections =1650, unique reflections 1353 (R_{int} 0.01%), observed reflections 1304. The structure was solved by direct methods using the SHELXS-97 program included in the WinGX v1.70.01 crystallographic software package. For the structural refinement, the non-hydrogen atoms were treated anisotropically, and the hydrogen atoms, included in the structure factor calculation, were refined isotropically. The final *R* indices were $[I > 2\sigma(I)]$ R1 = 3.3% and wR2 = 8.3%. Largest difference peak and hole were 0.144 and −0.133 e $Å^3$. The Olex2 v1.1.5 software[37] permitted calculation of the Flack[34] *x* = −0.0(3) and the Hooft[35] *y* = 0.1(1) parameters. For the inverted structure these parameters were *x* = 1.0(3) and *y* = 1.0(1), respectively. Crystallographic data (excluding structure factors) have been deposited (No. 1470326) at the Cambridge Crystallographic Data Centre. Copies of the data can be obtained free of charge on application to the CCDC, 12 Union Road, Cambridge CB2 1EZ, UK. Fax: +44-(0)1223-336033 or e-mail: deposit@ccdc.cam.ac.uk.

Vibrational Circular Dichroism. VCD and IR measurements were done on a BioTools dualPEM ChiralIR FT spectrophotometer. Samples of **8** and **13** (4 and 10 mg, respectively) were dissolved in $CDCl_3$ (150 μL) and placed in BaF_2 cells with a path length of 100 μm. Data for **8** and **13** were acquired at a resolution of 4 cm^{-1} for 7 and 6 h, respectively. The baseline was provided by subtracting the spectrum of the solvent acquired under the same conditions. The stability of samples was monitored by ^1H NMR measurements immediately before and after VCD measurements.

VCD Calculations. For the calculated VCD and IR spectra, Monte Carlo search protocols were carried out for **8** and **13** using the Merck Molecular Force Field (MMFF94) as implemented in the Spartan'04 program. An energy cutoff of 10 kcal/mol was considered, which yielded nine conformers for **8** and six for **13**. All conformers were examined to discard duplicates. The single-point energy of each conformer was calculated with the DFT B3LYP/6-31G(d) level of theory in the Spartan'04 program, giving three low-energy conformers for **8** and five for **13**. These structures were geometry optimized with DFT at the B3LYP/DGDZVP level of theory employing the Gaussian 03W program. The minimized structures in the first 3 kcal/mol, three for each compound (Table 5), were used to calculate the thermochemical parameters and the IR and VCD frequencies at 298 K and 1 atm. The six minimum energy structures were verified for the presence of no imaginary frequencies, and their relative free energies were employed to calculate their Boltzmann population. The Boltzmann-weighted IR and VCD spectra for each compound were calculated considering Lorentzian bands with half-widths of 6 cm^{-1}. Molecular visualization was carried out with the GaussView 3.0 program. Geometry optimization and vibrational calculations required some 12 h computational time per conformer when using a laptop computer operating at 2.20 GHz with 8 Gb RAM.

DOI: 10.1021/acs.jnatprod.6b00491
J. Nat. Prod. 2016, 79, 2570−2579

■ ASSOCIATED CONTENT

Supporting Information

The Supporting Information is available free of charge on the ACS Publications website at DOI: 10.1021/acs.jnatprod.6b00491.

^{1}H, ^{13}C, COSY, NOESY, HSQC or HETCOR, and HMBC spectra of compounds **1**−**13** and overlay plots of experimental and VCD spectra of **8** and **13** (PDF)

■ AUTHOR INFORMATION

Corresponding Authors

*E-mail (C. M. Cerda-García-Rojas): ccerda@cinvestav.mx. Tel: +52 55 5747 4035. Fax: +52 55 5747 7137.

*E-mail (R. E. del Río): ndelrio@umich.mx. Tel: +52 443 326 5788. Fax: +52 443 326 5790.

Notes

The authors declare no competing financial interest.

■ ACKNOWLEDGMENTS

We thank CIC-UMSNH for financial support. J.C.P.N. and H.M.A.G. are grateful to CONACYT-Mexico for scholarships 268710 and 295638, respectively. We are grateful to Prof. J. Rzedowski, Instituto de Ecología, A. C., Centro Regional del Bajío, Pátzcuaro, Michoacán, Mexico, for identifying the plant material.

■ REFERENCES

(1) García, P. G.; del Río, R. E.; Guzmán, M. R.; Martínez, G. M. I.; Scior, T. R. F. *Rev. Mex. Cienc. Farm.* **2011**, *42*, 45−51.

(2) Romo de Vivar, A.; Cuevas, L. A.; Guerrero, C. *Rev. Latinoam. Quim.* **1971**, *2*, 32−34.

(3) Bohlmann, F.; Jakupovic, J.; Lonitz, M. *Chem. Ber.* **1977**, *110*, 301−314.

(4) Guerrero, C.; Silva, M.; Maldonado, E.; Martínez, M. *Rev. Latinoam. Quím.* **1978**, *9*, 71−75.

(5) García, P. G.; García, S. E.; Martínez, G. I.; Scior, T. R. F.; Salvador, J. L.; Martínez, P. M. M.; del Río, R. E. *Rev. Bras. Farmacogn.* **2011**, *21*, 928−935.

(6) Cao, Y.; Wei, X.; Xu, H.; Tang, W. *Fitoterapia* **2010**, *81*, 1176−1179.

(7) Cuenca, M. D. R.; Catalán, C. A. N.; Díaz, J. G.; Herz, W. *J. Nat. Prod.* **1991**, *54*, 1162−1164.

(8) Wu, Q. H.; Liu, C. M.; Chen, Y. J.; Gao, K. *Helv. Chim. Acta* **2006**, *89*, 915−922.

(9) Li, X. Q.; Gao, K.; Jia, Z. J. *Planta Med.* **2003**, *69*, 356−360.

(10) Sumioka, H.; Harinantenaina, L.; Matsunami, K.; Otsuka, H.; Kawahata, M.; Yamaguchi, K. *Phytochemistry* **2011**, *72*, 2165−2171.

(11) Liu, X.; Wu, Q. X.; Shi, Y. P. *J. Chin. Chem. Soc.* **2005**, *52*, 369−374.

(12) Tamayo-Castillo, G.; Jakupovic, J.; Bohlmann, F.; Rojas, A.; Castro, V.; King, R. M. *Phytochemistry* **1988**, *27*, 2893−2897.

(13) Stojakowska, A.; Malarz, J.; Kisiel, W. *Acta Soc. Bot. Polym.* **2011**, *80*, 253−256.

(14) Mark, N.; Namchuk, J. D.; McCarter, A. B.; Trevor, A.; Stephen, G. W. *J. Am. Chem. Soc.* **2000**, *122*, 1270−1277.

(15) Carey, F. A.; Sundberg, R. J. *Advanced Organic Chemistry. Part A: Structure and Mechanisms*; Kluwer Academic/Plenum Publishers: New York, 2000; pp 276−290.

(16) De Pascual-T, J.; Bellido, I. S.; Torres, C.; Sastre, B. A.; Grande, M. *Phytochemistry* **1981**, *20*, 163−165.

(17) Stolow, R. D.; Sachdev, K. *Tetrahedron* **1965**, *21*, 1889−1895.

(18) Blumann, A.; Della, E. W.; Henrick, C. A.; Hodgkin, J.; Jefferies, P. R. *Aust. J. Chem.* **1962**, *15*, 290−295.

(19) Stolow, R. D.; Sachdev, K. *J. Org. Chem.* **1971**, *36*, 960−966.

(20) Turner, J. A.; Herz, W. *J. Org. Chem.* **1977**, *42*, 1895−1900.

(21) Zhang, T.; Chen, D. *J. Ethnopharmacol.* **2008**, *117*, 351−361.

(22) Wolf-Rainer, A.; Burghard, S.; Klaus, K. *Appl. Microbiol. Biotechnol.* **1986**, *24*, 24−30.

(23) De Pascual-Teresa, J.; Torres, C.; González, M. S.; Grande, M.; Bellido, I. S. *Phytochemistry* **1983**, *22*, 2749−2751.

(24) Joseph-Nathan, P.; Gordillo-Román, B. Vibrational Circular Dichroism Absolute Configuration Determination of Natural Products In *Progress in the Chemistry of Organic Natural Products*; Kinghorn, A. D., Falk, H., Kobayashi, J., Eds.; Springer International Publishing: Switzerland, 2015; Vol. *100*, pp 311−451.

(25) Burgueño-Tapia, E.; Joseph-Nathan, P. *Nat. Prod. Commun.* **2015**, *10*, 1785−1795.

(26) Höltje, H. D.; Folkers, G. In *Molecular Modeling. Basic Principles and Applications*; Mannhold, R.; Kubinyi, H.; Timmerman, H., Eds.; Methods and Principles in Medicinal Chemistry; VCH: Weinheim, 1996; Vol. *5*, Chapter 2, p 29.

(27) (a) Godbout, N.; Salahub, D. R.; Andzelm, J.; Wimmer, E. *Can. J. Chem.* **1992**, *70*, 560−571. (b) Andzelm, J.; Wimmer, E. *J. Chem. Phys.* **1992**, *96*, 1280−1303.

(28) Debie, E.; Gussem, E. D.; Dukor, R. K.; Herrebout, W.; Nafie, L. A.; Bultinck, P. *ChemPhysChem* **2011**, *12*, 1542−1549.

(29) Bustos-Brito, C.; Sánchez-Castellanos, M.; Esquivel, B.; Calderón, J. S.; Calzada, F.; Yépez-Mulia, L.; Joseph-Nathan, P.; Cuevas, G.; Quijano, L. *J. Nat. Prod.* **2015**, *78*, 2580−2587.

(30) Gordillo-Román, B.; Camacho-Ruiz, J.; Bucio, M. A.; Joseph-Nathan, P. *Chirality* **2012**, *24*, 147−154.

(31) Gordillo-Román, B.; Camacho-Ruiz, J.; Bucio, M. A.; Joseph-Nathan, P. *Chirality* **2013**, *25*, 939−951.

(32) García-Sánchez, E.; Ramírez-López, C. B.; Talavera-Alemán, A.; León-Hernández, A.; Martínez-Muñoz, R. E.; Martínez-Pacheco, M. M.; Gómez-Hurtado, M. A.; Cerda-García-Rojas, C. M.; Joseph-Nathan, P.; del Río, R. E. *J. Nat. Prod.* **2014**, *77*, 1005−1012.

(33) Gutiérrez-Nicolás, F.; Gordillo-Román, B.; Oberti, J. C.; Estévez-Braun, A.; Ravelo, A. G.; Joseph-Nathan, P. *J. Nat. Prod.* **2012**, *75*, 669−676.

(34) Flack, H. D.; Bernardinelli, G. *Chirality* **2008**, *20*, 681−690.

(35) Hooft, R. W. W.; Straver, L. H.; Spek, A. L. *J. Appl. Crystallogr.* **2008**, *41*, 96−103.

(36) Delord, T. J.; Malcolm, A. J.; Fronczek, F. R.; Fischer, N. H.; Watkins, S. F. *Acta Crystallogr., Sect. C: Cryst. Struct. Commun.* **1988**, *44*, 765−767.

(37) Dolomanov, O. V.; Bourhis, L. J.; Gildea, R. J.; Howard, J. A. K.; Puschmann, H. *J. Appl. Crystallogr.* **2009**, *42*, 339−341.

DOI: 10.1021/acs.jnatprod.6b00491
J. Nat. Prod. 2016, 79, 2570−2579

JOURNAL OF NATURAL PRODUCTS

Article

Cite This: J. Nat. Prod. 2018, 81, 63−71

pubs.acs.org/jnp

Methodology for the Absolute Configuration Determination of Epoxythymols Using the Constituents of *Ageratina glabrata*

Héctor M. Arreaga-González,[†] Julio C. Pardo-Novoa,[†] Rosa E. del Río,[†] Gabriela Rodríguez-García,[†] J. Martín Torres-Valencia,[‡] J. Jesús Manríquez-Torres,[§] Carlos M. Cerda-García-Rojas,*[,⊥] Pedro Joseph-Nathan,[⊥] and Mario A. Gómez-Hurtado*[,†]

[†]Instituto de Investigaciones Químico Biológicas, Universidad Michoacana de San Nicolás de Hidalgo, Ciudad Universitaria, Morelia, Michoacán 58030, Mexico

[‡]Área Académica de Química, Universidad Autónoma del Estado de Hidalgo, Km 4.5 Carretera Pachuca-Tulancingo, Mineral de la Reforma, Hidalgo 42184, Mexico

[§]Centro de Investigación Interdisciplinario. Área Académica de Nutrición, Instituto de Ciencias de la Salud, Universidad Autónoma del Estado de Hidalgo. Circuito Actopan-Tilcuautla s/n. Ex hacienda La Concepción, San Agustín Tlaxiaca, Hidalgo 42160, Mexico

[⊥]Departamento de Química, Centro de Investigación y de Estudios Avanzados del Instituto Politécnico Nacional, Apartado 14-740, Mexico City, 07000, Mexico

Supporting Information

ABSTRACT: A methodology to determine the enantiomeric excess and the absolute configuration (AC) of natural epoxythymols was developed and tested using five constituents of *Ageratina glabrata*. The methodology is based on enantiomeric purity determination employing 1,1′-bi-2-naphthol (BINOL) as a chiral solvating agent combined with vibrational circular dichroism (VCD) measurements and calculations. The conformational searching included an extensive Monte Carlo protocol that considered the rotational barriers to cover the whole conformational spaces. (+)-(8*S*)-10-Benzoyloxy-6-hydroxy-8,9-epoxythymol isobutyrate (**1**), (+)-(8*S*)-10-acetoxy-6-methoxy-8,9-epoxythymol isobutyrate (**4**), and (+)-(8*S*)-10-benzoyloxy-6-methoxy-8,9-epoxythymol isobutyrate (**5**) were isolated as enantiomerically pure constituents, while 10-isobutyryloxy-8,9-epoxythymol isobutyrate (**2**) was obtained as a 75:25 (8*S*)/(8*R*) scalemic mixture. In the case of 10-benzoyloxy-8,9-epoxythymol isobutyrate (**3**), the BINOL methodology revealed a 56:44 scalemic mixture and the VCD measurement was beyond the limit of sensitivity since the enantiomeric excess is only 12%. The racemization process of epoxythymol derivatives was studied using compound **1** and allowed the clarification of some stereochemical aspects of epoxythymol derivatives since their ACs have been scarcely analyzed and a particular behavior in their specific rotations was detected. In more than 30 oxygenated thymol derivatives, including some epoxythymols, the reported specific rotation values fluctuate from −1.6 to +1.4 passing through zero, suggesting the presence of scalemic and close to racemic mixtures, since enantiomerically pure natural constituents showed positive or negative specific rotations greater than 10 units.

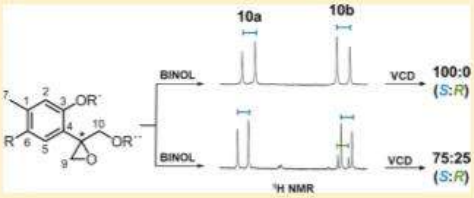

Epoxythymol derivatives constitute a widespread group of aromatic monoterpenoids with functionalizations at C-3, C-6, C-7, and/or C-10, which include hydroxy or ester groups, as well as an oxirane ring at C-8/C-9. Sixty epoxythymol derivatives with these structural characteristics have been reported from 67 vegetal species distributed in 32 genera of the family Asteraceae.[1] Despite the fact that there is a considerable number of epoxythymols, with some of them showing relevant biological activities, only the absolute configurations (ACs) for two members of this group have been described.[2,3] Also, the specific rotation of these substances has been reported for only some cases. Thus, levorotatory epoxythymol derivatives were found in *Callilepis laureola*,[4] *Eupatorium fortunei*,[5] and *Gaillarda aristata*,[6] while dextrorotatory epoxythymol dervatives have been reported from *Ageratina glabrata*,[7] *A. cylindrica*,[2] *Arnica acaulis*,[8] *Brasilia sickii*,[9] and *Inula crithmoides*.[10] Surprisingly, epoxythymol dervatives isolated from *Eupatorium stoechadosmum*[11] and *Piptothrix areolare*[12] were described as racemic mixtures. The presence of natural epoxythymol racemates in the latter species was supported by using chiral chemical shift reagents.[12] Some explanations about the racemization of 8,9-disubstituted thymol derivatives have referred to the isolation process[5] or the generation of artifacts in long-stored samples.[13] However, both enantiomerically pure and racemic thymol derivatives have been reported in the same plant,[5,14] although studies on the racemization susceptibility of epoxythymols have not been

Received: July 24, 2017
Published: December 26, 2017

DOI: 10.1021/acs.jnatprod.7b00637
J. Nat. Prod. 2018, 81, 63−71

addressed to date. In the present paper, the natural epoxythymol derivatives (+)-(8*S*)-10-benzoyloxy-6-hydroxy-8,9-epoxythymol isobutyrate (**1**), 10-isobutyryloxy-8,9-epoxythymol isobutyrate (**2**), 10-benzoyloxy-8,9-epoxythymol isobutyrate (**3**), (+)-(8*S*)-10-acetoxy-6-methoxy-8,9-epoxythymol isobutyrate (**4**), and (+)-(8*S*)-10-benzoyloxy-6-methoxy-8,9-epoxythymol isobutyrate (**5**), isolated from *Ageratina glabrata* (Figure 1), were evaluated to establish a methodology for the determination of their enantiomeric excess and AC. The methodology involves, on one hand, the use of 1,1′-bi-2-naphthol (BINOL)[15] as a chiral solvating agent in ^{1}H NMR spectroscopy and, on the other hand, vibrational circular dichroism (VCD) measurements and calculations.[16,17] The ^{1}H NMR-BINOL data provided the enantiomeric excess for **1**−**5**, while VCD spectroscopy allowed a determination of the AC of thymol derivatives **1**, **2**, **4**, and **5**. The racemization susceptibility of **1** under acid conditions is also described, comprising the chemical behavior observed in these compounds.

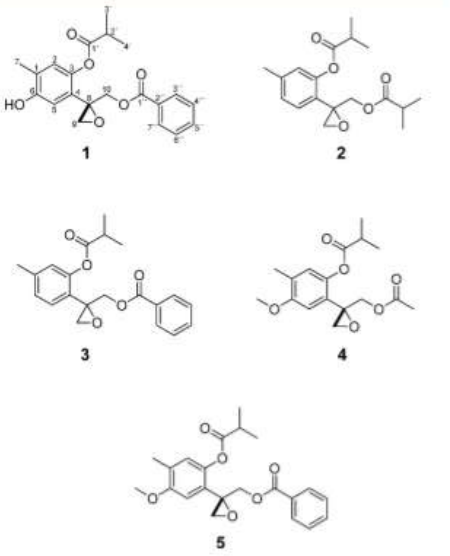

Figure 1. Thymol metabolites from *Ageratina glabrata*.

RESULTS AND DISCUSSION

The aerial parts of *A. glabrata* afforded compounds **1**−**5** after extraction with hexanes and CH_2Cl_2 followed by purification using column chromatography. The NMR data of (+)-(8*S*)-10-benzoyloxy-6-hydroxy-8,9-epoxythymol isobutyrate (**1**), 10-benzoyloxy-8,9-epoxythymol isobutyrate (**3**), and (+)-(8*S*)-10-benzoyloxy-6-methoxy-8,9-epoxythymol isobutyrate (**5**) were similar to those recently reported,[3] as was the case for 10-isobutyryloxy-8,9-epoxythymol isobutyrate (**2**),[18−20] which, interestingly, has been obtained from 40 different plants that represent 60% of the total reported vegetal species containing epoxythymol derivatives.[1] In spite of this previous work, there were no data about the absolute configuration of this compound. A sole ^{1}H NMR analysis of (+)-(8*S*)-10-acetoxy-6-methoxy-8,9-epoxythymol isobutyrate (**4**)[7] showed data with many discrepancies in comparison with those obtained herein. Our data followed therefore from 2D NMR spectroscopy. In the ^{1}H NMR spectrum of **4**, typical chemical shifts for a tetrasubstituted aromatic ring at δ 6.88 (H-5) and δ 6.79 (H-2) were found together with two AB systems for CH_2-10 (δ 4.54 and 4.19, J = 12.0 Hz) and for CH_2-9 at δ 3.03 and 2.80, J = 5.6 Hz. The ^{13}C NMR spectrum showed 17 signals, of which those at δ 175.6 and δ 170.3 were assigned to the isobutyrate and acetate carbonyl groups, respectively. The aromatic carbon atoms were observed within the δ 155.3−109.5 range, while the sp^3 carbon atoms appeared between δ 65.1 and 16.0, with those of CH_3-3′ and CH_3-4′ overlapping at δ 18.9. All the NMR assignments were supported by gHSQC and gHMBC experiments.

The specific rotation measurements of epoxythymols **1**−**5** caught our attention since the observed values for **1**, **2**, **4**, and **5** were found between $[\alpha]_{589}$ +10 and $[\alpha]_{589}$ +28, while that of **3** showed a very small dextrorotatory value ($[\alpha]_{589}$ +0.8 in $CHCl_3$), which differs in sign and magnitude from that reported ($[\alpha]_{589}$ −3.9 in $CHCl_3$).[3] This variation suggested that in both cases there were different scalemic mixtures with prevalence of opposite enantiomers, in line with several reports wherein epoxythymol derivatives have been isolated as racemates.[1,3] Thus, the design of an efficient method for the enantiomeric purity determination of chiral epoxythymol derivatives turned out to be desirable. To achieve this task, it was decided to explore the use of (*S*)-1,1′-bi-2-naphthol [(*S*)-BINOL] as a chiral solvating agent to differentiate the enantiomers by means of ^{1}H NMR measurements. This method has been employed successfully in the enantiomeric discrimination of some natural isoflavanones,[21] alkaloids,[22,23] and peptides,[24] as well as for pharmacologically active principles[25−27] and is based on the use of a chiral solvating agent for the enantioresolution of the NMR signals of two distereoisomeric host−guest complexes formed between a BINOL enantiomer and each enantiomer of the studied thymol derivative. This methodology has some advantages over other spectroscopic techniques for the estimation of the enantiomeric excess. For instance, measurement of the specific rotation depends on concentration and temperature and is very sensitive to small amounts of optically active impurities. The use of NMR chiral shift reagents could be an alternative, but it requires anhydrous conditions and in general induces some line broadening.

The ^{1}H NMR-BINOL analyses of **1**, **4**, and **5** revealed their 100% enantiomeric purity, since only one set of signals, slightly shifted upfield in comparison to their original ^{1}H NMR spectra, was observed for each compound (Figure 2). The most relevant chemical shift changes were observed for the CH_2-10 ($\Delta\delta$ up to 0.042) and CH_2-9 ($\Delta\delta$ up to 0.034) signals. Additionally, the signals of H-5, CH_3-3′, and CH_3-4′ showed variations within the $\Delta\delta$ 0.011−0.016 range. In the case of epoxythymol **2**, the ^{1}H NMR spectrum, in the presence of BINOL, showed two sets of signals for H-10b at δ 4.174 and 4.161 ($\Delta\delta$ 0.013) with different signal heights. Splitting of H-9a with $\Delta\delta$ 0.007 and H-9b with $\Delta\delta$ 0.004 was also observed (Figure 2). The remaining resonances only showed the typical shifts to upper field in comparison with the original ^{1}H NMR spectrum. The intensity of the split signals of **2** established that this epoxythymol exists as a 75:25 scalemic mixture. The ^{1}H NMR-BINOL analysis of thymol **3** revealed two sets of signals for H-10a and for H-10b with almost similar heights (Figure 2). It was noted that H-10b

DOI: 10.1021/acs.jnatprod.7b00637
J. Nat. Prod. 2018, 81, 63−71

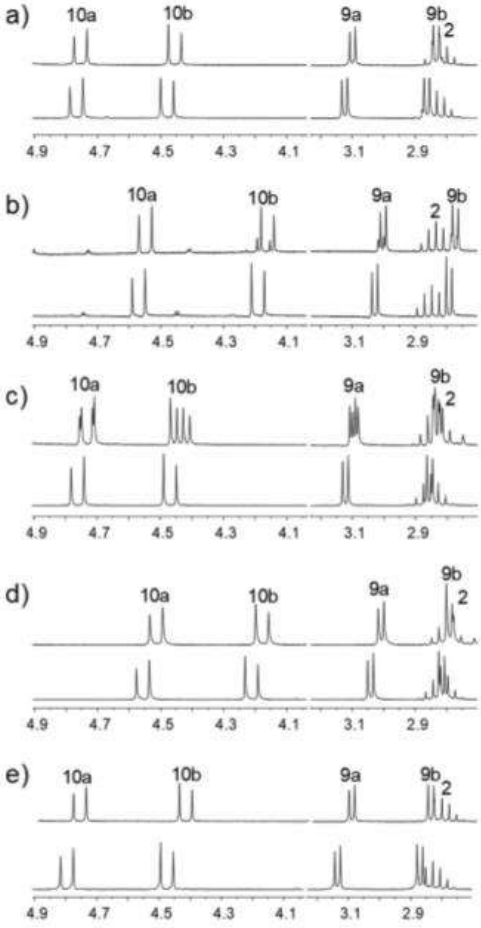

Figure 2. Comparison between the ^{1}H NMR spectra of epoxythymols **1**–**5** (lower traces) and those upon BINOL addition (upper traces) showing their enantiomeric proportions. Compounds (a) **1** 100:0 *S*/*R*; (b) **2** 75:25 *S*/*R*; (c) **3** 56:44 *S**/*R**; (d) **4** 100:0 *S*/*R*; and (e) **5** 100:0 *S*/*R*.

showed the major chemical shift splitting ($\Delta\delta$ 0.021) in comparison with that observed for H-10a ($\Delta\delta$ 0.006). Also, H-9a showed $\Delta\delta$ 0.009 and H-9b displayed $\Delta\delta$ 0.003, while no significant signal splitting was observed in the remaining resonances. Considering that the line width of the signals is the same in the split resonances, their height relationship indicated a 56:44 scalemic mixture, which is in agreement with the very low specific rotation ($[\alpha]_{589}$ +0.8) observed for **3**.

Once the presence of scalemic mixtures in **2** and **3** was demonstrated, it was important to induce partial racemization of an enantiomerically pure epoxythymol derivative (i.e., **1**, **4**, or **5**) to observe the split resonances upon addition of BINOL. At the same time, such an experiment could provide useful data to understand the susceptibility in the racemization of epoxythymols. Transesterification with oxirane cleavage of some epoxythymol derivatives has been proposed,[2,28] but the oxirane racemization has not been documented. Thus, epoxythymol **1** was selected to explore its racemization because it was isolated in good yields. Three aliquots of **1** were heated under reflux in benzene in the presence of silica gel as the catalyst using a Dean–Stark trap for 2, 4, and 6 h. The crude reaction products were purified by column chromatography and subjected to ^{1}H NMR-(*R*)-BINOL measurements, revealing a gradual scalemization of **1** that was dependent on the reaction time (Figure 3). After 2 h of reaction, two sets of signals for the CH_2-10 AB system centered at δ 4.58 indicated the presence of a 90:10 (ee 80%) scalemic mixture, and after 4 h of treatment there was an increase to an 87:13 mixture (ee 74%), while after 6 h of treatment the scalemic mixture increased to a 75:25 ratio

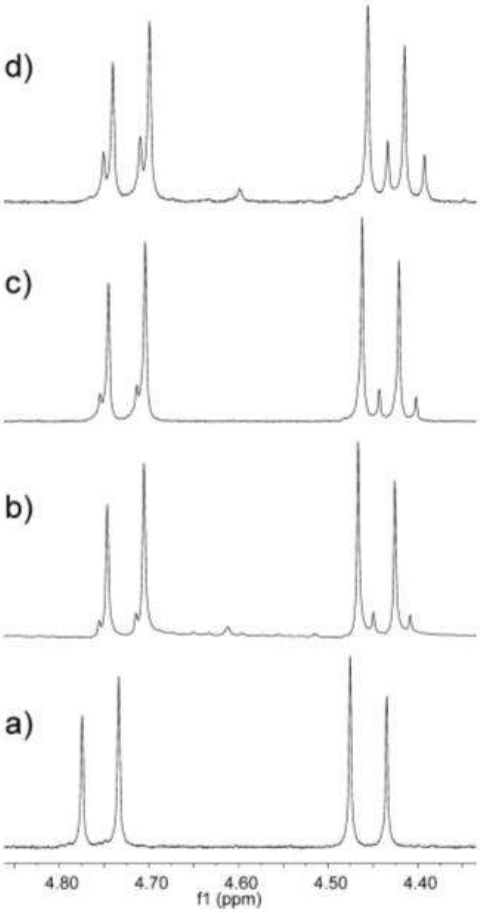

Figure 3. Enantiomeric ratio of the scalemization reactions of epoxythymol **1** evidenced by the ^{1}H NMR-BINOL methodology (a) determined at 0 h (100:0), (b) 2 h (90:10), (c) 4 h (87:13), and (d) 6 h (75:25).

DOI: 10.1021/acs.jnatprod.7b00637
J. Nat. Prod. 2018, 81, 63−71

(ee 50%). This experiment confirmed the 100% enantiomeric purity of natural epoxythymol **1** isolated from *A. glabrata* (see Figure 3 at time 0 h), as well as the ability of this compound to undergo racemization.

A concerted reaction mechanism could be proposed for the scalemization of epoxythymol **1** (Figure 4) in which a

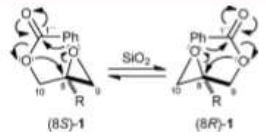

Figure 4. Concerted reaction mechanism proposed.

nucleophilic attack of the O-8 epoxide oxygen atom to the C-1″ carbonyl group could promote a transference of the acyl group from the oxygen atom at C-10 to the oxygen atom at C-9 with the concomitant C-8−O-8 bond breakage and the concerted O-10−C-8 bond formation. If this mechanism is reversible (Figure 4), the process will ultimately yield a racemic product passing through proportions of scalemic mixtures. A minor byproduct was detected during the progress of these experiments, which was isolated and identified as 10-benzoyloxy-9-isobutyryloxy-6,8-dihydroxythymol (Figure S25, Supporting Information). This ring-opening product may be formed by attack of a H_2O molecule to C-8 with the concerted epoxide ring rupture at the C-8−O-8 bond followed by transesterification of the isobutyryl residue from O-3 to O-9, as suggested by Bohlmann et al.[5] On the basis of the NMR data of this substance and the pertinent observations made by Bustos-Brito et al.,[28] we are herein proposing the revision of the 10-benzoyloxy-6,8,9-trihydroxythymol isobutyrate structure reported by our research group[29] to 10-benzoyloxy-9-isobutyryloxy-6,8-dihydroxythymol, since the spectroscopic data are identical to those provided in this paper (Figures S26 and S28, Supporting Information).

In the five compounds (**1**−**5**) studied, it was observed that the changes in chemical shifts upon addition of BINOL were more significant on those hydrogen atoms located near the stereogenic center, in concordance with the observed trends for other substances.[21−27,30] In some cases,[24] intermolecular interactions between BINOL and the studied molecules have been confirmed by X-ray diffraction analysis. On the basis of these findings, the formation of a transitory hydrogen bond between the hydroxy hydrogen of (*S*)-BINOL and the oxygen atoms O-10 and/or O-8 of the epoxythymols could be proposed, allowing an evident shielding phenomenon at the CH_2-10 and CH_2-9 hydrogen atoms caused by the naphthol moieties.

Once the enantiomeric ratio for thymol derivatives **1**−**5** was established (Figure 2), the absolute configuration determination by VCD analysis for enantiomerically pure **1**, **4**, and **5** was addressed. This technique involves a comparison between the calculated and experimental VCD and IR spectra, in which a statistical validation is required. This methodology has been recently employed for determining the AC of a thymol derivative[2] as well as for other monoterpenes.[31] For this purpose, molecular models of (8*S*)-10-benzoyloxy-6-hydroxy-8,9-epoxythymol isobutyrate (**1**), (8*S*)-10-acetoxy-6-methoxy-8,9-epoxythymol isobutyrate (**4**), and (8*S*)-10-benzoyloxy-6-methoxy-8,9-epoxythymol isobutyrate (**5**) were built and minimized using a molecular mechanics force field.[32] The conformational distribution of compound **1** was explored initially by the Monte Carlo protocol, and an energy window of 10 kcal/mol was established for the conformer selection. The whole set of conformers, consisting of 139 individuals, was subjected to a single-point density functional theory (DFT) energy optimization at the B3LYP/6-31G(d) level of theory. Those conformers within the range of 0−3 kcal/mol (109 conformers) were geometry optimized at the DFT PBEPBE/DGDZVP level of theory, and the VCD and IR spectra of those conformers within the 0−2 kcal/mol range (18 conformers) were calculated at the same level of theory. However, the statistical comparison of the Boltzmann-averaged calculated VCD and IR data with the experimental spectra, employing the Compare*VOA* algorithm[33] (BioTools Inc., Jupiter, FL, USA), reflected a low spectroscopic similarity. Therefore, a systematic conformational search was carried out taking into consideration a dihedral angle analysis of the rotatable bonds, focusing on those with a more restricted rotation. This procedure allowed the finding of 13 additional low-energy conformers, which were geometry optimized at the same level of theory. The whole set of 31 conformers was considered in a new VCD and IR spectra calculation (Figure 5). The Compare*VOA* analysis now provided a good spectroscopic similarity between the calculated and experimental spectra for compound **1** (S_{IR} = 90.9 and S_E 70.9%) and 100% confidence level for the correct enantiomer. Other essential data about the confidence level for the VCD and IR data of **1** are listed in Table 1, thus defining the absolute configuration of **1** as (8*S*).

The lack of many conformers in the initial Monte Carlo protocol of **1** gave evidence for the complexity of its conformational behavior that arises from unusually high rotational barriers present in the O-3−C-1′ and C-8−C-10 bonds. The peculiar conformational space of epoxythymols precluded the finding of all low-energy conformers by performing a Monte Carlo run starting from a single conformer. The rotational analysis in thymol derivatives **4** and **5** employing the PC Model program revealed that the rotational barrier energies in the C-3−O-3−C-1′−C-2′ and C-4−C-8−C-10−O-10 dihedral angles were higher than 10 kcal/mol. To overcome this difficulty, the conformational search of **4** and **5** was carried out with the Monte Carlo protocol starting from four different conformations, according to the four combinations obtained by 180 deg rotations of the mentioned dihedral angles. The four Monte Carlo searches for epoxythymol **4** yielded different amounts of conformers in the 0−10 kcal/mol range. The four groups were subjected separately to single-point energy calculations at the DFT B3LYP/6-31G(d) level, and those conformers within a 0−3 kcal/mol range were combined and filtered according to their energies and dihedral angles, to yield 64 conformers. Geometry optimization at the DFT PBEPBE/DGDZVP level afforded 20 conformers within the 0−2 kcal/mol range, for which the calculated frequencies and VCD and IR spectra at the same level of theory provided the Boltzmann-averaged spectra. The statistical comparison of the calculated with experimental VCD and IR spectra showed the Compare*VOA* values listed in Table 1 with a confidence level of 100% for the (8*S*)-**4** enantiomer (Figure 6).

Analysis of the AC of thymol **5** using the same methodology showed a similar behavior to that observed for **4**. In the single-point energy calculation at the DFT B3LYP/6-31G(d) level, it gave 62 conformers within the 0−3 kcal/mol range, while geometry optimization at the DFT PBEPBE/DGDZVP level

DOI: 10.1021/acs.jnatprod.7b00637
J. Nat. Prod. 2018, 81, 63−71

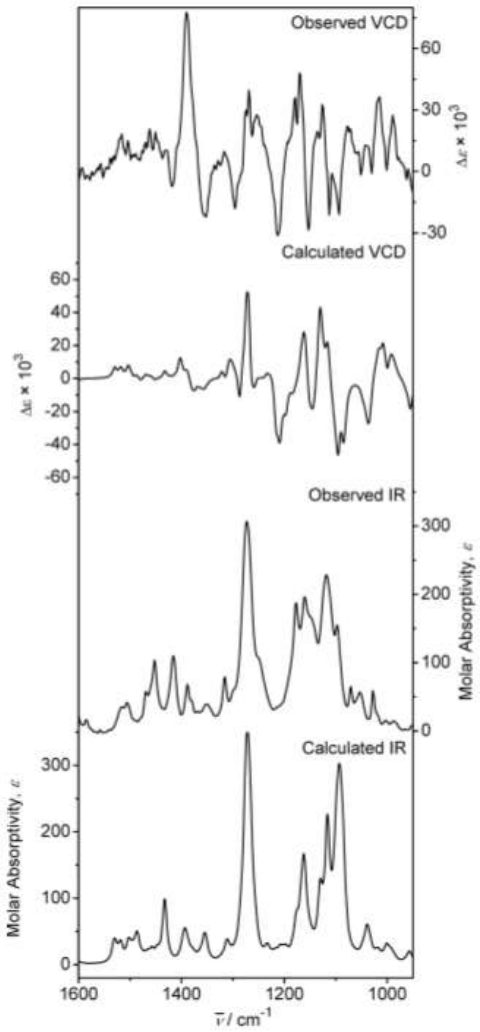

Figure 5. Comparison of the experimental and PBEPBE/DGDZVP-calculated VCD and IR spectra of (+)-(8*S*)-10-benzoyloxy-6-hydroxy-8,9-epoxythymol isobutyrate (**1**).

afforded 49 conformers within a 0−2 kcal/mol range. The calculated VCD and IR spectra were compared with the experimental ones (Figure 7), and the Compare*VOA* algorithm gave a confidence level of 100% (Table 1) for the (8*S*)-**5** enantiomer.

Once the effectiveness of the proposed methodology for the AC determination of epoxythymols was tested, the AC of the major enantiomer in the scalemic mixture of thymol **2** was approached. Despite the fact that thymol **2** was isolated from *A. glabrata* as a 75:25 scalemic mixture (ee 50%), its AC could be determined confidently by the VCD methodology presented herein. A conformational search by using the Monte Carlo protocol, also starting from the four different minimum-energy models, was carried out. The single-point calculations at the DFT B3LYP/6-31G(d) level were combined and then filtered to eliminate duplicates considering the energy and the dihedral angles, yielding 105 conformers within the 0−3 kcal/mol range. The geometry optimization of these conformers at the DFT PBEPBE/DGDZVP level afforded 48 conformers within the 0−2 kcal/mol range. The VCD and IR frequencies of this group were calculated using the same level of theory and were Boltzmann-averaged to obtain the calculated spectra. In this particular case, compound **2** with ee 50% still displayed strong VCD bands, mainly in the 1400−1000 cm^{-1} spectroscopic region. Therefore, only this region was subjected to comparison because the weak experimental bands present in other regions were hidden by the noise, causing some uncertainties. Thus, comparison of the calculated and experimental spectra of epoxythymol **2** showed a good correspondence for the (8*S*)-**2** enantiomer (Figure 8) with a level of confidence of 100% (Table 1). As mentioned, epoxythymol **2** has been reported as a natural product from 60% of the total plant species containing epoxythymol derivatives.[1] Therefore, the AC of this molecule present in other species could be determined by comparison of its specific rotation with that reported herein for (8*S*:8*R*)-(75:25 er)-**2** ($[\alpha]_{589}$ +17.3, *c* 0.6, $CHCl_3$), but considering in each case its particular enantiomeric ratio that could be measured by using the ^{1}H NMR-BINOL method. In the case of epoxythymol **3**, the VCD measurement was beyond the limit of accuracy, since the enantiomeric excess of the product isolated from *A. glabrata* was very small (ee 12%).

To conclude, in the determination of the AC of epoxythymol derivatives by VCD, several facts should be considered, which include the specific rotation analysis, the enantiomeric purity measurement using a chiral solvating agent such as $BINOL_9$ and a systematic conformational analysis or a statistical algorithm as the Monte Carlo method in which the rotational barriers must be identified previously. Thus, this report provides enough information for a rapid and accurate evaluation of the enantiomeric excess of new and known epoxythymol derivatives isolated as pure enantiomers or scalemic mixtures. It also describes a detailed VCD method to determine the AC of those epoxythymols isolated with ee higher than 50%.

Table 1. Confidence Level Data for the IR and VCD Spectra of 1, 2, 4, and 5 Calculated at the PBEPBE/DGDZVP Level of Theory

compound	anH[a]	S_{IR}[b]	S_E[c]	S_{-E}[d]	ESI[e]	C[f]
1	1.020	90.9	70.9	17.3	53.5	100
2	1.014	89.6	73.2	23.7	49.5	100
4	1.009	80.7	71.5	11.8	59.7	100
5	1.000	84.7	71.2	19.2	51.9	100

[a]Anharmonicity factor. [b]IR spectra similarity. [c]VCD spectra similarity for the correct enantiomer. [d]VCD spectra similarity for the incorrect enantiomer. [e]Enantiomer similarity index calculated as $S_E - S_{-E}$. [f]Confidence level in percentage for the configurational assignments.

EXPERIMENTAL SECTION

General Experimental Procedures. The melting point was determined on a Fisher-Johns apparatus and is uncorrected. Optical rotations were measured in $CHCl_3$ solution on a PerkinElmer 341 polarimeter. UV spectra were registered on a PerkinElmer Lambda 12 spectrophotometer. 1D and 2D NMR spectra were measured at 300 or 400 MHz for ^{1}H and at 75.4 or 100 MHz for ^{13}C on Varian Mercury

DOI: 10.1021/acs.jnatprod.7b00637
J. Nat. Prod. 2018, 81, 63−71

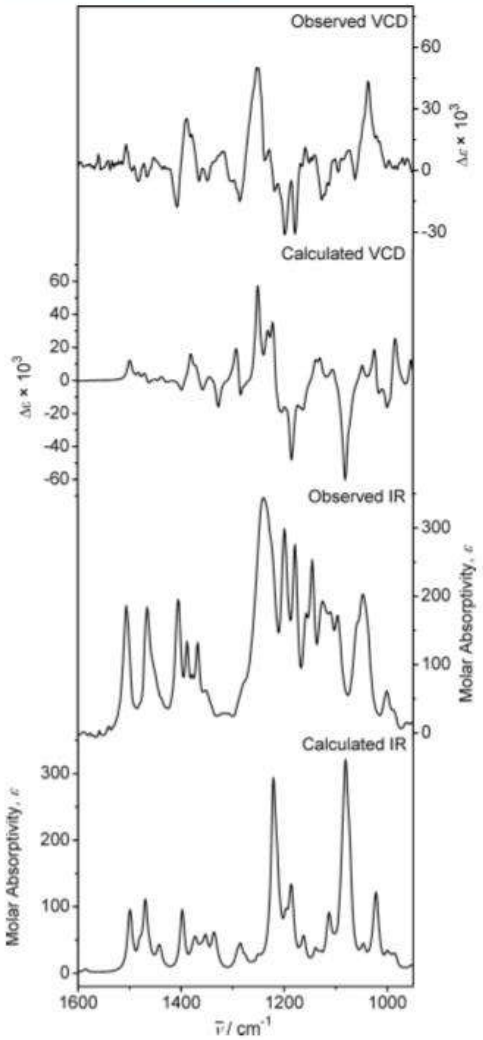

Figure 6. Comparison of the experimental and PBEPBE/DGDZVP-calculated VCD and IR spectra of (+)-(8*S*)-10-acetoxy-6-methoxy-8,9-epoxythymol isobutyrate (**4**).

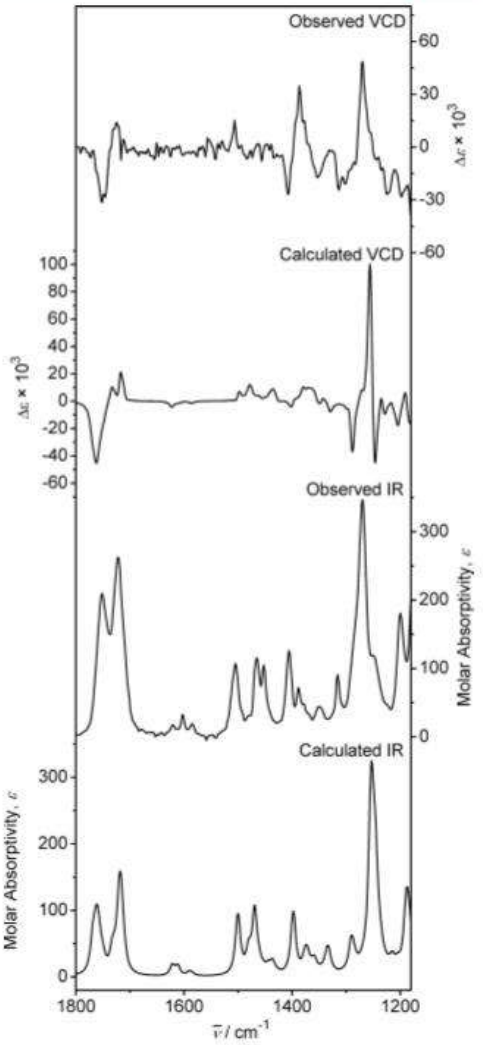

Figure 7. Comparison of the experimental and PBEPBE/DGDZVP-calculated VCD and IR spectra of (+)-(8*S*)-10-benzoyloxy-6-methoxy-8,9-epoxythymol isobutyrate (**5**).

300 or 400 NMR spectrometers, respectively, from $CDCl_3$ solution using tetramethylsilane as internal reference. Chemical shift values are reported in ppm, and coupling constants (*J*) are in Hz. Silica gel 230–400 mesh (Merck) was used for column chromatography.

Plant Material. *Ageratina glabrata* (Kunth) R.M.King & H.Rob. specimens were collected during the flowering stage, in February, 2014, near km 4.5 of the Pátzcuaro–Santa Clara del Cobre federal road no. 200, N 19°29.516′ W 101°35.273′ at 2285 m above sea level. A voucher specimen (No. 226133) was deposited at the Herbarium of Instituto de Ecología, A. C., Centro Regional del Bajío, Pátzcuaro, Michoacán, Mexico, where Prof. Jerzy Rzedowski identified the plant material.

Extraction and Isolation. Leaves and stems (1.5 kg, each) from *A. glabrata* were individually macerated with hexanes (3 × 10 L) at room temperature for 3 days. The leaves were subsequently macerated with CH_2Cl_2 (3 × 10 L). Filtration and evaporation of the hexanes and CH_2Cl_2 extracts of the leaves yielded 35 g (2.3%) and 147 g (9.8%), respectively, while the hexanes extract from the stems gave 30 g (2%) of a greenish oil. Column chromatography of an aliquot of the CH_2Cl_2 extract from the leaves (70 g), using hexanes–EtOAc mixtures in ascending polarity afforded **1** (3.9 g, 5.6%) with 4:1 hexanes–EtOAc as the eluent. Chromatography of the total hexanes extract from the leaves provided **2** (15 mg, 0.04%) with 19:1 hexanes–EtOAc, and **3**

DOI: 10.1021/acs.jnatprod.7b00637
J. Nat. Prod. 2018, 81, 63–71

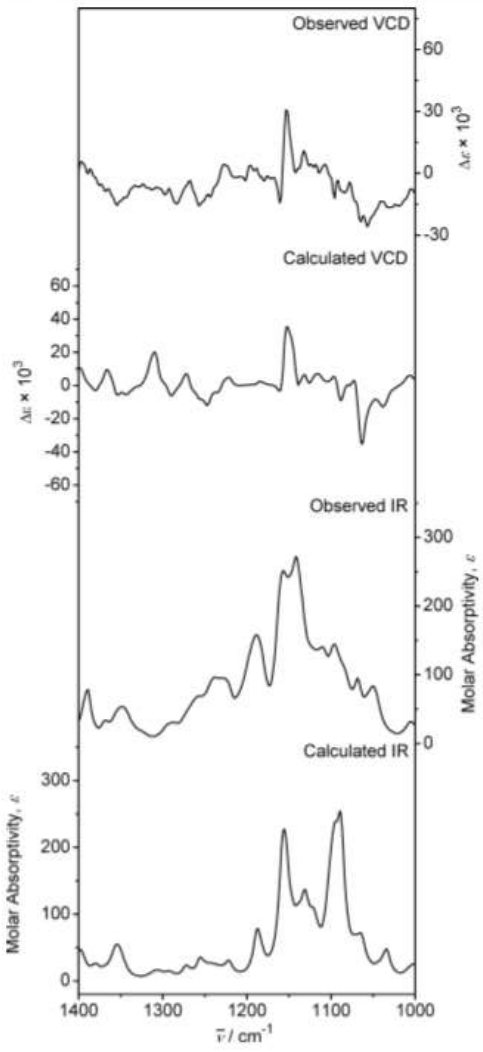

Figure 8. Comparison of the experimental and PBEPBE/DGDZVP-calculated VCD and IR spectra of (8*S*)-10-isobutyryloxy-8,9-epoxythymol isobutyrate (**2**).

(16 mg, 0.05%) and **5** (30 mg, 0.09%) with 4:1 hexanes−EtOAc, while the hexanes extract from the stems yielded **4** (235 mg, 0.8%).

Scalemization Reactions. Three suspensions of silica gel (1 g) in benzene (60 mL) were refluxed for 4 h using a Dean−Stark trap to eliminate moisture. Samples of enantiomerically pure **1** (100 mg) were added to each system, and the mixtures were refluxed for 2, 4, or 6 h. The crude reaction solutions were filtered, evaporated under a vacuum, and purified by column chromatography using hexanes−AcOEt (4:1) to give 15.3 mg (15%), 16.1 mg (16%), and 11.2 mg (11%) of scalemic mixtures of **1** as pale yellow oils.

Determination of Scalemic Proportions Using (*S*)-BINOL. The enantiomeric purity of epoxythymol derivatives was determined by ^{1}H NMR spectroscopy dissolving the samples (6 mg) in 0.7 mL of $CDCl_3$ and adding (−)-(*S*)-BINOL (Aldrich), unless otherwise indicated, as a chiral solvating agent (30 mg). The enantiomeric ratio (er) of each sample was obtained from the height of the signals considering that the width at half-height is constant.

*(+)-(8S)-10-Benzoyloxy-8,9-epoxy-6-hydroxythymol isobutyrate (**1**)*: colorless crystals; mp 112−114 °C; $[\alpha]_{589}$ +9.9, $[\alpha]_{578}$ +10.0, $[\alpha]_{546}$ +11.0, $[\alpha]_{436}$ +17.1, (*c* 0.8, $CHCl_3$).

*(8S:8R)-(75:25 er)-10-Isobutyryloxy-8,9-epoxythymol isobutyrate (**2**)*: yellow oil; $[\alpha]_{589}$ +17.3, $[\alpha]_{578}$ +17.5, $[\alpha]_{546}$ +18.9, $[\alpha]_{436}$ +30.5, $[\alpha]_{365}$ +53.1 (*c* 0.6, $CHCl_3$).

(8S:8R*)-(56:44 er)-10-Benzoyloxy-8,9-epoxythymol isobutyrate (**3**)*: yellow oil; $[\alpha]_{589}$ +0.8, $[\alpha]_{578}$ +0.8, $[\alpha]_{546}$ +0.9, $[\alpha]_{436}$ +1.5 (*c* 0.8, $CHCl_3$).

*(+)-(8S)-10-Acetoxy-6-methoxy-8,9-epoxythymol isobutyrate (**4**)*: yellow oil; $[\alpha]_{589}$ +28.0, $[\alpha]_{578}$ +29.0, $[\alpha]_{546}$ +33.1, $[\alpha]_{436}$ +58.6 (*c* 1.0, $CHCl_3$); UV (EtOH) λ_{max} (log ε) 221 (3.95), 278 (3.46), 284 (3.44) nm; IR ($CHCl_3$) ν_{max} 2983, 1746, 1506, 1466, 1179 cm^{-1}; ^{1}H NMR (400 MHz, $CDCl_3$) δ 6.88 (1H, s, H-5), 6.79 (1H, s, H-2), 4.54 (1H, d, J = 12.0 Hz, H-10a), 4.19 (1H, d, J = 12.0 Hz, H-10b), 3.81 (3H, s, OMe), 3.03 (1H d, J = 5.6 Hz, H-9a), 2.80 (1H, d, J = 5.6 Hz, H-9b), 2.80 (1H, sept, J = 7.0 Hz, H-2′), 2.17 (3H, s, H-7), 2.02 (3H, s, H-2″), 1.31 (3H, d, J = 7.0 Hz, H-3′), 1.30 (3H, d, J = 7.0 Hz, H-4′); ^{13}C NMR (100 MHz, $CDCl_3$) δ 175.6 (C, C-1′), 170.3 (C, C-1″), 155.3 (C, C-3), 141.3 (C, C-6), 128.2 (C, C-4), 126.6 (C, C-1), 124.3 (CH, C-2), 109.5 (CH, C-5), 65.1 (CH_2, C-10), 56.7 (C, C-8), 55.6 (CH_3, C-9), 50.6 (CH_3, OMe), 34.0 (CH, C-2′), 20.6 (CH_3, C-2″), 18.9 (CH_3, C-3′, C-4′), 16.0 (CH_3, C-7).

*(+)-(8S)-10-Benzoyloxy-6-methoxy-8,9-epoxythymol isobutyrate (**5**)*: yellow oil; $[\alpha]_{589}$ +10.3, $[\alpha]_{578}$ +10.7, $[\alpha]_{546}$ +12.0, $[\alpha]_{436}$ +20.3, $[\alpha]_{365}$ +31.5 (*c* 1.05, $CHCl_3$).

Vibrational Circular Dichroism Measurements. These data were obtained on a BioTools dualPEM Chiral*IR* FT spectrophotometer using 8.4, 8.8, 9.1, and 6.3 mg of **1**, **2**, **4**, and **5**, respectively. Each sample was dissolved in 100% D atom $CDCl_3$ (150 μL) and placed in BaF_2 cells with a path length of 100 μm. Data for **1**, **2**, **4**, and **5** were acquired at a resolution of 4 cm^{-1} for 6 h each, with the baseline provided by subtracting the spectrum of the solvent acquired under the same conditions, and the stability of samples was monitored by ^{1}H NMR measurements immediately before and after VCD measurements.

Vibrational Circular Dichroism Calculations. Monte Carlo search protocols were carried out for **1**, **2**, **4**, and **5**, using the Merck Molecular Force Field (MMFF94) as implemented in the Spartan'04 program. In the case of **1**, conformational searching was complemented with a systematic search, while for **2**, **4**, and **5** their rotational barriers were identified using the PCModel v7.0 software. Their Monte Carlo searches were carried out starting from four strategic low-energy conformers. An energy cutoff of 10 kcal/mol was considered, which yielded 139 conformers for **1**, 221 for **2**, 133 for **4**, and 128 for **5**. All conformers were examined to discard duplicates. The single-point energy of each conformer was calculated with the DFT B3LYP/6-31G(d) level of theory in the Spartan'04 program, giving 109 low-energy conformers for **1**, 105 for **2**, 64 for **4**, and 62 for **5**. These structures were geometry optimized with DFT at the PBEPBE/DGDZVP level of theory employing the Gaussian 03W or Gaussian 09 programs. The global minimum structures of **1**, **2**, **4**, and **5** are depicted in Figure 9. The minimized structures within the first 2 kcal/mol for these four compounds (Figures S21−S24, Supporting Information) were used to calculate the thermochemical parameters and the IR and VCD frequencies at 298 K and 1 atm. All minimum energy structures were verified for the absence of imaginary frequencies, and their relative free energies were employed to calculate their Boltzmann population. The Boltzmann-weighted IR and VCD spectra for each compound were calculated considering Lorentzian bands with half-widths of 6 cm^{-1}. Molecular visualization was carried out with the GaussView 3.0 program. Geometry optimization and vibrational calculations required some 30 h of computational time per

DOI: 10.1021/acs.jnatprod.7b00637
J. Nat. Prod. 2018, 81, 63−71

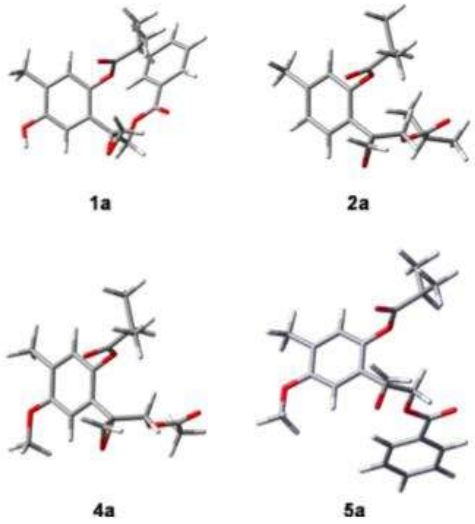

Figure 9. Global minimum energy conformers of thymol derivatives **1**, **2**, **4**, and **5**.

conformer when using a computer operating at 2.20 GHz with 8 Gb RAM and about 2 h when using Xiuhcoátl, the institutional supercomputer cluster hybrid.[34]

■ ASSOCIATED CONTENT

Supporting Information

The Supporting Information is available free of charge on the ACS Publications website at DOI: 10.1021/acs.jnatprod.7b00637.

Thermochemical analysis of epoxythymols **1**−**5**, copies of 1D and 2D NMR spectra of **1**−**5**, and minimum energy conformers of **1**−**5** (PDF)

■ AUTHOR INFORMATION

Corresponding Authors

*(C. M. Cerda-García-Rojas) E-mail: ccerda@cinvestav.mx. Tel: +52 55 5747 4035. Fax:+52 55 5747 7137.

*(M. A. Gómez-Hurtado) E-mail: magomez@umich.mx. Tel: +52 443 322 3500, ext. 4204. Fax: +52 443 326 5788.

ORCID

Carlos M. Cerda-García-Rojas: 0000-0002-5590-7908

Pedro Joseph-Nathan: 0000-0003-3347-3990

Notes

The authors declare no competing financial interest.

■ ACKNOWLEDGMENTS

We thank CIC-UMSNH and CONACYT-Mexico (Grant Nos. 238206 and 241053) for financial support. H.M.A.G. and J.C.P.N. are grateful to CONACYT-Mexico for scholarships 295638 and 268710, respectively. We are grateful to Professor Jerzy Rzedowski, Instituto de Ecología, A. C., Centro Regional del Bajío, Pátzcuaro, Michoacán, Mexico, for identifying the plant material, and acknowledge CGSTIC at CINVESTAV-IPN for providing HPC resources on the Hybrid Cluster Supercomputer "Xiuhcoátl" of the LANCAD CINVESTAV node for the scalemization of epoxythymol **1**.

■ REFERENCES

(1) Talavera-Alemán, A.; Rodríguez-García, G.; López, Y.; García-Gutiérrez, H. A.; Torres-Valencia, J. M.; del Río, R. E.; Cerda-García-Rojas, C. M.; Joseph-Nathan, P.; Gómez-Hurtado, M. A. *Phytochem. Rev.* **2016**, *15*, 251−277.

(2) Bustos-Brito, C.; Sánchez-Castellanos, M.; Esquivel, B.; Calderón, J. S.; Calzada, F.; Yepez-Mulia, L.; Hernández-Barragán, A.; Joseph-Nathan, P.; Cuevas, G.; Quijano, L. *J. Nat. Prod.* **2014**, *77*, 358−363.

(3) Bustos-Brito, C.; Vázquez-Heredia, V. J.; Calzada, F.; Yépez-Mulia, L.; Calderón, J. S.; Hernández-Ortega, S.; Esquivel, B.; García-Hernández, N.; Quijano, L. *Molecules* **2016**, *21*, 1132.

(4) Bohlmann, F.; Zdero, C. *Phytochemistry* **1977**, *16*, 1854−1855.

(5) Tori, M.; Ohara, Y.; Nakashima, K.; Sono, M. *J. Nat. Prod.* **2001**, *64*, 1048−1051.

(6) Bohlmann, F.; Niedballa, U.; Schulz, J. *Chem. Ber.* **1969**, *102*, 864−871.

(7) Bohlmann, F.; Jakupovic, J.; Lonitz, M. *Chem. Ber.* **1977**, *110*, 301−314.

(8) Herz, W.; Sosa, V. E. *Phytochemistry* **1988**, *27*, 155−159.

(9) Bohlmann, F.; Grenz, M.; Jakupovic, J.; King, R. M.; Robinson, H. *Phytochemistry* **1983**, *22*, 1213−1218.

(10) Marco, J. A.; Sanz-Cervera, J. F.; Manglano, E. *Phytochemistry* **1993**, *33*, 875−878.

(11) Trang, N. D.; Wanner, M. J.; Koomen, G. J.; Dung, N. X. *Planta Med.* **1993**, *59*, 480−481.

(12) Hernández, J. D.; Román, L. U.; Rodríguez, M. J.; Espiñeira, J.; Joseph-Nathan, P. *Phytochemistry* **1986**, *25*, 1743−1744.

(13) Delle-Monache, G.; Delle-Monache, F.; Becerra, J.; Silva, M.; Menichini, F. *Phytochemistry* **1984**, *23*, 1947−1950.

(14) Wang, Y.; Li, J.; Wang, H.; Jin, D. Q.; Chen, H.; Xu, J.; Ohizumi, Y.; Guo, Y. *Phytochem. Lett.* **2014**, *7*, 190−193.

(15) Du, G.; Li, Y.; Ma, S.; Wang, R.; Li, B.; Guo, F.; Zhu, W.; Li, Y. *J. Nat. Prod.* **2015**, *78*, 2968−2974.

(16) Joseph-Nathan, P.; Gordillo-Román, B. In *Progress in the Chemistry of Organic Natural Products*; Kinghorn, A. D., Falk, H., Kobayashi, J., Eds.; Springer International Publishing: Cham, Switzerland, 2015; Vol. *100*, pp 311−451.

(17) Burgueño-Tapia, E.; Joseph-Nathan, P. *Nat. Prod. Commun.* **2015**, *10*, 1785−1795.

(18) Mossa, J. S.; El-Feraly, F. S.; Muhammad, I.; Zaw, K.; Mbwambo, Z. H.; Pezzuto, J. M.; Fong, H. H. S. *J. Nat. Prod.* **1997**, *60*, 550−555.

(19) Zee, O. P.; Kim, D. K.; Lee, K. R. *Arch. Pharmacal Res.* **1998**, *21*, 618−620.

(20) Werner, H.; Sosa, V. E. *Phytochemistry* **1988**, *27*, 155−159.

(21) Yi, J.; Du, G.; Yang, Y.; Li, Y.; Li, Y.; Guo, F. *Tetrahedron: Asymmetry* **2016**, *27*, 1153−1159.

(22) Antkowiak, R.; Antkowiak, W. Z.; Nowak-Wydra, B. *Heterocycles* **2002**, *58*, 137−146.

(23) Yuste, F.; Sánchez-Obregón, R.; Díaz, E.; García-Carrillo, M. A. *Tetrahedron: Asymmetry* **2014**, *25*, 224−228.

(24) Hu, X.; Yang, Y.; Shi, S.; Shan, Z. *Chirality* **2016**, *28*, 784−788.

(25) Borowiecki, P. *Tetrahedron: Asymmetry* **2015**, *26*, 16−23.

(26) Redondo, J.; Capdevila, A.; Ciudad, S. *Chirality* **2013**, *25*, 780−786.

(27) Redondo, J.; Capdevila, A.; Latorre, I. *Chirality* **2010**, *22*, 472−478.

(28) Bustos-Brito, C.; Esquivel, B.; Calzada, F.; Yepez-Mulia, L.; Calderón, J. S.; Porras-Ramirez, J.; Quijano, L. *Chem. Biodiversity* **2016**, *13*, 1281−1289.

(29) García, P. G.; García, S. E.; Martínez, G. I.; Scior, R. F. T.; Salvador, J. L.; Martínez, P. M. M.; del Río, R. E. *Rev. Bras. Farmacogn.* **2011**, *21*, 928−935.

(30) Silva, M. S.; Pietrobom, D. *New J. Chem.* **2015**, *39*, 8240−8244.

(31) Pardo-Novoa, J. C.; Arreaga-González, H. M.; Gómez-Hurtado, M. A.; Rodríguez-García, G.; Cerda-García-Rojas, C. M.; Joseph-Nathan, P.; del Río, R. E. *J. Nat. Prod.* **2016**, *79*, 2570−2579.
(32) Höltje, H. D.; Folkers, G. In *Molecular Modeling. Basic Principles and Applications*; Mannhold, R.; Kubinyi, H.; Timmerman, H., Eds.; Methods and Principles in Medicinal Chemistry; VCH: Weinheim, 1996; Vol. *5*, Chapter 2, pp 23−29.
(33) Debie, E.; Gussem, E. D.; Dukor, R. K.; Herrebout, W.; Nafie, L. A.; Bultinck, P. *ChemPhysChem* **2011**, *12*, 1542−1549.
(34) http://clusterhibrido.cinvestav.mx/.

DOI: 10.1021/acs.jnatprod.7b00637
J. Nat. Prod. 2018, 81, 63−71

JOURNAL OF NATURAL PRODUCTS

Article

Cite This: J. Nat. Prod. XXXX, XXX, XXX−XXX

pubs.acs.org/jnp

Biomimetic Transformation of *p*-Menthene Glucosides into *p*-Cymenes and Carvotanacetone

Julio C. Pardo-Novoa,[†] Héctor M. Arreaga-González,[‡] Sinuhé Galván-Gómez,[‡] Gabriela Rodríguez-García,[‡] Rosa E. del Río,[‡] Carlos M. Cerda-García-Rojas,*[,†] Pedro Joseph-Nathan,[†] and Mario A. Gómez-Hurtado*[,‡]

[†]Departamento de Química, Centro de Investigación y de Estudios Avanzados del Instituto Politécnico Nacional, Apartado 14-740, Mexico City 07000, Mexico

[‡]Instituto de Investigaciones Químico-Biológicas, Universidad Michoacana de San Nicolás de Hidalgo, Ciudad Universitaria, Morelia, Michoacán 58030, Mexico

Supporting Information

ABSTRACT: A biomimetic transformation of *p*-menthene glucosides into aromatic monoterpenoids that alluded to mechanisms for essential oil metabolism, which lines up with the precepts of molecular economy, is described. Acid treatment of (−)-(3*S*,4*S*,6*R*)-3,6-dihydroxy-1-menthene 3-*O*-*β*-D-glucopyranoside (**1**) and (−)-(3*S*,4*R*,5*R*,6*S*)-3,5,6-trihydroxy-1-menthene 3-*O*-*β*-D-glucopyranoside (**2**), from *Ageratina glabrata*, yielded *p*-cymene (**7**) and carvacrol (**9**). The stable oxidized intermediates (+)-(3*S*,4*S*,6*R*)-3,6-dihydroxy-1-menthene (**3**), (+)-(1*S*,4*S*,6*R*)-1,6-dihydroxy-2-menthene (**4**), (+)-(1*R*,4*S*,6*R*)-1,6-dihydroxy-2-menthene (**5**), (+)-(4*S*,6*R*)-yabunikkeol (**6**), (+)-(4*S*)-carvotanacetone (**8**), (+)-(1*S*,4*S*,5*R*,6*R*)-1,5,6-trihydroxy-2-menthene (**15**), (+)-(1*R*,4*S*,5*R*,6*R*)-1,5,6-trihydroxy-2-menthene (**16**), and the new (+)-(4*S*,5*R*,6*S*)-1(7),2-menthadiene (**17**) permitted establishment of the reaction mechanisms. The reactivity of the hydroxy groups of **4** and **5**, as well as those of **15** and **16**, was compared by acetylation reactions and supported by DFT calculations, revealing diminished reactivity in **4** and **15** due to the *cis* configuration of their hydroxy groups at C-1 and C-6. In addition, *p*-cymene (**7**) was detected as one of the major constituents of the essential oil of *A. glabrata*, which matches well with the biomimetic study.

Ageratina glabrata

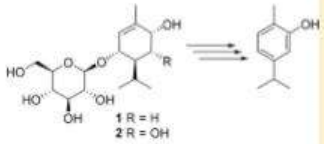

The biosynthetic pathway of *p*-menthenes assumes the isomerization of geranyl diphosphate to neryl diphosphate, followed by cyclization through an allylic cation−diphosphate ion-pair to afford an *α*-terpinyl cation, which is an intermediate in the formation of several mono- and bicyclic monoterpenes.[1] Oxidation, isomerization, transposition, and other reactions lead to an extensive variety of monoterpenes, of which many are found in essential oils. The biosynthetic pathway of aromatic monoterpenes is closely related to *γ*-terpinene,[2] limonene, menthene, and carvone through dehydrogenation reactions,[3] while the storage of volatile compounds in plants proceeds through nonvolatile glycosides, which after enzymatic glycolysis liberate the volatile aglycone and the sugar residue.[4−7] Nonetheless, due to the molecular economy observed in cell metabolic processes, we can visualize the relationship between the storage of volatile compounds and the presence of a few strategic precursors capable of providing essential oil constituents. Therefore, the understanding of anabolic and catabolic mechanisms, related to volatile compounds, becomes relevant to the biosynthetic pathways of these metabolites for subsequent chemical, biological, biotechnological, and industrial applications.[8]

Previously we described the absolute configuration determination of (−)-(3*S*,4*S*,6*R*)-3,6-dihydroxy-1-menthene 3-*O*-*β*-D-glucopyranoside (**1**) and (−)-(3*S*,4*R*,5*R*,6*S*)-3,5,6-trihydroxy-1-menthene 3-*O*-*β*-D-glucopyranoside (**2**), from *Ageratina glabrata*, and their derivatives (+)-(3*S*,4*S*,6*R*)-3,6-dihydroxy-1-menthene (**3**), (+)-(1*S*,4*S*,6*R*)-1,6-dihydroxy-2-menthene (**4**), (+)-(1*R*,4*S*,6*R*)-1,6-dihydroxy-2-menthene (**5**), (+)-(1*S*,4*S*,5*R*,6*R*)-1,5,6-trihydroxy-2-menthene (**15**), and (+)-(1*R*,4*S*,5*R*,6*R*)-1,5,6-trihydroxy-2-menthene (**16**), obtained by acid hydrolysis.[9]

In this paper the biomimetic transformations of **1** and **2** into aromatic monoterpene derivatives and other essential oil constituents, by dehydration and oxidation processes, are described. Dihydroxy-*p*-menthene derivatives **3**−**5**, (+)-(4*S*,6*R*)-yabunikkeol (**6**), 1,5,6-triols **15** and **16**, and the new (+)-(4*S*,5*R*,6*S*)-1(7),2-menthadiene (**17**), as reaction intermediates in the formation of *p*-cymene (**7**) and carvacrol

Special Issue: Special Issue in Honor of Drs. Rachel Mata and Barbara Timmermann

Received: October 14, 2018

DOI: 10.1021/acs.jnatprod.8b00855
J. Nat. Prod. XXXX, XXX, XXX−XXX

(9), were suggested. (+)-(4*S*)-Carvotanacetone (8) was also observed as a dehydration product of 4 and 5, while oxidation with iodine suggested that *p*-cymene (7) and carvacrol (9) could arise from a common precursor, 4. The reactivity of the tertiary hydroxy group of 4, 5, 15, and 16 was studied through the preparation of their respective acetyl derivatives 10−13 and 18−21, determining that the *trans*-1,6-diol disposition found in 5 and 16 was more reactive than the *cis* arrangement found in 4 and 15 and that the steric effects of the isopropyl group are insignificant, while fewer hydroxy group intramolecular interactions favor reactivity. All compounds were characterized by physical and spectroscopic data, while GC-MS analysis of the essential oil of the aerial parts from *A. glabrata* revealed *p*-cymene (7) as a main constituent,[10] supporting the herein proposed chemical pathways.

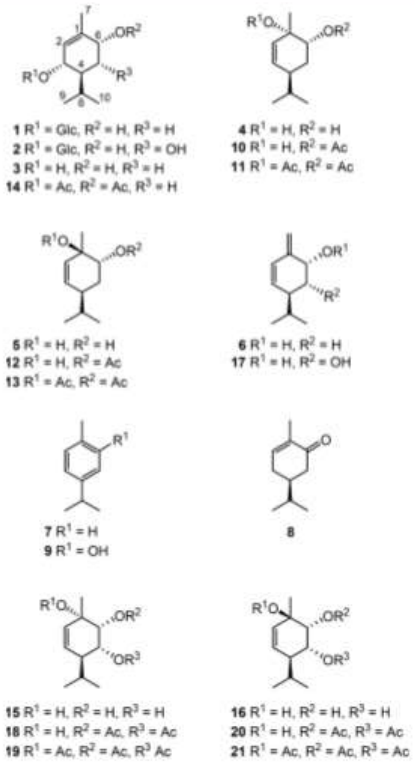

Figure 1. Formulas of *p*-Menthenes 1−21.

■ RESULTS AND DISCUSSION

Menthene glucosides 1 and 2 were individually hydrolyzed using diluted HCl to generate hydroxy-*p*-menthenes 3−5 from 1, and 15 and 16 from 2.[9] Considering 4, 5, 15, and 16 arise from H_2O trapping an allylic carbocation, induced by elimination at C-3 in 2 or 3, these molecules were considered as possible essential oil constituent intermediates. Such an idea is in accord with several investigations where glycosides function as a storage mechanism for volatile compounds.[4−7]

Carbocation formation was induced by acid hydrolysis in a polar protic medium. Dehydration of *p*-menthene 4 and/or 5 using 10% HCl yielded a mixture of (+)-yabunikkeol (6), *p*-cymene (7), and (+)-(4*S*)-carvotanacetone (8) in a 1:4:10 ratio, establishing 8 as the most favored isomer. Furthermore, acid hydrolysis of 6, under the same reaction conditions used for 4 or 5, afforded *p*-cymene (7), suggesting that 6 is a subsequent intermediate in the aromatization process from glucoside 1 to 7. Thus, (Scheme 1), acid hydrolysis of 1 provides *p*-menthene 3[9] as the first intermediate, followed by protonation of the C-3 hydroxy group and subsequent dehydration to give allylic carbocation **I**, which is quenched by addition of water at C-1, yielding 4 and 5 as the next diol intermediates. Based on steric considerations a less probable route for generating 4 and 5 would involve an allylic alcohol exchange via hydroxylation at C-1 of 3. Activation of 4 or 5 via protonation at the tertiary hydroxy group favors dehydration at C-1 by proton loss from CH_3-7 to give 6. Finally, loss of the C-5 protonated hydroxy group from 6 to give **II** (path a) and subsequent deprotonation at C-5 provides triene **III**, whose acid-catalyzed rearrangement leads to *p*-cymene (7). The aromatization could occur by a concerted mechanism or via a carbocation pathway as depicted in Scheme 1.

For the generation of (+)-(4*S*)-carvotanacetone (8) from 1, the aforementioned steps leading to the formation of 4 or 5 could afford the allylic carbocation **IV**, directly or through 6 followed by protonation of the $\Delta^{1(7)}$ double bond (path b). A subsequent 1,3-hydride shift from C-5 to C-3 would give **V**, which would be susceptible to a 1,2-hydride shift from C-6 to C-5 in concert with deprotonation of the 6-hydroxy group to afford ketone 8. The above route is supported by density functional theory (DFT) calculations at the B3LYP/6-31G(d) level of theory of the reaction intermediates **IV** and **V**, as in several mechanistic proposals for terpene syntheses, including those for *p*-menthene derivatives.[11−14] In the present case 98.6% of the population of **IV** showed an H-3−C-3−C-5−H-5 relative orientation of −75.5 ± 4.7° and a C-3−C-5 distance of 2.47 ± 0.008 Å to favor the 1,3-hydride shift. The measured parameters for **V** (P = 97.7%) revealed a H-5−C-5−C-6−H-6 dihedral angle (θ = −71.5 ± 3.9°) and a C-5−C-6 bond distance (d = 1.47 Å) to permit the 1,2-hydride shift.

(+)-Yabunikkeol (6) was described as an oxidation derivative of (−)-α-phellandrene,[15] although the (4*R*,6*S*) absolute configuration was wrongly assigned, while *p*-cymene (7) and (+)-(4*S*)-carvotanacetone (8) are widely reported as essential oil components. In addition, 7 has been considered a good-quality essential oil ingredient in *Origanum* species[16] or a low-quality ingredient in lemon essential oil.[17]

Since allylic alcohol intermediates 4−6 lead to aromatic 7, iodine was considered as the aromatization reagent.[18,19] Thus, *p*-menthenediol 4 was refluxed in the presence of iodine for 3 h to yield 8 and 9 (1:2), while aromatization for 5 h only provided carvacrol (9). Therefore, 8 is an intermediate in the aromatization process as suggested in Scheme 1, where the coordination of iodine to the tertiary hydroxy group of 4, as depicted in **IX**, facilitates dehydration and formation of 6, whose protonation at C-7 by HI favors allylic carbocation **IV**. Subsequent 1,3-hydride shifts to **V** and 1,2-hydride shifts afforded 8. Formation of the iodoiranium intermediate **VI** is followed by rupture of the C-2−I bond to allow formation of the Δ^2 double bond in intermediate **VII**. Deiodination affords carbocation **VIII**, which on deprotonation at C-4 and spontaneous tautomerization would generate 9. Thus,

DOI: 10.1021/acs.jnatprod.8b00855
J. Nat. Prod. XXXX, XXX, XXX−XXX

Scheme 1. Putative Mechanism for the Aromatization of *p*-Menthenes 4 and 5

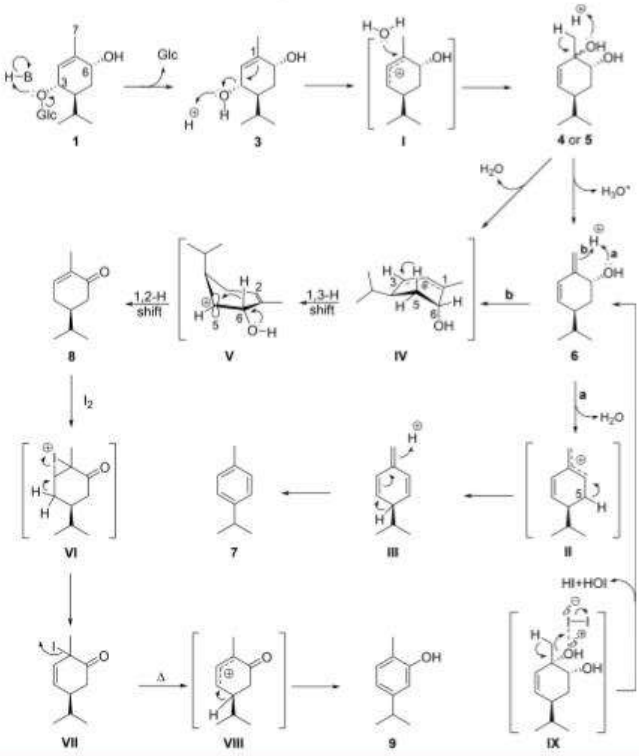

iodoiranium-assisted aromatization intermediates become plausible since acid conditions deactivate the carbonyl moiety in **8**, via keto−enol tautomerism, which at the end may contribute to the aromatization process, but avoiding dehydration by acid catalysis as in the formation of *p*-cymene (**7**). Consequently, (+)-(4*S*)-carvotanacetone (**8**) can be considered as a common constituent in essential oils related to the aromatic monoterpene biosynthesis. This mechanistic proposal is based on those described for terpene aromatization using iodine as a mild reagent.[18,19]

Although **4** and **5** provided the same aromatization products, their reactivity was assessed by acetylation of the C-1 hydroxy group, since reactivity variations in the crude reaction outcomes were observed by ^{1}H NMR. A 25:1 mixture of **10** and **11** was obtained from **4**, while **5** yielded the *p*-menthene mixture of **12** and **13** in a 10:1 ratio. Thus, the 1-hydroxy group in **5** is a more favorable nucleophile than that at **4**, perhaps due to a reduced hydroxy group interaction due to their *trans* disposition. These results also discard possible steric effects exerted by the isopropyl group, as revealed by **5**. In support of conformational preferences of **4** and **5**, calculations were done with the Monte Carlo protocol using a molecular model force field (MMFF). All conformer energies were optimized at the DFT B3LYP/6-31G(d) level of theory, a methodology successfully employed for the conformational analysis of aliphatic[9] and aromatic *p*-menthene derivatives,[20] thus providing 29 conformers for **4** and 43 conformers for **5** in 10 kcal/mol energy gaps. Measurements of the O-1−H-1···O-6, O-6−H-6···O-1, and O-1···O-6 bond lengths and angles (Table S1, Supporting Information) suggested that 99.9% of the conformational population of **4** favor weak hydrogen-bonding interactions, while in **5** only 50% of the conformational population favor probable hydrogen-bonding interactions.[21,22] In turn, acetylation of **3** gave the expected diacetate **14**.

Once the behavior of *p*-menthenediols **4** and **5** was studied under acid- and iodine-catalyzed reaction conditions, glucoside **2** was evaluated under the same conditions. Acid hydrolysis of **2** yielded the triol epimers **15** and **16**,[9] which were individually dissolved in tetrahydrofuran (THF) and treated with 10% HCl. In either case two compounds were obtained and separated by column chromatography, affording carvacrol (**9**) and a sample of amorphous material, whose ^{1}H NMR data suggested the Δ^2 endocyclic double bond conjugated with an exocyclic $\Delta^{1(7)}$ olefinic bond, whose signals were observed in the δ 6.18−5.12 range. In addition, two hydrogen signals geminal to hydroxy groups resonated at δ 4.33 (H-6) and 3.75 (H-5). The ^{13}C NMR spectrum showed the expected 10 signals for a *p*-menthene skeleton, including four signals assigned to the conjugated diene moiety in the δ 143.5−115.2 range and two signals at δ 71.6 and 71.4 attributed to C-6 and C-5, respectively. The HRESIMS data confirmed the $C_{10}H_{16}O_2$

DOI: 10.1021/acs.jnatprod.8b00855
J. Nat. Prod. XXXX, XXX, XXX−XXX

Scheme 2. Putative Mechanism for the Aromatization of *p*-Menthenes 15 and 16

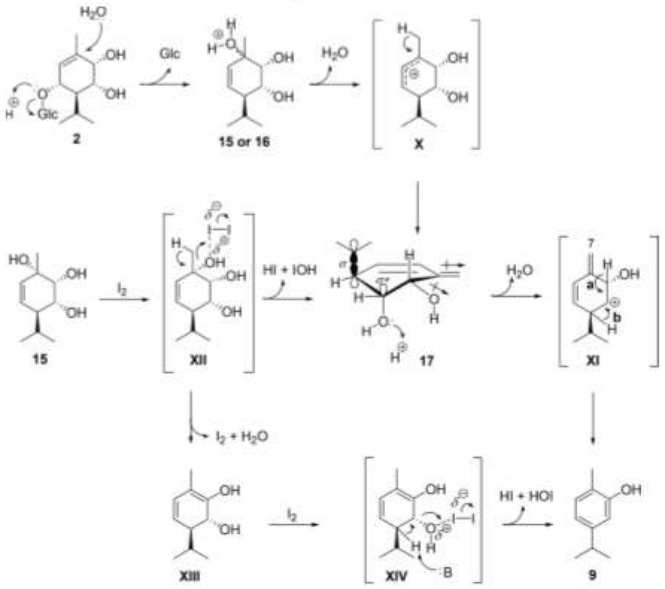

composition showing the $[M + NH_4]^+$ molecular ion at m/z 186.1497 (calcd as $C_{10}H_{16}O_2 + NH_4^+$, 186.1494), while the specific rotation was dextrorotatory. These data suggested the identity of the compound as the new *p*-menthene derivative (+)-(4*S*,5*R*,6*S*)-5,6-dihydroxy-1(7),2-menthadiene (**17**). Unequivocal structure assignment of **17** was supported by HETCOR, COSY, NOESY, and HMBC spectra. Treatment of **17** with 10% HCl for 24 h yielded carvacrol (**9**).

Based on the overall chemical transformations, an aromatization reaction mechanism of **2**, through **15**−**17** to carvacrol (**9**), including stable reaction intermediates, is suggested in Scheme 2, which involves protonation of the allylic tertiary hydroxy group of **15** and/or **16** followed by dehydration. The allylic carbocation intermediate **X** is stabilized through deprotonation at C-7, yielding **17**. This stable diol has the potential to also undergo a dehydration at C-5 affording conjugated diene carbocation **XI**, which can be deprotonated at C-6 as shown in **XI** (shift a), followed by protonation at C-7 and concomitant deprotonation at C-4 to generate carvacrol (**9**). The other alternative, shown in **XI** (shift b), involves deprotonation at C-4, providing a conjugated triene, which aromatizes to **9**. The possibility to obtain thymol as the final aromatic compound, via dehydration at C-6, was unsuccessfully searched.

To explain the regiospecific dehydration in **17**, conformational population calculations were done by the Monte Carlo protocol using MMFF. All conformer energies were optimized at the DFT B3LYP/6-31G(d) level of theory as described above. This procedure provided 22 conformers in a 10 kcal/mol range, of which 74% of the conformer population revealed the C-5 hydroxy group and the isopropyl group in a *pseudo-trans* diaxial arrangement with a dihedral angle of 152 ± 7.4°, favoring $\sigma-\sigma^*$ conformational interactions, as depicted in Scheme 2, increasing the reactivity of the 5-hydroxy group and directing regiospecificity toward formation of **9**. In addition, the polar reaction medium stabilizes the equatorial 6-hydroxy group via a dipole−dipole interaction with the exocyclic double bond.[23] Coupling constant analysis was not used for the conformational analysis since H-5 and H-6 resonated as undefined broad signals.

A reactivity comparison of the hydroxy groups at C-1 in **15** and **16** was done as for **4** and **5**. Acetylation of **15** gave a 10:1 mixture of **18** and **19**. From the acetylation of **16** the formation of compounds **20** and **21** was expected. However, the ^{1}H NMR spectrum revealed the presence of **20**, a complex mixture of acetylated compounds of undefined identity, and traces of **21**, readily recognized by its typical H-2 signal at δ 6.13 (Figure S54, Supporting Information). It thus seems that **20** suffers degradation via reaction of the hydroxy group at C-1 since hydrogen atoms geminal to the C-5 and C-6 acetoxy groups at δ 5.72−4.76 and acetoxy signals at δ 2.23−2.00 were observed. This evidences a higher reactivity of the hydroxy group at C-1 in **16** than in **15**, which is similar to the case of **5**. As done for **4** and **5**, DFT calculations for **15** and **16** were performed, affording 37 conformers for **15** and 48 conformers for **16** in 10 kcal/mol gaps. These calculations revealed intramolecular hydrogen bonding interactions in 99.7% of the conformational population of **15**, of which essentially all involve the oxygen atom at C-1. In turn, only 24% of the conformational population of **16** shows this type of interaction, thus inhibiting the tertiary hydroxy group from interacting, and consequently the nucleophilicity of the hydroxy group at C-1 in **16** is higher than in **15**. Modification of reaction conditions for the acetylation permitted the preparation of **20** and **21** (see Experimental Section).

The iodine aromatization reaction of **15** gave carvacrol (**9**) as the regiospecific aromatization product. This reaction is similar to the acid-catalyzed aromatization of **15**, despite the

DOI: 10.1021/acs.jnatprod.8b00855
J. Nat. Prod. XXXX, XXX, XXX−XXX

fact that thymol and/or carvacrol (**9**) formation might be possible. Thus, a plausible reaction mechanism (Scheme 2) for the transformation of **15** involves the charged iodine-bonded adduct at the tertiary hydroxy group in **XII** followed by dehydration, yielding the $\Delta^{1(6)}$ double bond in **XIII**. Since keto−enol tautomerism of this intermediate is expected, deactivation of the hydroxy group at C-6 leads to dehydration at C-5 to yield **9**, via adduct **XIV**. Alternatively, dehydration of the hydroxy group at C-1, via iodine charged complex **XII**, to form **17** followed by dehydration of the hydroxy group at C-5, via **XI** (shift a or b), favors aromatization to **9**. In the latter alternative, regiospecificity could be induced by conformational effects, as well as dipole−dipole interactions in the considered intermediate **17**, since the polarity of the reaction medium increases due to H_2O and HI formation during the reaction process.

Interestingly, NMR and GC-MS essential oil analysis of the leaves revealed the presence of *p*-cymene (**7**) as a main constituent in the mixture, thus supporting the present biomimetic study. On the above basis it seems that several biochemical processes may be related to laboratory studies, under the principle that chemistry rules are applied in any reaction system, but probably stereospecificity and reaction rates are the most important differences between enzymatic and chemical systems. In addition, biomimetic studies provide chemical pathways applied to two targets: the synthesis of organic molecules of interest[24−26] and understanding the observed biosynthetic pathways of natural products in living systems.[27] Moreover, glucosides **1** and **2** may favor the formation of aromatic *p*-menthene derivatives **7** and **9** through catabolic processes, which could be related to several anabolic pathways providing multifunctionalized thymol derivatives, similar to those reported from *Ageratina glabrata*.[20,28,29] Other relevant conclusions are the observation of precise chemical routes for molecular transformations and the observation of chemical economy during these processes.

■ EXPERIMENTAL SECTION

General Experimental Procedures. Melting points (uncorrected) were determined on a Fisher−Johns apparatus. Optical rotations were recorded in $CHCl_3$ solutions at room temperature on a PerkinElmer 341 polarimeter. 1D and 2D NMR spectra were measured at 300 or 400 MHz for ^{1}H and at 75.4 or 100 MHz for ^{13}C on Varian Mercury 300 or 400 spectrometers from $CDCl_3$ solutions using tetramethylsilane as the internal reference. Chemical shift values are reported in parts per million, and coupling constants (*J*) are in Hz. HRMS data were acquired on a Waters Synapt G2 spectrometer at the Department of Chemistry and Biochemistry, University of Colorado, Boulder, CO, USA. Silica gel 230−400 mesh (Merck) was used for column chromatography.

Compounds. Menthene derivatives **1**−**5**, **15**, and **16** were obtained as described.[9] A combination of vibrational circular dichroism, single-crystal X-ray diffraction, and chemical correlations allowed securing[9] their absolute configuration (AC). Since all other chiral molecules of the present study were also chemically correlated with the above molecules, their AC is also fully substantiated. In turn, monoterpenes **7**−**9** are known molecules.[30−33] In cases when more than one acetyl group was present, the signal distinction followed from gHSQC and gHMBC NMR measurements.

Dehydration and Aromatization Reactions. Solutions of **4** or **5** (100 mg each) in THF (1 mL) were treated with aqueous 10% HCl (5 mL) and stirred at room temperature for 5 h. Each reaction mixture was washed with a saturated $NaHCO_3$ solution, poured over ice−H_2O, extracted with CH_2Cl_2, dried over anhydrous Na_2SO_4, filtered, and evaporated to dryness. Each residue was column chromatographed on silica gel using hexanes−CH_2Cl_2 mixtures as eluent. Fractions 4−7 (hexanes−CH_2Cl_2, 4:1) afforded **8** (24 mg, 30%), fractions 8−12 (hexanes−CH_2Cl_2, 1:1) yielded **6** (11 mg, 12%), and fractions 15−17 (hexanes−CH_2Cl_2, 3:7) gave **7** (52 mg, 58%). Similarly, a solution of **15** and **16** (70 mg) was treated as above. Column chromatography of the residue afforded **9** (19 mg, 34%) in fractions 8−11 (hexanes−CH_2Cl_2, 3:2) and **17** (42 mg, 66%) in fractions 15−19 (CH_2Cl_2−MeOH, 49:1). Acid treatment of **6** (20 mg), as above, yielded **7** (11 mg, 63%) in fractions 3−5 (hexanes−CH_2Cl_2, 4:1), while **17** (40 mg) for 5 h afforded **9** (28 mg, 80%) in fractions 5−7 (hexanes−CH_2Cl_2, 3:2).

Samples of **4** or **15** (40 mg each) were dissolved in toluene (10 mL), and iodine (40 mg) was added. Each reaction mixture was stirred under reflux for 5 h. Each residue was washed with a saturated $Na_2S_2O_3$ solution, $NaHCO_3$, and NaCl, poured over ice−H_2O, extracted with hexanes, dried over anhydrous Na_2SO_4, filtered, and evaporated to yield 28 mg (80%) of **9** from **4** and 30 mg (94%) from **15**. Similarly, a solution of **4** (30 mg) in toluene (10 mL) was treated with iodine (30 mg) for 3 h. The residue was column chromatographed on silica gel using hexanes−CH_2Cl_2. Fractions 3−5 (hexanes−CH_2Cl_2, 3:2) afforded **9** (17 mg, 64%), and fractions 5−7 (hexanes−CH_2Cl_2, 3:7) gave **8** (7 mg, 26%).

Acetylation Reactions. Solutions of **3** (40 mg), **4**, **5**, **15**, or **16** (30 mg each) were dissolved in pyridine (1 mL), and Ac_2O (1 mL) was added. Each reaction mixture was stirred at room temperature for 24 h, or 3 h for **3**, poured over ice−H_2O, and extracted with EtOAc. Each organic layer was washed with aqueous 10% HCl, H_2O, aqueous $NaHCO_3$, and H_2O, dried over anhydrous Na_2SO_4, filtered, and evaporated. The residue from the reaction of **3** was extracted to yield **14** (38 mg, 85%). Column chromatography of the reaction of **4** afforded **10** (18 mg, 48%) and **11** (11 mg, 25%), while that of **5** yielded **12** (26 mg, 70%) and **13** (3 mg, 7%). Chromatography of the residue from **15** afforded **18** (25 mg, 57%) and **19** (3 mg, 6%), while that from **16** yielded **20** (20 mg, 46%) and **21** (8 mg, 16%).

Reactivity Assay of 4, 5, 15, and 16. The studies were done by acetylation using the above reaction conditions for 12 h, and the crude reaction mixtures were analyzed by ^{1}H NMR spectroscopy.

(+)-(4S,6R)-Yabunikkeol (6): colorless oil; $[\alpha]_{589}$ +5, $[\alpha]_{578}$ +5, $[\alpha]_{546}$ +5, $[\alpha]_{436}$ +13, $[\alpha]_{365}$ +23 (*c* 0.1, $CHCl_3$); lit.[30] $[\alpha]_{589}$ +5.0 (*c* 0.8, $CHCl_3$); lit.[15] $[\alpha]_{589}$ +4.2 (*c* 3.1, $CHCl_3$); IR ($CHCl_3$) ν_{max} cm^{-1} 3411, 2957, 2925, 1675, 1464, 1038, 892; ^{1}H NMR ($CDCl_3$, 400 MHz) δ 6.14 (1H, dd, *J* = 10.1, 2.6 Hz, H-3), 5.83 (1H, dd, *J* = 10.1, 1.0 Hz, H-2), 5.06 (1H, br s, H-7), 4.96 (1H, br s, H-7′), 4.42 (1H, m, H-6), 2.34 (1H, m, H-4), 1.91 (1H, m, H-5), 1.72 (1H, septd, *J* = 6.8, 1.1 Hz, H-8), 1.55 (1H, m, H-5′), 0.93 (6H, d, *J* = 6.8 Hz, CH_3-9 and CH_3-10); ^{13}C NMR ($CDCl_3$, 100 MHz) δ 145.3 (C, C-1), 134.0 (CH, C-2), 126.6 (CH, C-3), 112.9 (CH_2, C-7), 69.4 (CH, C-6), 37.2 (CH, C-4), 32.5 (CH_2, C-5), 31.5 (CH, C-8), 19.6 (CH_3, C-9), 19.60 (CH_3, C-10); IR and ^{1}H and ^{13}C NMR data in agreement with published values.[15,34,35]

(+)-(1S,4S,6R)-6-Acetoxy-1-hydroxy-2-menthene (10): colorless oil; $[\alpha]_{589}$ +9, $[\alpha]_{578}$ +9, $[\alpha]_{546}$ +12, $[\alpha]_{436}$ +28, $[\alpha]_{365}$ +64 (*c* 2.7, $CHCl_3$); IR ($CHCl_3$) ν_{max} 3582, 2959, 2870, 1727, 1464, 1375 cm^{-1}; ^{1}H NMR (400 MHz, $CDCl_3$) δ 5.67 (1H, ddd, *J* = 10.4, 2.8, 1.2 Hz, H-3), 5.59 (1H, ddd, *J* = 10.4, 2.4, 1.2 Hz, H-2), 4.94 (1H, ddd, *J* = 6.4, 2.4, 1.2 Hz, H-6), 2.10 (3H, s, Ac), 2.10 (1H, m, H-4), 2.02 (1H, tdd, *J* = 13.0, 6.0, 1.2 Hz, H-5), 1.64 (1H, m, H-8), 1.58 (1H, ddd, *J* = 13.0, 8.8, 2.4 Hz, H-5′), 1.29 (3H, s, CH_3-7), 0.89 (3H, d, *J* = 7.0 Hz, CH_3-9), 0.88 (3H, d, *J* = 7.0 Hz, CH_3-10); ^{13}C NMR (100 MHz, $CDCl_3$) δ 170.8 (C, Ac), 131.9 (CH, C-2), 131.2 (CH, C-3), 75.8 (CH, C-6), 69.0 (C, C-1), 38.1 (CH, C-4), 31.4 (CH, C-8), 26.9 (CH_2, C-5), 21.3 (CH_3, Ac) 27.0 (CH_3, C-7), 19.5 (CH_3, C-9), 19.4 (CH_3, C-10); HRESIMS *m*/*z* 235.1312 [M + Na]$^+$ (calcd for $C_{12}H_{20}O_3$ + Na$^+$, 235.1308).

(+)-(1S,4S,6R)-1,6-Diacetoxy-2-menthene (11): colorless oil; $[\alpha]_{589}$ +65, $[\alpha]_{578}$ +68, $[\alpha]_{546}$ +78, $[\alpha]_{436}$ +144, $[\alpha]_{365}$ +253 (*c* 1.2, $CHCl_3$); IR ($CHCl_3$) ν_{max} 2058, 1728, 1370 cm^{-1}; ^{1}H NMR (400 MHz, $CDCl_3$) δ 6.01 (1H, ddd, *J* = 10.0, 2.4, 0.7 Hz, H-2), 5.73 (1H, dd, *J* = 10.0, 2.8 Hz, H-3), 5.23 (1H, dd, *J* = 8.0, 2.8 Hz, H-6), 2.16 (1H, m, H-4), 2.10 (3H, s, Ac), 2.03 (1H, m, H-5), 2.01 (3H, s, Ac),

DOI: 10.1021/acs.jnatprod.8b00855
J. Nat. Prod. XXXX, XXX, XXX−XXX

1.71 (1H, m, H-8), 1.65 (3H, s, CH_3-7), 1.64 (1H, m, H-5′), 1.57 (3H, s, H-7), 0.92 (6H, d, J = 7.0 Hz, CH_3-9, CH_3-10); ^{13}C NMR (100 MHz, $CDCl_3$) δ 170.5 (C, Ac), 170.1 (C, Ac), 132.5 (CH, C-3), 128.8 (CH, C-2), 78.3 (C, C-1), 73.4 (CH, C-6), 38.8 (CH, C-4), 31.7 (CH, C-8), 25.9 (CH_2, C-5), 23.3 (CH_3, C-7), 22.1 (CH_3, Ac), 21.2 (CH_3, Ac), 19.7 (CH_3, C-9), 19.5 (CH_3, C-10); HRESIMS m/z 277.1414 $[M]^+$ (calcd for $C_{14}H_{22}O_4$, 277.1410).

(+)-(1R,4S,6R)-6-Acetoxy-1-hydroxy-2-menthene (12): colorless oil; $[\alpha]_{589}$ +1, $[\alpha]_{578}$ +1, $[\alpha]_{546}$ +2, $[\alpha]_{436}$ +7, $[\alpha]_{365}$ +22 (c 0.8, $CHCl_3$); IR ($CHCl_3$) ν_{max} 3592, 2956, 1722, 1374, 1035 cm^{-1}; ^{1}H NMR (400 MHz, $CDCl_3$) δ 5.74 (1H, dd, J = 10.2, 2.7 Hz, H-3), 5.61 (1H, ddd, J = 10.2, 2.3, 1.0 Hz, H-2), 4.97 (1H, dd, J = 6.0, 3.8 Hz, H-6), 2.08 (3H, s, Ac), 2.06 (1H, m, H-4), 1.81 (1H, m, H-8), 1.79 (1H, m, H-5), 1.68 (1H, m, H-5′), 1.27 (3H, s, CH_3-7), 0.91 (3H, d, J = 6.8 Hz, CH_3-10), 0.92 (3H, d, J = 6.8 Hz, CH_3-9); ^{13}C NMR (100 MHz, $CDCl_3$) δ 171.0 (C, Ac), 132.4 (CH, C-2), 131.6 (CH, C-3), 75.6 (CH, C-6), 69.3 (C, C-1), 38.4 (CH, C-4), 31.6 (CH, C-8), 26.4 (CH_2, C-5), 24.3 (CH_3, C-7), 21.3 (CH_3, Ac), 19.8 (CH_3, C-9), 19.7 (CH_3, C-10); HRESIMS m/z 235.1310 $[M]^+$ (calcd for $C_{12}H_{20}O_3$, 235.1308).

(−)-(1R,4S,6R)-1,6-Diacetoxy-2-menthene (13): colorless oil; $[\alpha]_{589}$ −77, $[\alpha]_{578}$ −80, $[\alpha]_{546}$ −92, $[\alpha]_{436}$ −164, $[\alpha]_{365}$ −275 (c 1.8, $CHCl_3$); IR ($CHCl_3$) ν_{max} 1731, 1370, 1248, 1042 cm^{-1}; ^{1}H NMR (400 MHz, $CDCl_3$) δ 6.07 (1H, ddd, J = 10.3, 2.8, 1.0 Hz, H-2), 5.80 (1H, ddd, J = 10.3, 2.8, 0.6 Hz, H-3), 5.21 (1H, ddd, J = 4.6, 3.1, 1.0 Hz, H-6), 2.08 (1H, m, H-4), 2.07 (3H, s, Ac), 1.95 (3H, s, Ac), 1.83 (1H, m, H-5), 1.80 (1H, m, H-5′), 1.71 (1H, septd, J = 6.8, 1.3 Hz, H-8), 1.49 (3H, s, CH_3-7), 0.90 (3H, d, J = 6.8 Hz, CH_3-9), 0.89 (3H, d, J = 6.8 Hz, CH_3-10); ^{13}C NMR (100 MHz, $CDCl_3$) δ 170.4 (C, Ac), 169.6 (C, Ac), 133.6 (CH, C-3), 128.4 (CH, C-2), 77.9 (C, C-1), 72.5 (CH, C-6), 37.7 (CH, C-4), 31.3 (CH, C-8), 25.5 (CH_2, C-5), 22.1 (CH_3, Ac), 21.2 (CH_3, Ac), 21.1 (CH_3, C-7), 19.5 (CH_3, C-9), 19.2 (CH_3, C-10); HRESIMS m/z 277.1418 $[M + Na]^+$ (calcd for $C_{14}H_{22}O_4 + Na^+$, 277.1410).

(−)-(3S,4S,6R)-3,6-Diacetoxy-1-menthene (14): colorless oil; $[\alpha]_{589}$ −85, $[\alpha]_{578}$ −88, $[\alpha]_{546}$ −99, $[\alpha]_{436}$ −160, $[\alpha]_{365}$ −234 (c 2.6, $CHCl_3$); IR ($CHCl_3$) ν_{max} 1721, 1466, 1371, 1022 cm^{-1}; ^{1}H NMR (400 MHz, $CDCl_3$) δ 5.58 (1H, dd, J = 2.3, 1.5 Hz, H-2), 5.22 (1H, m, H-3), 5.20 (1H, m, H-6), 2.08 (3H, s, Ac), 2.07 (3H, s, Ac), 1.83 (1H, m, H-5), 1.78 (1H, m, H-8), 1.77 (1H, m, H-4), 1.71 (3H, br t, J = 1.4, CH_3-7), 1.58 (1H, m, H-5′), 0.92 (3H, d, J = 6.7, CH_3-9), 0.83 (3H, d, J = 6.7, CH_3-10); ^{13}C NMR (100 MHz, $CDCl_3$) δ 170.7 (C, Ac), 170.6 (C, Ac), 135.3 (C, C-1), 127.4 (CH, C-2), 71.0 (CH, C-3), 69.2 (CH, C-6), 39.4 (CH, C-4), 26.9 (CH_2, C-5), 26.4 (CH, C-8), 21.1 (CH_3, Ac), 21.0 (CH_3, Ac), 20.3 (CH_3, C-9), 19.9 (CH_3, C-7), 17.2 (CH_3, C-10); HRESIMS m/z 277.1408 $[M + Na]^+$ (calcd for $C_{14}H_{22}O_4 + Na^+$, 277.1410).

(+)-(4S,5R,6S)-5,6-Dihydroxy-1(7),2-menthadiene (17): white solid; mp 86−88 °C ($CHCl_3$); $[\alpha]_{589}$ +113, $[\alpha]_{578}$ +118, $[\alpha]_{546}$ +135, $[\alpha]_{436}$ +235, $[\alpha]_{365}$ +377 (c 1.1, $CHCl_3$); IR ν_{max} 3556, 2958, 1389 1056 cm^{-1}; ^{1}H NMR (400 MHz, $CDCl_3$) δ 6.18 (1H, dd, J = 10.0, 2.1 Hz, H-2), 5.70 (1H, dd, J = 10.0, 2.6 Hz, H-3), 5.26 (1H, br s, H-7), 5.12 (1H, br s, H-7′), 4.33 (1H, br s, H-6), 3.75 (1H, br s, H-5), 2.25 (1H, m, H-4), 1.96 (1H, septd, J = 6.8, 1.7 Hz, H-8), 1.05 (3H, d, J = 6.8 Hz, CH_3-9), 0.89 (3H, d, J = 6.8 Hz, CH_3-10); ^{13}C NMR (100 MHz, $CDCl_3$) δ 143.5 (C, C-1), 129.0 (CH, C-3), 127.3 (CH, C-2), 115.2 (CH_2, C-7), 71.8 (CH, C-6), 71.4 (CH, C-5), 46.8 (CH, C-4), 28.3 (CH, C-8), 21.1 (CH_3, C-9), 18.5 (CH_3, C-10); HRESIMS m/z 186.1497 $[M + NH_4]^+$ (calcd for $C_{10}H_{16}O_2 + NH_4^+$, 186.1489).

(+)-(1S,4S,5R,6R)-5,6-Diacetoxy-1-hydroxy-2-menthene (18): white solid; mp 78−80 °C; $[\alpha]_{589}$ +113, $[\alpha]_{578}$ +118, $[\alpha]_{546}$ +134, $[\alpha]_{436}$ +234, $[\alpha]_{365}$ +379 (c 0.1, $CHCl_3$); IR ($CHCl_3$) ν_{max} 3584, 2963, 2875, 1743, 1371 cm^{-1}; ^{1}H NMR (400 MHz, $CDCl_3$) δ 5.65 (1H, ddd, J = 10.4, 2.3, 1.1 Hz, H-2), 5.59 (1H, dd, J = 10.4, 2.5 Hz, H-3), 5.20 (1H, dd, J = 2.2, 1.1 Hz, H-6), 5.11 (1H, dd, J = 8.3, 2.2 Hz, H-5), 2.38 (1H, ddt, J = 8.4, 3.6, 2.5 Hz, H-4), 2.15 (3H, s, Ac), 2.05 (3H, s, Ac), 1.80 (1H, septd, J = 6.8, 3.6 Hz, H-8), 1.38 (3H, d, J = 1.0 Hz CH_3-7), 1.02 (3H, d, J = 6.8 Hz, CH_3-10), 0.83 (3H, d, J = 6.8 Hz, CH_3-9); ^{13}C NMR (100 MHz, $CDCl_3$) δ 170.8 (C, Ac), 170.5 (C, Ac) 132.9 (CH, C-2), 126.1 (CH, C-3), 74.8 (CH, C-6), 70.7 (CH, C-5), 70.2 (C, C-1), 43.0 (CH, C-4), 27.5 (CH, C-8), 26.8 (CH_3, C-7), 21.1 (CH_3, Ac), 21.1 (CH_3, Ac), 20.5 (CH_3, C-10), 17.8 (CH_3, C-9); HRESIMS m/z 293.1365 $[M]^+$ (calcd for $C_{14}H_{22}O_5$, 293.1359).

(+)-(1S,4S,5R,6R)-1,5,6-Triacetoxy-2-menthene (19): colorless oil; $[\alpha]_{589}$ +96, $[\alpha]_{578}$ +103, $[\alpha]_{546}$ +116, $[\alpha]_{436}$ +204, $[\alpha]_{365}$ +333 (c 0.8, $CHCl_3$); IR ($CHCl_3$) ν_{max} 2954, 1731, 1369, 1053 cm^{-1}; ^{1}H NMR (400 MHz, $CDCl_3$) δ 6.04 (1H, ddd, J = 10.4, 2.5, 1.6 Hz, H-2), 5.70 (1H, t, J = 2.0 Hz, H-6), 5.66 (1H, dd, J = 10.4, 2.2 Hz, H-3), 5.08 (1H, dd, J = 9.6, 2.0 Hz, H-5), 2.50 (1H, dq, J = 9.6, 2.9 Hz, H-4), 2.12 (3H, s, Ac), 2.05 (3H, s, Ac), 1.99 (3H, s, Ac), 1.84 (1H, septd, J = 6.8, 2.9 Hz, H-8), 1.71 (3H, s, CH_3-7), 1.02 (3H, d, J = 6.8 Hz, CH_3-10), 0.81 (3H, d, J = 6.8 Hz, CH_3-9); ^{13}C NMR (100 MHz, $CDCl_3$) δ 170.6 (C, Ac), 170.1 (C, Ac), 169.6 (C, Ac), 129.2 (CH, C-2), 126.9 (CH, C-3), 79.8 (C, C-1), 72.7 (CH, C-6), 69.4 (CH, C-5), 42.0 (CH, C-4), 26.7 (CH, C-8), 24.7 (CH_3, C-7), 22.0 (CH_3, Ac), 20.9 (CH_3, Ac), 20.9 (CH_3, Ac), 20.3 (CH_3, C-10), 19.3 (CH_3, C-9); HRESIMS m/z 335.1473 $[M + Na]^+$ (calcd for $C_{16}H_{24}O_6 + Na^+$, 335.1465).

(+)-(1R,4S,5R,6R)-5,6-Diacetoxy-1-hydroxy-2-menthene (20): colorless oil; $[\alpha]_{589}$ +47, $[\alpha]_{578}$ +49, $[\alpha]_{546}$ +56, $[\alpha]_{436}$ +97 (c 1.2, $CHCl_3$); IR ($CHCl_3$) ν_{max} 3594, 2964, 2875, 1734, 1600, 1370 cm^{-1}; ^{1}H NMR (400 MHz, $CDCl_3$) δ 5.70 (1H, dd, J = 10.3, 2.2 Hz, H-3), 5.63 (1H, ddd, J = 10.3, 2.2, 1.3 Hz, H-2), 5.29 (1H, dd, J = 9.0, 2.5 Hz, H-5), 5.21 (1H, dd, J = 2.5, 1.3 Hz, H-6), 2.36 (1H, m, H-4), 2.09 (3H, s, Ac), 2.02 (3H, s, Ac), 1.84 (1H, septd, J = 7.0, 3.6 Hz, H-8), 1.27 (3H, s, CH_3-7), 1.02 (3H, d, J = 7.0 Hz, CH_3-10), 0.82 (3H, d, J = 7.0 Hz, CH_3-9); ^{13}C NMR (100 MHz, $CDCl_3$) δ 170.6 (C, Ac), 170.6 (C, Ac) 131.2 (CH, C-2), 128.7 (CH, C-3), 74.7 (CH, C-6), 70.4 (C, C-1), 69.5 (CH, C-5), 42.2 (CH, C-4), 27.0 (CH, C-8), 25.1 (CH_3, C-7), 21.0 (CH_3, Ac), 21.0 (CH_3, Ac), 20.4 (CH_3, C-10), 17.5 (CH_3, C-9); HRESIMS m/z 293.1358 $[M]^+$ (calcd for $C_{14}H_{22}O_5$, 293.1359).

(−)-(1R,4S,5R,6R)-1,5,6-Triacetoxy-2-menthene (21): colorless oil; $[\alpha]_{589}$ −35, $[\alpha]_{578}$ −36, $[\alpha]_{546}$ −43, $[\alpha]_{436}$ −80, $[\alpha]_{365}$ −145 (c 0.6, $CHCl_3$); IR ($CHCl_3$) ν_{max} 2959, 1735, 1463, 1369, 1052 cm^{-1}; ^{1}H NMR (300 MHz, $CDCl_3$) δ 6.14 (1H, ddd, J = 10.3, 2.4, 1.2 Hz, H-2), 5.75 (1H, dd, J = 10.3, 2.7 Hz, H-3), 5.39 (1H, dd, J = 2.6, 1.2 Hz, H-6), 5.30 (1H, dd, J = 9.0, 2.6 Hz, H-5), 2.35 (1H, ddd, J = 9.0, 3.0, 2.7 Hz, H-4), 2.10 (3H, s, Ac), 2.03 (3H, s, Ac), 2.00 (3H, s, Ac), 1.85 (1H, septd, J = 7.0, 3.0 Hz, H-8), 1.51 (3H, s, CH_3-7), 1.01 (3H, d, J = 7.0 Hz, CH_3-10), 0.80 (3H, d, J = 7.0 Hz, CH_3-9); ^{13}C NMR (75.4 MHz, $CDCl_3$) δ 170.5 (C, Ac), 170.3 (C, Ac), 169.5 (C, Ac), 130.1 (CH, C-3), 128.6 (CH, C-2), 79.1 (C, C-1), 72.2 (CH, C-6), 68.9 (CH, C-5), 42.2 (CH, C-4), 27.1 (CH, C-8), 22.0 (CH_3, Ac), 21.0 (CH_3, Ac), 20.9 (2CH_3, Ac and C-7), 20.8 (CH_3, C-10), 20.3 (CH_3, C-9); HRESIMS m/z 335.1479 $[M + Na]^+$ (calcd for $C_{16}H_{24}O_6 + Na^+$, 335.1465).

Conformational Calculations. Monte Carlo search protocols using the Merck molecular force field (MMFF94) followed by single-point energy calculations using DFT at the B3LYP/6-31G(d) level of theory, both implemented in the Spartan'04 software, were carried out. The MMFF step provided 29, 43, 37, 48, 22, six, and six conformers for **4**, **5**, **15**, **16**, **17**, **IV**, and **V**, respectively, in energy gaps of 10 kcal/mol, while after single-point calculations these conformers appeared in 8.79, 5.51, 8.53, 7.61, 5.68, 3.90, and 5.10 kcal/mol energy gaps, respectively. Bond distances and dihedral angles of each conformer were extracted using the Spartan'04 software. Averaged and standard errors of these data were estimated using the Microsoft Excel program. Calculations were performed using a laptop computer operating at 2.20 GHz with 8 Gb RAM.

■ ASSOCIATED CONTENT

Supporting Information

The Supporting Information is available free of charge on the ACS Publications website at DOI: 10.1021/acs.jnatprod.8b00855.

DOI: 10.1021/acs.jnatprod.8b00855
J. Nat. Prod. XXXX, XXX, XXX−XXX

Copies of 1D and 2D NMR spectra of **1**−**21**; minimum energy conformers, bond lengths, and angles of **4**, **5**, **15**, **16**, **17**, **IV**, and **V** (PDF)

AUTHOR INFORMATION

Corresponding Authors

*(C. M. Cerda-García-Rojas) E-mail: ccerda@cinvestav.mx. Tel: +52 55 5747 4035. Fax: +52 55 5747 7137.

*(Mario A. Gómez-Hurtado) E-mail: magomez@umich.mx. Tel: +52 443 3265788. Fax: +52 443 326 5790.

ORCID

Julio C. Pardo-Novoa: 0000-0002-7807-1074

Héctor M. Arreaga-González: 0000-0002-3746-0137

Sinuhé Galván-Gómez: 0000-0001-6006-8523

Gabriela Rodríguez-García: 0000-0002-9840-9968

Rosa E. del Río: 0000-0001-8932-552X

Carlos M. Cerda-García-Rojas: 0000-0002-5590-7908

Pedro Joseph-Nathan: 0000-0003-3347-3990

Mario A. Gómez-Hurtado: 0000-0002-2386-4819

Notes

The authors declare no competing financial interest.

ACKNOWLEDGMENTS

We thank CIC-UMSNH and CONACYT-Mexico (Grant No. 284194) for financial support. J.C.P.N., H.M.A.G., and S.G.G. are grateful to CONACYT-Mexico for scholarships 446483, 295638, and 619406. We are grateful to Professor Jerzy Rzedowski, Instituto de Ecología, A. C., Centro Regional del Bajío, Pátzcuaro, Michoacán, Mexico, for identifying the plant material.

DEDICATION

Dedicated to Dr. Rachel Mata, Universidad Nacional Autónoma de México, Mexico City, Mexico, for her pioneering work on bioactive natural products.

REFERENCES

(1) Dewick, P. M. *Nat. Prod. Rep.* **2002**, *19*, 181−222.

(2) Friedman, M. *J. Agric. Food Chem.* **2014**, *62*, 7652−7670.

(3) Talapatra, S. K.; Talapatra, B. *Chemistry of Natural Products, Stereochemistry, Conformation, Synthesis, Biology, and Medicine*; Springer: Berlin, 2015; pp 348−349.

(4) Šulniūtė, V.; Baranauskienė, R.; Ragažinskienė, O.; Venskutonis, P. R. *Flavour Fragrance J.* **2017**, *32*, 254−264.

(5) Pérez, A. G.; Cert, A.; Ríos, J. J.; Olías, J. M. *J. Agric. Food Chem.* **1997**, *45*, 4393−4397.

(6) Mastelić, J.; Jerković, I.; Vinković, M.; Džolić, Z.; Vikić-Topić, D. *Croat. Chem. Acta* **2004**, *77*, 491−500.

(7) Mastelić, J.; Jerković, I. *Food Chem.* **2003**, *80*, 135−140.

(8) Stahl-Biskup, E.; Intert, F.; Holthuijzen, J.; Stengele, M.; Schulz, G. *Flavour Fragrance J.* **1993**, *8*, 61−80.

(9) Pardo-Novoa, J. C.; Arreaga-González, H. M.; Gómez-Hurtado, M. A.; Rodríguez-García, G.; Cerda-García-Rojas, C. M.; Joseph-Nathan, P.; del Río, R. E. *J. Nat. Prod.* **2016**, *79*, 2570−2579.

(10) Pimienta-Ramírez, L.; García-Rodríguez, Y. M.; Ríos-Ramírez, E. M.; Linding-Cisneros, R.; Espinosa-García, F. J. *J. Essent. Oil Res.* **2016**, *28*, 113−120.

(11) Doering, W. E.; Schimdt, E. K. G. *Tetrahedron* **1971**, *27*, 2005−2030.

(12) Gutta, P.; Tantillo, D. J. *J. Am. Chem. Soc.* **2006**, *128*, 6172−6179.

(13) Gutta, P.; Tantillo, D. J. *Org. Lett.* **2007**, *9*, 1069−1071.

(14) Hong, Y. J.; Tantillo, D. J. *J. Am. Chem. Soc.* **2010**, *132*, 5375−5386.

(15) Montiel, V.; López, M.; Aldaz, A. *Synth. Commun.* **1987**, *17*, 993−996.

(16) Lukas, B.; Schmiderer, C.; Novak, J. *Phytochemistry* **2015**, *119*, 32−40.

(17) Pérez-Galindo, P.; Martínez-Raya, A.; Francia, J. R.; Jiménez, J.; Navarro, C. *J. Essent. Oil Res.* **2005**, *17*, 651−655.

(18) Domingo, V.; Prieto, C.; Silva, L.; Rodilla, J. M.; Quílez del Moral, J. F.; Barrero, A. F. *J. Nat. Prod.* **2016**, *79*, 831−837.

(19) Pollastro, F.; Caprioglio, D.; Marotta, P.; Moriello, A. S.; De Petrocellis, L.; Taglialatela-Scafati, O.; Appendino, G. *J. Nat. Prod.* **2018**, *81*, 630−633.

(20) Arreaga-González, H. M.; Pardo-Novoa, J. C.; del Río, R. E.; Rodríguez-García, G.; Torres-Valencia, J. M.; Manríquez-Torres, J. J.; Cerda-García-Rojas, C. M.; Joseph-Nathan, P.; Gómez-Hurtado, M. A. *J. Nat. Prod.* **2018**, *81*, 63−71.

(21) Batsanov, S. S. *Inorg. Mater.* **2001**, *37*, 871−885. Translated from *Neorganicheskie Materialy* **2001**, *37*, 1031−1046.

(22) Scheiner, S. *Hydrogen Bonding: A Theoretical Perspective*; University Press: New York, 1997; pp 14−18.

(23) Basco, E. A.; Kaiser, C.; Rittner, R.; Lambert, J. B. *J. Org. Chem.* **1993**, *58*, 7865−7869.

(24) Yoder, R. A.; Johnston, J. N. *Chem. Rev.* **2005**, *105*, 4730−4756.

(25) Tran, D. N.; Cramer, N. *Chem. - Eur. J.* **2014**, *20*, 1−7.

(26) Lam, H. C.; Spence, J. T. J.; George, J. H. *Angew. Chem., Int. Ed.* **2016**, *55*, 1−5.

(27) Dewick, P. M. *Medicinal Natural Products. A Biosynthetic Approach*, 3rd ed.; John Wiley & Sons: Chichester, 2009; pp 233−234.

(28) Bohlmann, F.; Jakupovic, J.; Lonitz-Über, M. *Chem. Ber.* **1977**, *110*, 301−314.

(29) Bustos-Brito, C.; Vázquez-Heredia, V. J.; Calzada, F.; Yépez-Mulia, L.; Calderón, J. S.; Hernández-Ortega, S.; Esquivel, B.; García-Hernández, N.; Quijano, L. *Molecules* **2016**, *21*, 1−13.

(30) Alencar, J. W.; de Vasconcelos Silva, M. G.; Lacerda Machado, M. I.; Craveiro, A. A.; de Abreu Matos, F. J.; de Abreu Magalhães, R. *Spectroscopy* **1997**, *13*, 265−273.

(31) Işcan, G.; Kırımer, N.; Demirci, F.; Demirci, B.; Noma, Y.; Başerd, K. H. C. *Chem. Biodiversity* **2012**, *9*, 1525−1532.

(32) Ross, S. A.; El Sayed, K. A.; El Sohly, M. A.; Hamann, M.; Abdel-Halim, O. B.; Ahmed, A. F.; Ahmed, M. M. *Planta Med.* **1997**, *63*, 479−482.

(33) Jeong, E. Y.; Lim, J. H.; Kim, H. G.; Lee, H. S. *J. Food Prot.* **2008**, *71*, 351−355.

(34) Escher, S.; Keller, U.; Willhalm, B. *Helv. Chim. Acta* **1979**, *62*, 2061−2072.

(35) Weyerstahl, P.; Marschall, H.; Splittgerber, U.; Son, P. T.; Giang, P. M.; Kaul, V. K. *Flavour Fragrance J.* **1999**, *14*, 225−229.

DOI: 10.1021/acs.jnatprod.8b00855
J. Nat. Prod. XXXX, XXX, XXX−XXX